Escola de Camins
Escola Tècnica Superior d'Enginyeria de Camins, Canals i Ports
UPC BARCELONATECH

PROJECTE O TESINA D'ESPECIALITAT

Títol

STORM-INDUCED CHANGES IN THE CATALAN COAST USING LIDAR: THE ST. ESTEVE STORM (26/12/2008) CASE

Autor/a

ANA PLANA CASADO

Tutor/a

JOSÉ ANTONIO JIMÉNEZ QUINTANA

Departament

DEPARTAMENT D'ENGINYERIA HIDRÀULICA, MARÍTIMA I AMBIENTAL

Intensificació

ENGINYERIA MARÍTIMA

Data

GENER DE 2013

ABSTRACT

Storm events represent a major factor controlling short-to-medium-term morphological evolution of beaches. The storm of Sant Esteve 2008 was a significant event that hit the whole Catalan coast on 26th December 2008. The ICC registered its effects on different coastal areas through LIDAR surveys which took place shortly after the storm. Moreover, the pre-storm situation had been recorded in a previous flight, and the state of the beaches was surveyed again in summer 2009.

This work analyses the LIDAR data to evaluate the storm-induced changes on the Tordera-Blanes area and its post-storm recovery. Both the qualitative response and the sediment volumes involved are evaluated. The description of the morphological changes in the emerged part of the beach is completed by the modelling of the behaviour of the submerged part. The modelling tools used perform unevenly: the Convolution Method poses problems related to the beach geometrical definition, while the SBEACH model has accurate results that match the observations on the emerged part of the beach.

The joint analysis of measured and modelled data shows that the response of the beach of S'Abanell was general erosion driven by cross-shore transport, but that local variations were caused by longshore sediment transport boosted by the existing beach nourishment. In Malgrat de Mar, the changing orientation of the coast translated in a heterogeneous response to the storm characterized by erosion with scattered accretion spots. In both cases important overwash occurred.

Key words: LIDAR, beach morphology, overwash, storm-induced erosion, SBEACH, Convolution Method.

ACKNOWLEDGEMENTS

I offer my sincerest gratitude to my tutor, Professor José Jiménez Quintana, who has supported me throughout this research project with his patience and knowledge.

I would also like to thank the Institut Cartogràfic de Catalunya for providing the LIDAR data, the very cornerstone around which this work is constructed.

Barcelona, January 2013

CONTENTS

ABSTRACT ii

ACKNOWLEDGMENTS iii

CONTENTS 01

1. INTRODUCTION 03
    1.1. Motivation 03
    1.2. Objectives 03
    1.3. Structure 04

2. BACKGROUND 05
    2.1 LIDAR technology and data 05
    2.2 Study area 09

3. THE STORM OF SANT ESTEVE 2008 11
    3.1 Meteorology 11
    3.2 Deepwater storm classification 12
    3.3 Water level: Storm surge and astronomical tide 15
    3.4 Runup and overtopping 15
    3.5 Wave propagation 22
    3.6 Expected beach response 27

4. LIDAR-BASED ANALYSIS OF THE COAST MORPHOLOGICAL EVOLUTION 28
    4.1 Available datasets and methodology 28
    4.2 Morphological response to the storm 29
    4.3 Morphological recovery after the storm 43
    4.4 Summary 53

5. MODELLED EROSION 54
    5.1 Methodology 54
    5.2 Convolution method 56
    5.3 SBEACH numerical model 64
    5.4 Model comparison and total erosion 67

6. BEACH RESPONSE TO THE EVENT 75
    6.1 Storm-induced changes in S'Abanell 75
    6.2 Storm-induced changes in the beaches of Malgrat 78
    6.3 Storm induced changes in the mouth of the River Tordera 85

7. CONCLUSIONS 87

BIBLIOGRAPHY 89

ANNEX 1

ANNEX 2

Chapter 1

INTRODUCTION

1.1. Motivation

Highly-energetic storms hit the Catalan shores periodically, threatening the population and the economical activities that concentrate in the coastal areas. In the event of possible changing storm regimes, understanding these extreme events is crucial to implement adequate coastal management and protection measures.

Beaches are complex systems whose defining parameters vary enormously from one location to another. As a result, the accurate characterization of a given coastal zone cannot be solely based on analytical analysis and modelling. In order to fully understand the processes that occur, as much field data as possible have to be included in the studies.

At present, the Institut Cartogràfic de Catalunya (ICC) is developing the use of LIDAR to monitor the evolution of the coast. The highly accurate and dense LIDAR data can be an outstanding tool for fast response after major events and to quantify the evolution of the coast.

The storm of Sant Esteve 2008 was a significant event that hit the whole Catalan coast, causing important material damages and even the loss of human lives. The ICC registered its effects on different coastal areas through LIDAR surveys which took place shortly after the storm. Moreover, the pre-storm situation had been recorded in a previous flight. Lastly, the state of the beaches was surveyed again in summer 2009.

The availability of this information provides an excellent opportunity to evaluate the storm-induced changes in the beach morphology and its recovery after the extreme event of Sant Esteve 2008. The study can thus contribute to a better understanding of the potential effects of storms on the beaches of the study area and how they recover after these extreme events.

1.2. Objectives

The main objective of this work is to evaluate the morphological changes that the storm of Sant Esteve 2008 induced in the beaches of the Tordera-Blanes area. The specific goals regarding this evaluation are:

- To describe the morphological changes that occurred in the beaches of the area both during the storm and in the post-storm recovery
- To quantify the sediment volumes involved
- To explain the physical processes behind the beach response to the storm

In addition, this work aims to provide meaningful insight on the advantages and limitations of the application of LIDAR techniques to the case of the Catalan coast.

1.3. Structure

The first part of this work consists on the description of the LIDAR technology and the study area (Chapter 2). After that, but prior to the evaluation of the beach response to the studied event, the storm of Sant Esteve 2008 is characterized (Chapter 3). The LIDAR data are then analysed in Chapter 4. Chapter 5 complements the study with modelling techniques in order to overcome the limitations of LIDAR data. Finally, the results of all the previous chapters are analysed comprehensively in Chapter 6 to draw the picture of the storm-induced changes in the area.

Chapter 2

BACKGROUND

2.1. LIDAR technology and data

2.1.1. LIDAR concepts and applications

Nowadays, a large-scale approach to land survey is possible thanks to different remote sensing methods. Satellite images, either radar or optical, are been used in a wide range of professional activities and research areas. However, in many cases they have to be combined with topographic techniques to obtain high resolution three dimensional data. Depending on the scale of the project, the accurate topography needed is usually obtained by conventional topographic data collection or using GPS techniques.

LIDAR (*LIght Detection And Ranging* or *Laser Imaging Detection And Ranging*) combines the advantages of remote sensing with high vertical accuracy and precision, even though it cannot yet match the quality of classical topography. At the origin (mid-1960s), LIDAR was a military system used to detect submarines in shallow water. The technology entered the civil industry at the beginning of the 1990s (Heurtefeux, 2008).

The principle behind LIDAR technology is the reflexion of light and its dispersion in translucent environments. LIDAR instruments are active devices that fire high frequency beams of laser light towards an obstacle and measure the time it takes for each pulse to bounce back.

Even though the instrument can be ground-based, the most widespread system for coastal applications is Airborne LIDAR. The tool itself is constituted by the laser scanning system and an Inertial Navigation System (INS) tied to a differential GPS disposed on board of an aircraft or a helicopter. A video camera can be added to the system to provide images and better analyse the data obtained.

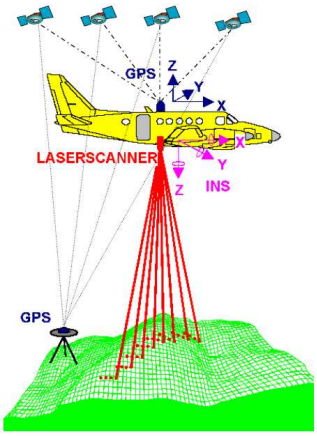

Figure 2.1. Airborne LIDAR (Ruiz and Kornus, 2003).

The data density and the strip width of the surface covered by each LIDAR survey depend on the sensors used. The output can be almost automatically converted to a Digital Model of the Terrain (MDT), allowing getting models of a region shortly after the flight and showing and almost instantaneous picture of the situation (Ruiz et al., 2008). Verification is made using control areas or previous flights.

The productivity of LIDAR is very high. For example, in 2008 almost the entire Catalan coast was covered by only four flights sessions. The vertical precision is usually of 10-25 cm and the XY error around 30-60 cm.

There are different kinds of LIDAR systems depending on the lasers employed. The data used in this work was obtained by topographic LIDAR, which uses near infrared lasers (wavelength of 1064 µm). Light of this frequency does not penetrate water, but topographic LIDAR is very cost-effective.

Bathymetric LIDAR is a much more expensive system which is used when underwater data are needed. This second kind of LIDAR uses, in addition to the infrared laser, a green laser light (532 µm) that is returned by the sea floor. Both lasers operate at the same time, and water depth is retrieved from the difference in return time of the two beams. Current bathymetric systems combine both sensors and can survey simultaneously the surface above and below the sea. This second kind of LIDAR has great potential, but its civil operational applications are often limited because of its economical cost and because the quality of the data obtained is very dependent on the clearness of the water.

There are other kinds of Airborne LIDAR sensors adapted to specific needs. For example, for forest and vegetation monitoring the sensors used emit two pulses, allowing detecting the different heights of trees.

The advantages of Airborne LIDAR over photogrammetry and conventional topography are:

- Higher productivity (less data collection and processing time).
- Data processing can be automated to a high degree.
- It needs less control points.
- Weather and light independence.
- It is very appropriate on flat terrain.
- It does not have the deformations problems that stereoscopic vision has with the presence of water or low texture sand.

- Higher density.
- Minimum number of control points required.

However, LIDAR surveys have technical requirements regarding the GPS satellites positions, and the distance to the fixed GPS stations used on land should not exceed 15 km (Heurtefeux, 2008).

Airborne LIDAR data can be used for a wide range of activities related to coastal dynamics, including:

- Volume computation of sand movements and shoreline change.
- Cataloguing of coastal defences and man-made structures.
- Dunes and beach morphological classification.
- Detailed coastal cartography.
- Detailed digital terrain modelling of floodplains for mapping and risk analysis.
- Shallow waters bathymetry.

Some of its applications in other domains are:

- Surface classification (crops, vegetation)
- Development and emergency planning
- Detection of buildings in protected areas
- 3D models for landscape analysis
- Monitoring of changes of the objects on the terrain, buildings and vegetation
- Snow monitoring (Fig. 2.2)
- City modelling (Fig. 2.2)

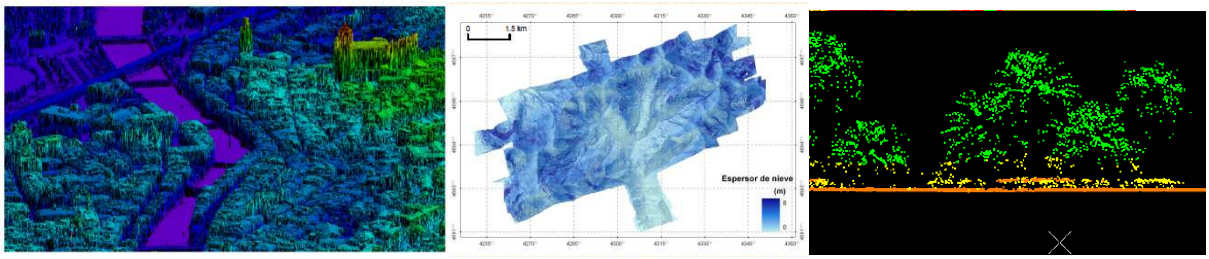

Figure 2.2. Examples of data obtained in Catalonia using LIDAR. From left to right: 3D model of the city of Girona; snow depths at La Vall de Núria (Pyrenees); point cloud image of Salou's maritime promenade obtained with a terrestrial mobile LIDAR device. (Institut Cartogràfic de Catalunya).

Finally, it has to be noted that LIDAR is not only a geosciences technique. Terrestrial LIDAR systems, either fixed or mobile, are used in many technological activities. Even today, 50 years after its invention, LIDAR is showing its potential in new applications as the development of autonomous cars.

2.1.2. Previous experiences

In the USA, the United States Geological Survey (USGS), the National Aeronautics and Space Agency (NASA) and the National Oceanic and Atmospheric Administration (NOAA) are collaborating to monitor the coast with LIDAR since 1995. In addition, LIDAR data has been used in many studies of the impact of extreme weather events on the coast (e.g. Stockdon et al., 2007; Sallenger et al., 2006).

In Catalonia, LIDAR techniques have started to be used much more recently. In 2001 the *Institut Cartogràfic de Catalunya* (ICC) purchased its first sensor, an OPTECH ALTM 3025. Many works were carried out with this sensor, including:

- Fluvial areas management plan (PEFCAT project).
- Airport modelling for AENA.
- Modelling of the Italian region of Emilia-Romagna.

Ruiz and Kornus (2009) made the first estimations of volumetric changes in Catalan beaches using LIDAR after the storms of the first months of 2002.

However, the ICC's flagship project in this area is LIDARCAT, which started in 2006. It aim to cover the entire surface of Catalonia (32114 km^2) every 4 years. Regarding coastal areas, between 2007 and 2008 all the Catalan coastline (a strip of 1200 metres) was covered with a density of 1 p/m^2 and a vertical precision of 10 cm. The survey was repeated in 2009. Several other flights have been made since then, but it has been impossible to complete annual surveys.

In 2008 the ICC purchased a new sensor, a LEICA ALS50 phase II. The data used in this work were obtained with this sensor.

Figure 2.3. LIDAR at the ICC. Left: Cessna Caravan 208B, one of the planes used for the surveys; Right: LIDAR sensor LEICA ALS50 phase II (ICC).

At present, the ICC is employing topographic LIDAR technology in various areas, and the results suggest that LIDAR data is a good option to complement conventional techniques in some applications and completely replace them in some others. Bathymetric LIDAR is being tested in the harbour of Mataró. The results up to this date prove that the technology is useful up to a depth of 22 metres, and provides results with a vertical error of 15-20 cm.

2.1.3. Datasets

Shortly after the storm of Sant Esteve 2008, the ICC carried out LIDAR surveys to assess the impact of the event in three areas of the Catalan coast: Barcelona, Mataró, and Tordera-Blanes.

Data of the existing situation before the storm at the three locations had been recorded in October 2008 in the framework of the LIDARCAT program (LIDAR COSTA program). Additional surveys took place during the summer of 2009, providing a picture of the post-storm situation. This work analyses the data corresponding to the area of Tordera-Blanes.

The data was obtained using a sensor LEICA ALS50 phase II. The parameters for each of the flights are specified in Table 2.1.

Table 2.1. (Flight specifications of the LIDAR surveys (ICC).

	PRE-STORM SURVEY	POST-STORM SURVEY	RECOVERY SURVEY
SENSOR		LEICA ALS50 phase II	
FLIGHT DATE	16/10/2008	17/01/2009	17/08/2009
ABOVE GROUND LEVEL	2250 m	950 m	1000 m
SCAN RATE	22 Hz	30.6 Hz	30.6 Hz
PULSE FREQUENCY	88000 Hz	90600 Hz	90600 Hz
AVERAGE POINT DENSITY	0.5 point/m^2	1 point/m^2	1 point/m^2
PRECISION IN HEIGHT	15 cm	15 cm	9 cm
PRECISION IN PLAN	32 cm	32 cm	14 cm

The initial processing of the rough LIDAR data was made by the ICC. This work is based on the Terrain Digital Models (MDT) that ensued from this first step.

2.2. Study area

Figure 2.4. Study area (ortophotos from the ICC; maps based on d-maps.com).

The study area, shown in Figure 2.4, covers approximately 9 kilometres of the Catalan coast, from Blanes' harbour at the north to the southern end of Malgrat de Mar.

The Catalan towns of Blanes and Malgrat de Mar (hereafter referred as Malgrat) are located on the north and south banks of the River Tordera. Both towns are important touristic destinations.

Blanes is located in the county of La Selva (province of Girona). It has a population of about 40000, but the number increases significantly during the summer holidays. The coastline of the town is divided into two parts by the headland of Sa Palomera. The beach of the Bay of Blanes lies at the north, nestled between the harbour and the headland and backed by a maritime promenade. South from Sa Palomera, the beach of S'Abanell stretches for over 2400 metres. The town limits are at approximately 600 meters from the River Tordera. From that point to the mouth of the river, the land is occupied by a small forest area and camping sites. Both beaches are approximately 40 metres wide.

Malgrat, which belongs to Maresme (Barcelona), has a population of 19000. Its coastline does not have any natural division, but it is usually divided into three parts: Malgrat Centre, La Conca and Punta de la Tordera. It is a very wide beach (up to 140 metres), and in many areas there are houses in the sand. As in S'Abanell, the section closest to the river mouth is occupied by camping sites. Between the camping sites and the town there is a low density area, and in this part the beach landward limits are the road and railway.

The beaches of the study area are highly reflective, and their sediment is coarse sand (see Table 2.2).

Table 2.2. Sediment characteristics for study area (IGC, Institut Geològic de Catalunya, 2010.

	Grain size, D_{50}	**Sediment type**
Bay of Blanes	1153 µm	Well sorted very coarse sand
S'Abanell	1398 µm	Very well sorted very coarse sand
Malgrat		
Punta de la Tordera	906 µm	Very well sorted very coarse sand
La Conca	1333 µm	Well sorted very coarse sand
Malgrat Centre	1806 µm	Very well sorted very coarse sand

The river Tordera flows for 60 km and has a pluvio-torrential regime. The river basin covers only 894 km^2, resulting in low mean flow of about 5 m^3/s and low sediment transport capacity in standard conditions (Agència Catalana de l'Aigua, 2002). However, significant rain episodes produce sudden and important increases of the river water flow and sediment transport rate known as *Torderades*. The mouth of the river is characterized by a delta covering an area of 8 km^2 which reaches a maximum width of 6400 metres at the coast.

In its lowest part, the Tordera suffers from strong anthropic pressure. Firstly, the growth of the urban settlements around the river has forced its embankment in many sections. In addition, both the river and the underlying aquifer are over-exploited to guarantee the water supply for domestic, industrial and agricultural usage in the area. As a result, the water level and flow velocity at the river mouth are usually very low, causing sea water intrusion. Nowadays, the delta suffers from regression and salinization.

Over the years, the Laboratory of Marine Engineering of the Polytechnic University of Catalunya (LIM) has carried out many studies and research projects in S'Abanell and its surrounding area. The knowledge gained concerning its behaviour and characteristics has proven to be a key factor to orientate this work, understand the results and reach profitable conclusions.

Chapter 3

THE STORM OF SANT ESTEVE 2008

The direct analysis of the LIDAR elevation data describing the storm-induced changes in the study area without a prior study of the event could result in the oversight of important processes.

The aim of this chapter is to characterize the storm of Sant Esteve 2008 and its interaction with the coast, thus providing a reference framework to understand the beach response to the extreme conditions registered.

3.1 Meteorology

Previous to the storm, the meteorological situation along the Catalan coast was stable and dominated by south and southwest winds (*Tramuntana*). The situation started to change on 25th December 2008, when a shallow depression arrived to the Balearic Sea from the Northeast with a minimum pressure of 1012 hPa. Its interaction with a high pressure centre over Northern Europe of 1047 hPa originated strong winds from the East (Figure 3.1, left).

Storms coming from the East are common on the Catalan coast and are called *Llevantades*. They are amongst the strongest in the area. Even though they have been widely studied, in this specific case the numerical model of the Catalan Meteorological Service failed to predict its real scale (Figure 3.1, right).

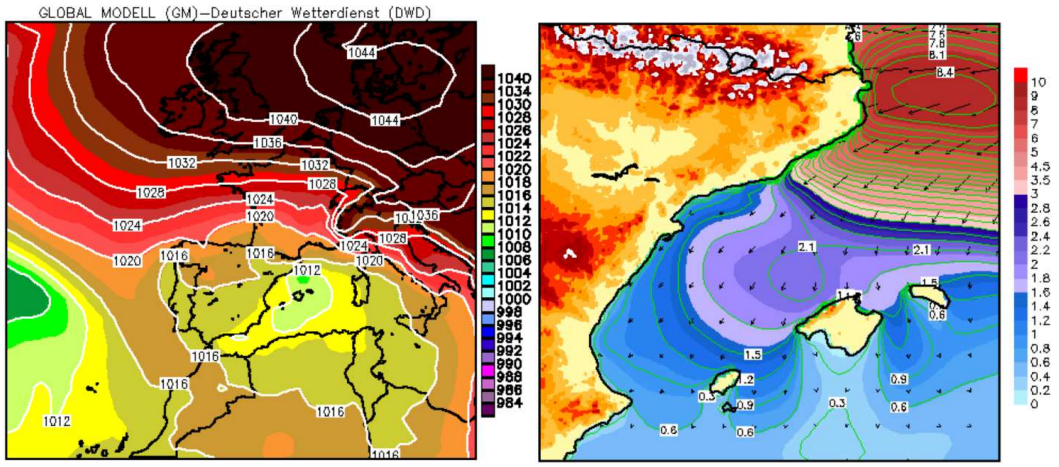

Figure 3.1. Left: Interaction between a high pressure centre and a depression, 26/12/2008-12Z. Right: Wave height prediction for 26/12/2008-18Z (Servei Meteorològic de Catalunya).

The storm affected the entire Catalan coast but its intensity decreased from Northeast to Southwest, and hence the worst-affected coastal towns were the northern ones (e.g. Roses, Palamós, l'Escala, Cadaqués). In these locations the storm hit the coast with an unusually

high strength that, according to the media and collective memory, was last seen more than 60 years ago.

In the central zone of the Catalan coast the storm was less intense and destructive, but wave heights in Barcelona reached six metres, with a mean height of around four metres. Unfortunately, this was enough to cause the death of three people.

Although the storm weakened towards the Southwest, its effects were noticeable even at the southernmost end of Catalonia, Ebro Delta.

The study area of this work is described in Chapter 2 and covers the beaches that lie between the harbour of Blanes and the southern end of Malgrat de Mar, in the limit between the provinces of Barcelona and Girona. The storm struck the area with high intensity, but it was not part of the most affected zones of the Catalan coast.

3.2 Deepwater storm classification

Mendoza et al. (2011), define a storm as the extreme event during which the significant deep-water wave height H_s is greater that 2 metres during at least six hours. Two of such events are considered non-independent if they are less than 72 hours apart and if during this in-between period H_s is lower than 1.5 metres for less than six hours.

Using this criterion, the storm of Sant Esteve 2008 in the area of the Tordera Delta was a single continuous event that started on 26th December 2008 at 12:00 a.m. and lasted until 29th December 2008 at 06:00 a.m. Its deep-water characteristics were:

- Duration: 66 hours
- Maximum significant height, Hs_{max}: 4.65 m (26/12/2008, 06:00-07:00 p.m.)
- Maximum peak period, Tp_{max}: 14.3 s (27/12/08, 01:00-02:00 a.m.)
- Prevailing wave direction: East

Figure 3.2 and 3.3 depict the evolution of wave heigths, periods and directions during the entire event. The data were recorded by a buoy belonging to the Catalan network XIOM (*Xarxa d'Instruments Oceanogràfics i Meteorològics)* and located in front of the harbour of Blanes.

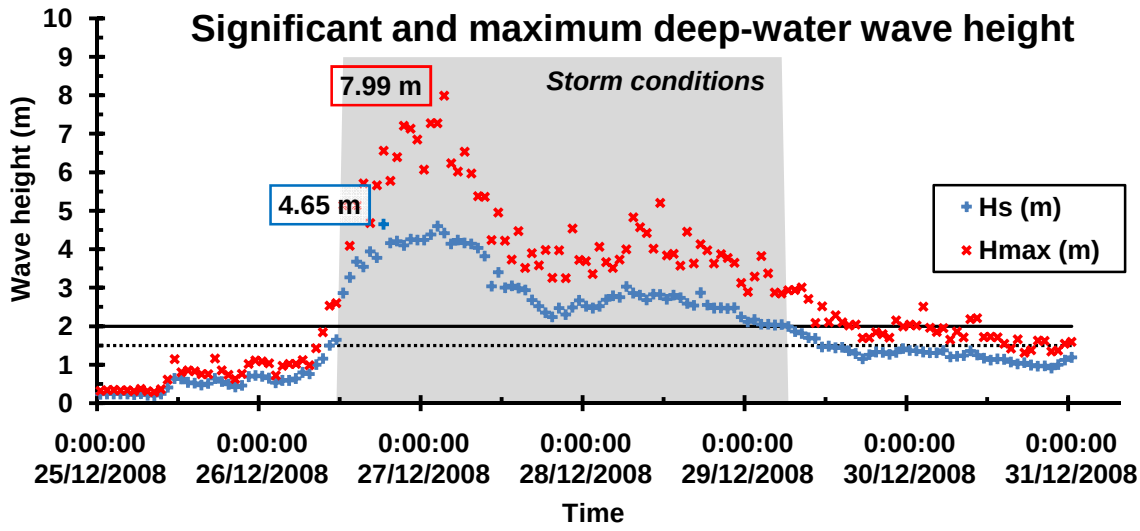

Figure 3.2. Deep-water wave heights during the event.

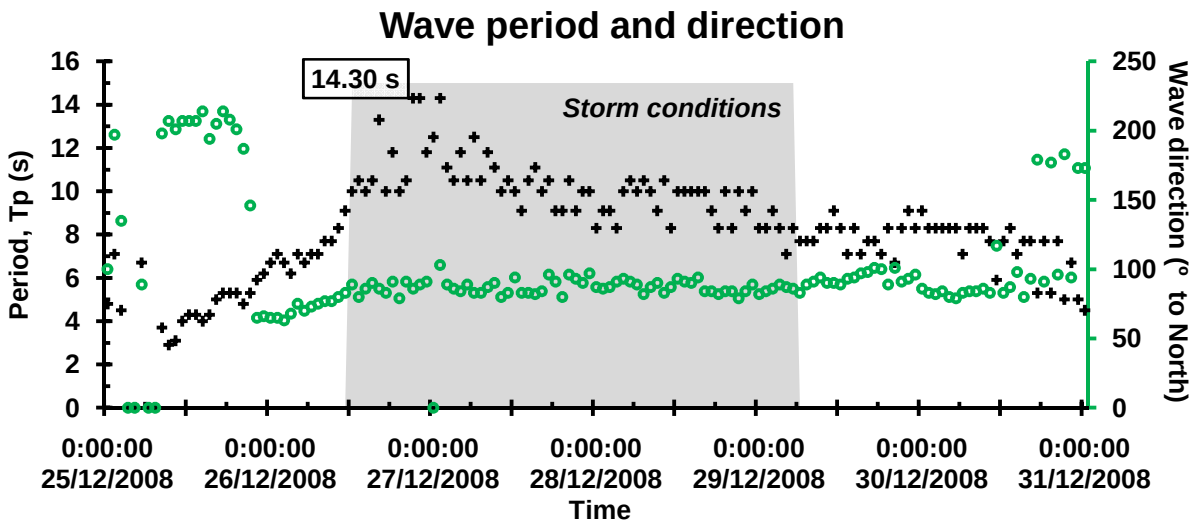

Figure 3.3. Wave period and direction during the event.

Figure 3.3 shows that prior to the storm the waves were coming from the South and the Southwest, with some instability intervals. On Christmas Day they started to veer towards the North and finally the East. This direction prevailed until the first week of January 2009. Table 3.1 displays the distribution of the wave directions during the time when storm conditions were met.

Table 3.1. Distribution of the wave directions during the storm.

Distribution of wave directions	
N	1.5%
NE	0.0%
E	98.5%
SE	0.0%
S	0.0%
SO	0.0%
O	0.0%
NO	0.0%

Mendoza et al. (2011) propose an intensity scale to classify coastal storms in the Catalan sea using their energy content as the main classification criterion. The energy content, which implicitly contains H_s and storm duration, is described as in (Eq. 3.1).

$$E = \int_{t1}^{t2} {H_s}^2 \cdot dt \qquad \text{(Eq. 3.1)}$$

Where t_1 and t_2 are the beginning and end of the event. As wave height values are discrete data, (Eq. 3.1) turns into a sum of $t_2 - t_1$ squared wave heights. For the studied event, the result is

$$E = 2.37 \cdot 10^6 \ m^2 \cdot s = 658 \ m^2 \cdot h \qquad \text{(Eq. 3.2)}$$

The energy flux is then

$$F = \int_{t1}^{t2} {H_s}^2 \cdot Tp \cdot dt = 25.385 \cdot 10^6 \ m^2 \cdot s^2 \qquad \text{(Eq. 3.3)}$$

The class limits proposed by Mendoza et al. are given in Table 3.2.

Table 3.2. Class limits of the storm intensity scale proposed by Mendoza et al. (2011).

CLASS	ENERGY CONTENT (m^2/h)
I	24-250
II	251-500
III	501-700
IV	701-1200
V	>1200

Accordingly, the storm in the study area was a type III event, because:

$$E = 658\ m^2 \cdot h\ \in\ [501\ m^2 \cdot h\ ;700\ m^2 \cdot h\ ] \quad \text{(Eq. 3.4)}$$

Comparing this result with the averaged characteristics of storm classes recorded in Catalonia during the period 1988-2008 (Table 3.3), it is noted that both the mean significant wave height and the event duration were slightly low for this category.

$$D = 66\ h < 77h \quad \text{(Eq. 3.5)}$$

$$\overline{H_s} = 3.08\ m < 4.4m \quad \text{(Eq. 3.6)}$$

Table 3.3. Averaged characteristics of storm classes recorded during the period 1988-2008 in the Catalan sea (Mendoza et al., 2011).

Storm class	H_s max (m)	$T_{p,max}$ (s)	Duration (h)	Energy (m^2h)
I	2.8	9.2	19	110 (24-250)
II	3.5	10.8	52	350 (250-500)
III	4.4	11.6	77	610 (501-700)
IV	5.1	12.1	86	950 (701-1200)
V	6.6	12.6	99	1300 (>1200)

Type III storms are described as “Significant” and sum up to 3% of the total number of storms. They belong to the 6% most destructive events.

The authors of the intensity scale give indicative values of the effects that each type of storm can have on the coast. They are only preliminary and potential values, because the real response depends not only on the storm but also on the geomorphology of the coast. Nonetheless, it is interesting to keep them in mind to compare them with the results of the following chapters of this work. For a type III event hitting a reflective coast, the predicted potential runup is about 3 metres and the beach potential erosion approximately 60-65 m^3/m.

Mendoza et al. classified the storm of Sant Esteve 2008 as a type V event. The discrepancy with the above results is explained by the delimitation of the impact zone. Mendoza et al. classified the storm impacting on the Catalan coast as a whole, and thus used the storm worst-scenario characteristics. As it has been said in the previous section, the study area was not amongst the worst-affected parts of the Catalan coast.

3.3 Water level: Storm surge and astronomical tide

One of the effects of a storm is a general increase of the water level, called storm tide. The storm tide is the combination of two factors, the first of which is the usual water-level variation due to the astronomical tide. The second one is the storm surge, defined as the rise of water generated by the meteorological forcing: intense cyclonic winds moving around the storm pile up the water against the shore. The low pressures associated with intense storms have also an impact on the storm surge, but they represent a small contribution in comparison with the wind impact.

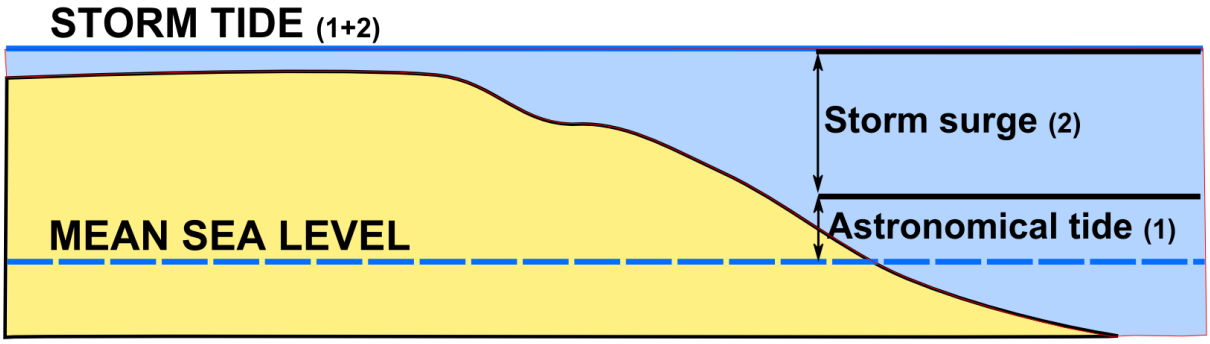

Figure 3.4. Storm tide.

The storm surge depends on factors ranging from changes in the storm intensity to the slope and characteristics of the coastal features. The complexity of the phenomenon makes it very difficult to accurately predict or model and it is preferred to work with measured data when possible.

In the study area there is an observation station recording water levels, but the available data only encompass the period from 2009 to 2012. The data used in this work were recorded by a station located in Barcelona's harbour, about 60 km south. As the storm was substantially weaker in Barcelona, the water level in the study area might be underestimated.

Barcelona's station measured both the storm surge and the astronomical tide hourly during the entire event. The resulting storm tide is the water level above the harbour "zero" level.

The storm tide has to be taken into consideration for the runup and overtopping studies in order to not underestimating them. However, given that in the Mediterranean Sea storm tides are not as destructive as in oceans, the error made using data from Barcelona is supposed to be acceptable.

3.4 Runup and overtopping

Runup is defined as the vertical distance above the still water level that a wave travels up a beach face (Laudier, 2009). It results from two dynamically different processes: (1) maximum setup, $\eta(y)$, the time-averaged water-level elevation resulting from wave breaking, and (2) swash, $S(y,t)$, the time-varying location of the intersection between the ocean and the beach (Stockdon, 2006). Thus, runup depends on the alongshore location y and on the time t.

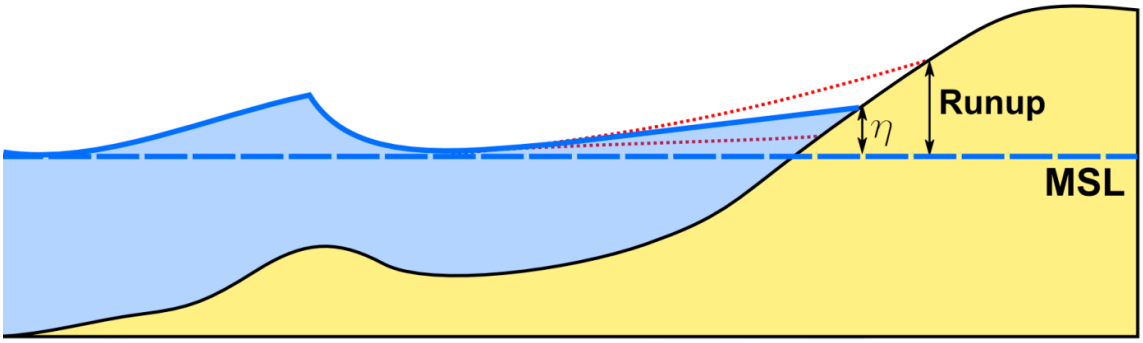

Figure 3.5. Runup.

Many experiments have been conducted to measure and model runup, but the vast majority deal with sloped dikes and seawalls. The studies for natural beaches are fewer and the results vary deeply between them. However, the basis for all the expressions proposed to estimate runup is Hunt's relationship (1959). Hunt characterized runup as a function (Eq. 3.7) of the offshore wave height H_0 and the Iribarren number ξ (Eq. 3.8).

$$R = KH_0\xi \quad \text{(Eq. 3.7)}$$

$$\xi = \frac{\tan\beta}{\sqrt{H_0/L_0}} \quad \text{(Eq. 3.8)}$$

Where β is the slope of the beach profile.

By convention, wave runup is always parameterized in terms of the exceedance of the highest 2% of the wave runup, $R_{2\%}$. Stockdon et al (2006) proposal to represent runup is equation (Eq. 3.9)

$$R_{2\%} = \bar{\eta} + \frac{S}{2} \quad \text{(Eq. 3.9)}$$

Where

$$\bar{\eta} = 0.35\tan\beta\,(L_0H_0)^{1/2} \quad \text{(Eq. 3.10)}$$

$$S = \sqrt{S_{inc}^2 + S_{IG}^2} \quad \text{(Eq. 3.11)}$$

(Eq. 3.10) represents wave setup and (Eq. 3.11) the swash, which has contributions from both incident (Eq. 3.12) and infragravity (Eq. 3.13) waves, which are parameterized as

$$S_{inc} = 0.75\beta(L_0H_0)^{1/2} \quad \text{(Eq. 3.12)}$$

$$S_{IG} = 0.06(L_0H_0)^{1/2} \quad \text{(Eq. 3.13)}$$

(Eq. 3.14) is the resulting expression for the total runup proposed by Stockdon et al.

$$R_{2\%} = 0.35\tan\beta\,(L_0H_0)^{1/2} + \frac{\sqrt{0.75\tan\beta\,(L_0H_0)^{1/2} + 0.06(L_0H_0)^{1/2}}}{2} \quad \text{(Eq. 3.14)}$$

A limitation of this approach is that, as swash is very dependent on the foreshore beach slope, using it for beaches with significant alongshore variable slopes can result in

pronounced errors. This fact is magnified in reflective beaches as Malgrat and S'Abanell, where runup is dominated by incident wave energy (Laudier, 2009). In order to minimize the error it is necessary to divide the beach into sections where the slope can be assumed to have very little variations. This issue will be addressed later in this work.

Another approach to runup estimation is indirectly proposed by Hedges and Reis (1998) in their model for overtopping, which explicitly incorporates runup. The parameterization, modified by Maese et al (2003), is

$$R_{37\%} = \begin{cases} 0.38 + 1.67\xi \; for \; 0 < \xi \leq 2.2 \\ 4.46 - 0.23\xi \; for \; 2.2 < \xi \leq 9.0 \\ 2.51 \; for \; 9.0 < \xi \end{cases} \quad \text{(Eq. 3.15)}$$

Where $R_{37\%}$ is equivalent to $R_{1\%}$ and $R_{1\%} = 1.08R_{2\%}$.

Both runup estimations use the same parameters: wave height (H_0), wave length (L_0) and beach slope ($\tan\beta$). Thus, it is necessary to define the three of them before using the relationships to the beaches of the study area.

The offshore wave height used is $H_0 = H_s$, and the wave length is given by (Eq. 3.16).

$$L_0 = \frac{gT_p^2}{2\pi} \quad \text{(Eq. 3.16)}$$

The remaining parameter, $\tan\beta$, characterizes the beach. Its accurate estimation presents some difficulties because it varies alongshore and with time. Figure 3.6 shows the pre and post storm slopes along the study area. The intersection of the two situations gives the map of average slopes. As runup is very dependent on the slope, it is necessary to take into account the three cases: pre-storm, post-storm and average slopes. The freeboard is also represented, because it is a parameter needed for the overtopping study.

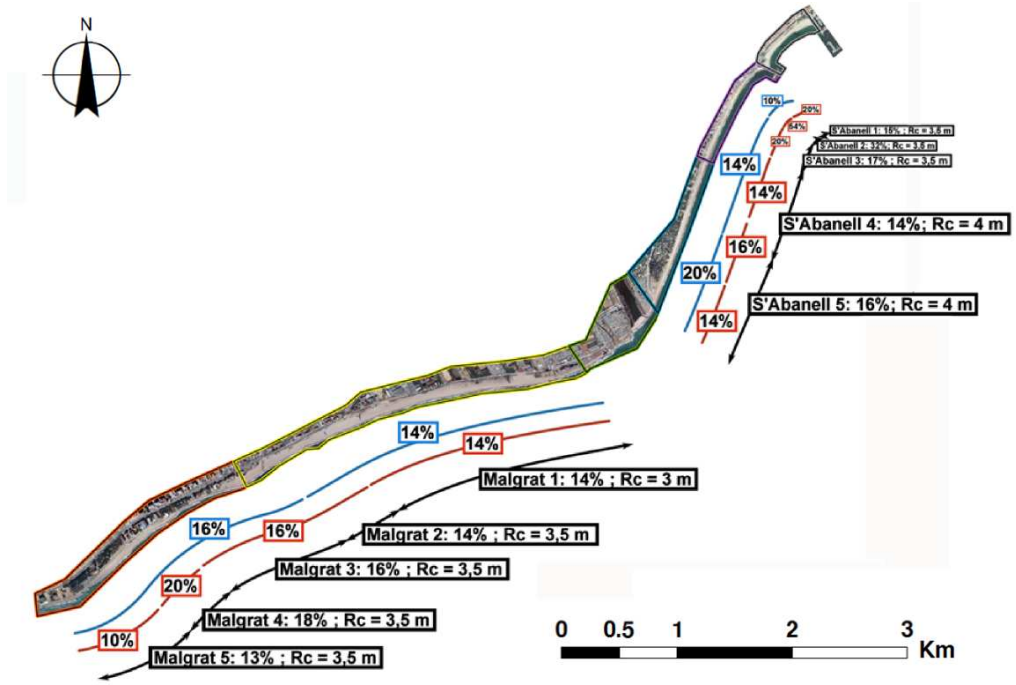

Figure 3.6. Slope and freeboard along the study area. Blue: Pre-storm situation; Red: Post-storm situation; Black: Average.

The data needed to obtain Figure 3.6 have been extracted from the analysis of the LIDAR elevation datasets of the pre and post storm situations (see Chapter 4).

The results show a substantial difference between the runup calculated with Stockdon's expression and the values obtained using the approach of Hedges and Reis. The figures for the entire set study area can be found in Annex 1. The section named Malgrat 4 is given herein as an example:

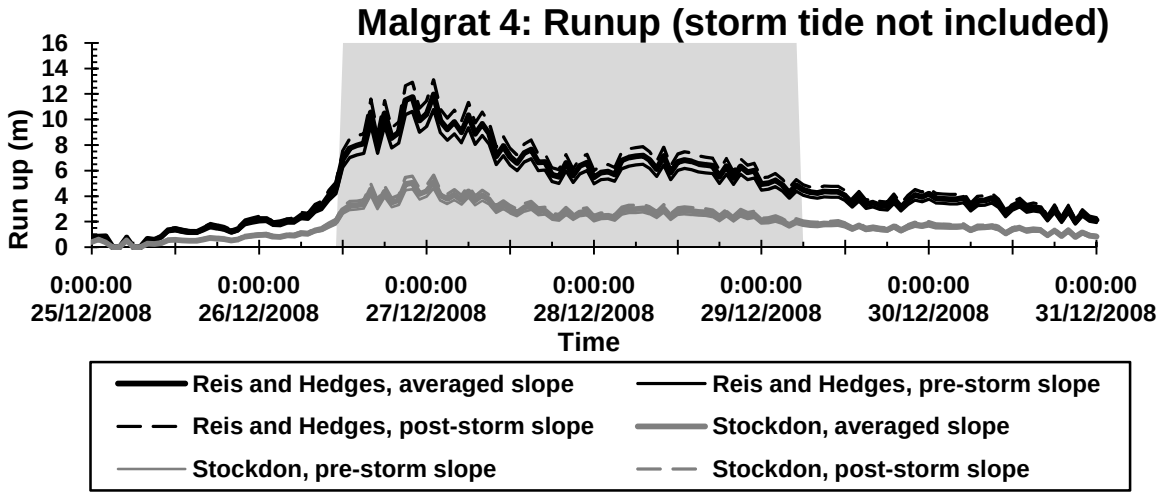

Figure 3.7. Comparison between the runup values in Malgrat 4 calculated with Stockdon's and Reis and Hedges' expressions. The grey area is the duration of the storm. The results do not account for the storm tide.

To understand the meaning of these values and establish whether they are appropriate for the study area it is necessary to study the overtopping. Overtopping occurs when the water elevation is higher that the freeboard of the section. It is a coastal process that has been broadly studied, and there are many empirical, semiempirical and numerical models available to estimate the mean discharge when random waves overtop seawalls. However, and as for the runup, the models for natural beaches are scarce.

Hedges and Reis' (1998) semiempirical model in based on the physical equation for discharge over a weir as analogous to discharge over a berm. This model imposes two conditions aiming towards physical accuracy: 1) wave overtopping is zero when the runup is inferior to the freeboard, and 2) the overtopping discharge remains finite when the freeboard equals zero (Laudier, 2009). The proposed expression for the discharge is (Eq. 3.17).

$$\frac{q}{\sqrt{gR_{max}^3}} = \begin{cases} A\left(1 - \frac{R_c}{\gamma_r R_{max}}\right)^B \; for \; 0 \le \frac{R_c}{\gamma_r R_{max}} < 1 \\ 0 \; for \; \frac{R_c}{\gamma_r R_{max}} \ge 1 \end{cases} \qquad \text{(Eq. 3.17)}$$

The coefficients were obtained through experiments and are given by (Eq. 3.18) and (Eq. 3.19).

$$A = \begin{cases} 0.033 \; for \; 0.05 \le \tan\beta < 0.083 \\ 0.033 + \frac{0.0025}{\tan\beta} \; for \; 0.083 < \tan\beta \le 1 \end{cases} \qquad \text{(Eq. 3.18)}$$

$$B = \begin{cases} 10.2 - \dfrac{0.275}{\tan\beta} \; for \; 0.05 \leq \tan\beta < 0.13 \\ 2.8 + \dfrac{0.65}{\tan\beta} \; for \; 0.13 \; < \tan\beta \leq 1 \end{cases} \qquad \text{(Eq. 3.19)}$$

The freeboard R_c has been obtained from the LIDAR data and corresponds to the maximum elevation of each beach section (details about the beach profiles and the use of the LIDAR elevation data are given in Chapter 3). The maximum elevation is generally the berm height, but in the locations were the beach is very narrow or where the berm is hardly developed R_c has been set to the elevation of the maritime promenade. The freeboard height values are relative to the reference water level used in Spain, the mean water level in Alicante (NMMA).

R_{max} is defined by Reis and Hedges as the maximum runup value for which no overtopping occurs, and its most probable value corresponds to a value not exceeded in 37% of the cases for a Rayleigh distribution of runup for 100 waves, $R_{37\%}$. This value has been calculated previously for the estimate of the runup, but cannot be directly compared to the freeboard R_c to establish when overtopping can occur. To obtain the real height that waves can reach during their uprush, it is necessary to add the levels of the storm tide obtained in Section 3.3 to the runup heights themselves (De Mas, 2010). After doing so, the resulting values of runup have to be transformed to have their origin match the origin of the LIDAR elevation data, which is the NMMA and not Barcelona's harbour zero. *Puertos del Estado* provides the necessary information to do so: all the runup values have to be reduced to -0.179 metres.

The last parameter that appears in the discharge estimation (Eq. 3.17) is γ_r. It is a reduction factor that accounts for non-normal wave incident angle, berm characteristics and permeability. γ_r is generally used to tune the model. It has been found that it over-estimates the overtopping because, as many other models, it is based on experiments obtained on impermeable planar laboratory beaches. Typical values for γ_r range from 0.70 to 0.95. In the rest of this study a standard value of $\gamma_r = 0.90$ is used.

The comparison between the freeboard and the final runup shows when overtopping occurs. Figure 3.8 shows the results for one of the profiles in S'Abanell (average slope). All the other figures can be found in.

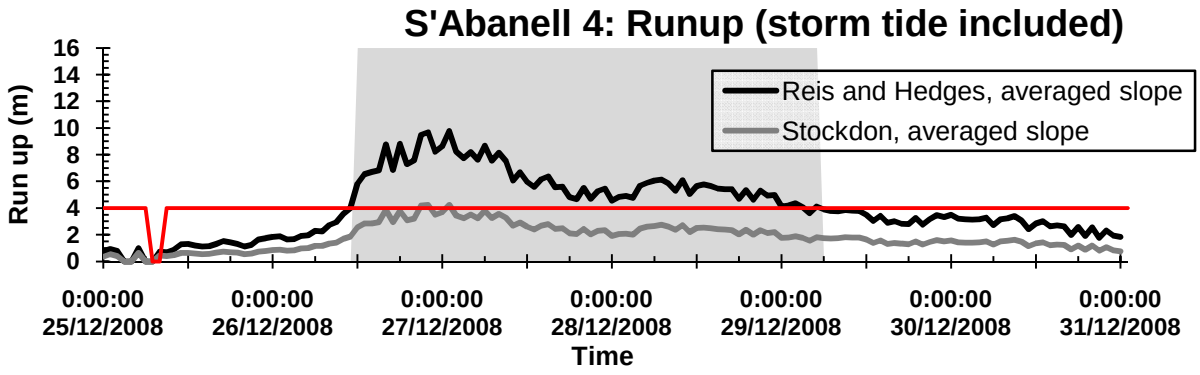

Figure 3.8. Comparison between the runup values in S'Abanell 4 calculated with Stockdon's and Reis and Hedges' expressions. The grey area is the duration of the storm. In this area, the storm did not modify the beach slope.

The differences between Stockdon's and Reis and Hedges' results can now be interpreted. According to Stockdon, runup never exceeded the freeboard for this profile, and thus there

was no overtopping. The situation is very similar in the rest of the profiles, with none or very little overtopping time for Stockdon's values of runup. Nevertheless, according to other studies and to the media, the seafront promenade was destroyed in this particular part of S'Abanell (see Fig. 3.9), and sand was transported to the inland of Blanes. Stockdon's expression systematically underestimates runup values, not only in this study (Laudier, 2009).

Figure 3.9. S'Abanell's promenade destroyed by the storm (Departament de Territori i Sostenibilitat, Generalitat de Catalunya. Press released, 23/12/2009).

In the light of these results it seems more appropriate to use Reis and Hedges' proposal for runup. However, the fact remains that the proposed expressions depend deeply on the beach slope, and the values for the slopes calculated in this study are only a discrete approximation of a continuous variable. In addition, they do not take into consideration the variations of the beach slope during the storm. Therefore, the resulting values have to be taken only as indicative values.

The figures describing the runup situation for each area can be found in Annex 1. Using Reis and Hedges expression the runup values are higher than those expected for a type III event (around 3 metres), a discrepancy partly explained by the fact that Mendoza et al. (2011) employed Stockdon's formulation.

The results show that the runup height exceeded the freeboard in some moment of the storm along the entire study area. The overtopping times are high in most cases, and so are the runup values during the entire storm. Nevertheless, this does not imply that the resulting overtopping was a continuous process, because under random wave conditions overtopping is dominated by a few waves with large runup. As it can be seen on the example on Figure 3.10, this was the case for the studied event.

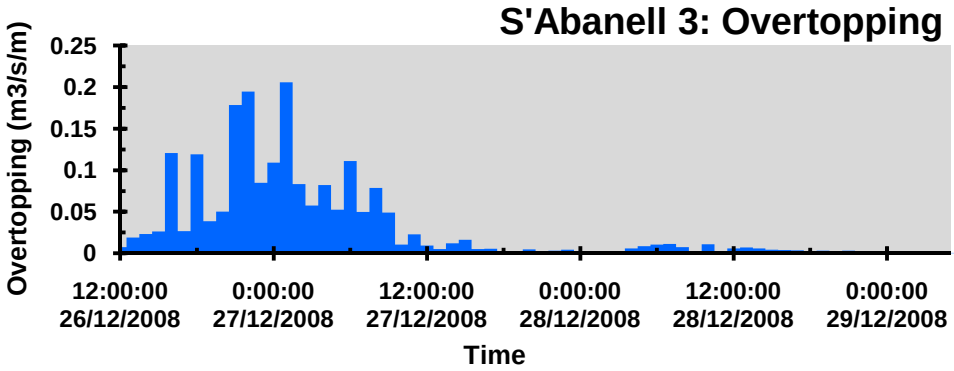

Figure 3.10. Overtopping in S'Abanell 3 according to Reis and Hedges for the duration of the storm and using the averaged beach slope.

Almost all the overtopping occurred between 26th December 2008 at 12:00 a.m. and 27th December 2008 at 12:00 a.m., but the runup values did not drop drastically after this period. The situation was the same in the entire study area. The overtopping took place around the peak runup values, when water level increased suddenly but for a small time lapse.

The total discharge in each zone is calculated by adding all the discrete values of discharge for said zone and multiplying the result by the time step (Eq. 3.20).

$$Q_i\left(\frac{m^3}{m}\right) = \sum q_i\left(\frac{m^3}{s}/m\right) \cdot 3600s \qquad \text{(Eq. 3.20)}$$

This amounts to a total volume of water of:

$$V_i(m^3) = Q_i(m^3/m) \cdot L_i(m) \qquad \text{(Eq. 3.21)}$$

Where L_i is the length of the area. Table 3.4 summarizes the results obtained.

Table 3.4. Overtopping values along the study area. Case of the average beach slope.

	LENGHT (m)	DISCHARGE (m^3/m)	WATER VOLUME (m^3)
S'Abanell 1	100	3256	325635
S'Abanell 2	150	65804	9870623
S'Abanell 3	300	7097	2129151
S'Abanell 4	820	877	718800
S'Abanell 5	970	3863	3747546
Malgrat 1	2120	4372	9268403
Malgrat 2	515	1997	1028630
Malgrat 3	1120	4944	5537577
Malgrat 4	455	9737	4430397
Malgrat 5	910	1117	1016453

The overtopping volumes calculated thusly vary deeply depending on which slope is used, as shown on Table 3.5. The difference is higher for steeper profiles (reaching a x5 factor in some cases). The existing models to estimate runup and overtopping have been mostly developed for gentle-sloping dissipative beaches, and their limitations are very noticeable in steep beaches as the ones of the study area of this work.

Table 3.5. Effects of the variation of the beach slope on the overtopping results.

	Using the pre-storm slope		Using the post-storm slope	
	DISCHARGE (m^3/m)	DIFFERENCE TO AVERAGE SLOPE	DISCHARGE (m^3/m)	DIFFERENCE TO AVERAGE SLOPE
S'Abanell 1	299	-91%	16586	+409 %
S'Abanell 2	299	-99 %	52321	-20 %
S'Abanell 3	1997	-72 %	16586	+134 %
S'Abanell 4	877	0 %	884	+1 %
S'Abanell 5	10205	+16 %	884	-77 %
Malgrat 1	4372	0 %	4397	+1 %
Malgrat 2	1997	0 %	2011	+1 %
Malgrat 3	4944	0 %	4974	+1 %
Malgrat 4	4944	-49 %	16586	+70 %
Malgrat 5	4944	+343 %	302	-73 %

A better estimate of the volumes could be done if the evolution of beach slope during the storm was known. It would then be possible to implement the runup equations in a semi-continuous manner, and therefore determine whether the real overtopping values were closer to the upper or to the lower limits of the range. Obtaining this kind of dynamic topographic information by direct measure is challenging, but it could be modelled using numerical methods. However, for this work it is only the values corresponding to the mean slope that are used. The modelling of the slope evolution and its implementation in the overtopping estimates could be object of further research. The figures describing the overtopping situation for each area can be found in Annex 2.

This section has dealt with runup and overtopping estimation in the beaches of Malgrat and S'Abanell. The area surrounding the mouth of the Tordera and the Bay of Blanes have been left aside from the study because they are not free beaches. A possible extension of this work is the adaptation of the runup and overtopping models to these two special cases, where wave conditions (for the bay) and beach profiles (for the area around the river mouth) suffer transformations for which the original models do not account.

3.5 Wave propagation

The variables that appear in the empirical expressions used in previous sections of this chapter are related to deep-water wave conditions. However, to fully understand the storm characteristics and the variation of its effects on the coast it is essential to know how it impacted the different zones of the study area.

3.5.1 Physical processes

As waves approach the coastline, their velocity, shape, height and direction are modified by the sea bottom bathymetry; only the wave period remains constant. Therefore, the waves that hit S'Abanell during the storm of Sant Esteve 2008 were not the same that the ones that reached Malgrat.

The main processes that modify waves approaching the coast are shoaling, refraction and breaking. To a minor degree (if there are no special obstacles), they are also affected by diffraction, reflexion and energy dissipation due to friction.

Shoaling (Figure 3.11, Left) consists on the gradual variation of wave height and velocity as the water depth decreases. The nearly sinusoidal deep-water profile of the swell is transformed in wave trains with a series of high peaked crests separated by relatively flat troughs (Komar, 1998). The variations are caused by the changes in the group celerity c_g. They can be calculated imposing energy conservation (Eq. 3.22).

$$E_{cn} = \left(\frac{1}{8} p g H^2\right) c \left[\frac{1}{2}\left[1 + \frac{2kh}{\sinh 2kh}\right]\right] = (E_{cn})_0 = constant \qquad \text{(Eq. 3.22)}$$

Using the simplifications of lineal theory a much more operational expression (Eq. 3.23) can be obtained to link shallow waters wave height (H) to deep waters wave height (H_0):

$$H = H_0 \sqrt{\frac{c_{g0}}{c_g}} \quad and \quad \frac{H}{H_0} = K_S = Shoaling\ coefficient \qquad \text{(Eq. 3.23)}$$

Refraction (Figure 3.11, right) is also related to celerity, but in this case it is wave directions that are modified. Wave crests gradually modify their orientation and tend to be as parallel to the bottom bathymetry as possible. This behaviour is due to the celerity gradient inside the wave caused by the water depth differences.

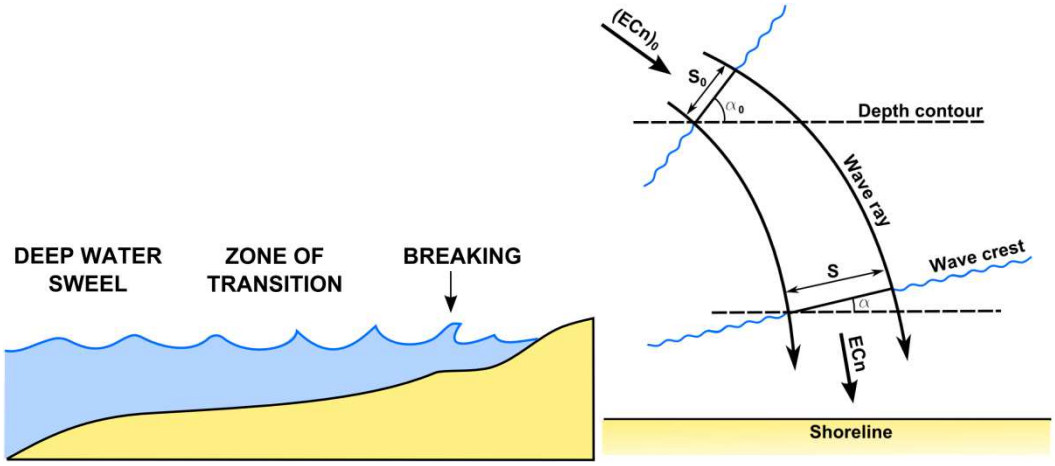

Figure 3.11. Wave shoaling and refraction. Adapted from Komar, 1998.

Wave refraction can be characterized using a refraction partial coefficient:

$$K_r{}' = \sqrt{\frac{s_0}{s}} \qquad \text{(Eq. 3.24)}$$

For an idealized linear beach geometry and parallel bathymetry, the distances can be calculated using Snell's Law and the relation:

$$\frac{s_0}{s} = \frac{\cos\alpha_0}{\cos\alpha} \qquad \text{(Eq. 3.25)}$$

Shoaling and refraction are usually studied together and represented by a unique coefficient, the total refraction coefficient K_r (Eq. 3.26).

$$K_r = K_S K_r = \sqrt{\frac{c_{g0}}{c_g}}\sqrt{\frac{s_0}{s}} \qquad \text{(Eq. 3.26)}$$

Lastly, **wave breaking** depends primarily on the ratio between wave height and wave length. Breaking can be predicted using the following empirical expression:

$$\frac{H_b}{L_b} = 0.142\tanh\left(\frac{2\pi h_b}{L_b}\right) \qquad \text{(Eq. 3.27)}$$

This general expression can be simplified for deep-water conditions and for shallow-water conditions. However, it does not take into account that beach characteristics also affect the breaking of the wave.

Evaluating the processes described in this section is a challenging task when the bathymetry and wave characteristics are real data and not a simplification to an ideal situation. Their correct estimation requires the use of calibrated wave propagation models that take all the variables into account.

3.5.2 Wave propagation modelling

The modelling software used in this work is Mike 21, by DHI. Mike 21 has been chosen because it is a very robust simulation tool widely used in coastal sciences, but at the same time simple and which does not require much input data. The two kinds of input data needed in order to run a basic wave propagation simulation on Mike 21 are bathymetric data and wave characteristics in deep water conditions.

The bathymetry for this work (Figure 3.12) has been obtained combining various datasets covering different parts of the study area. It dates from 2010, but can be used because sediment transport along the coast modifies the bathymetry only in a narrow buffer zone around the shoreline.

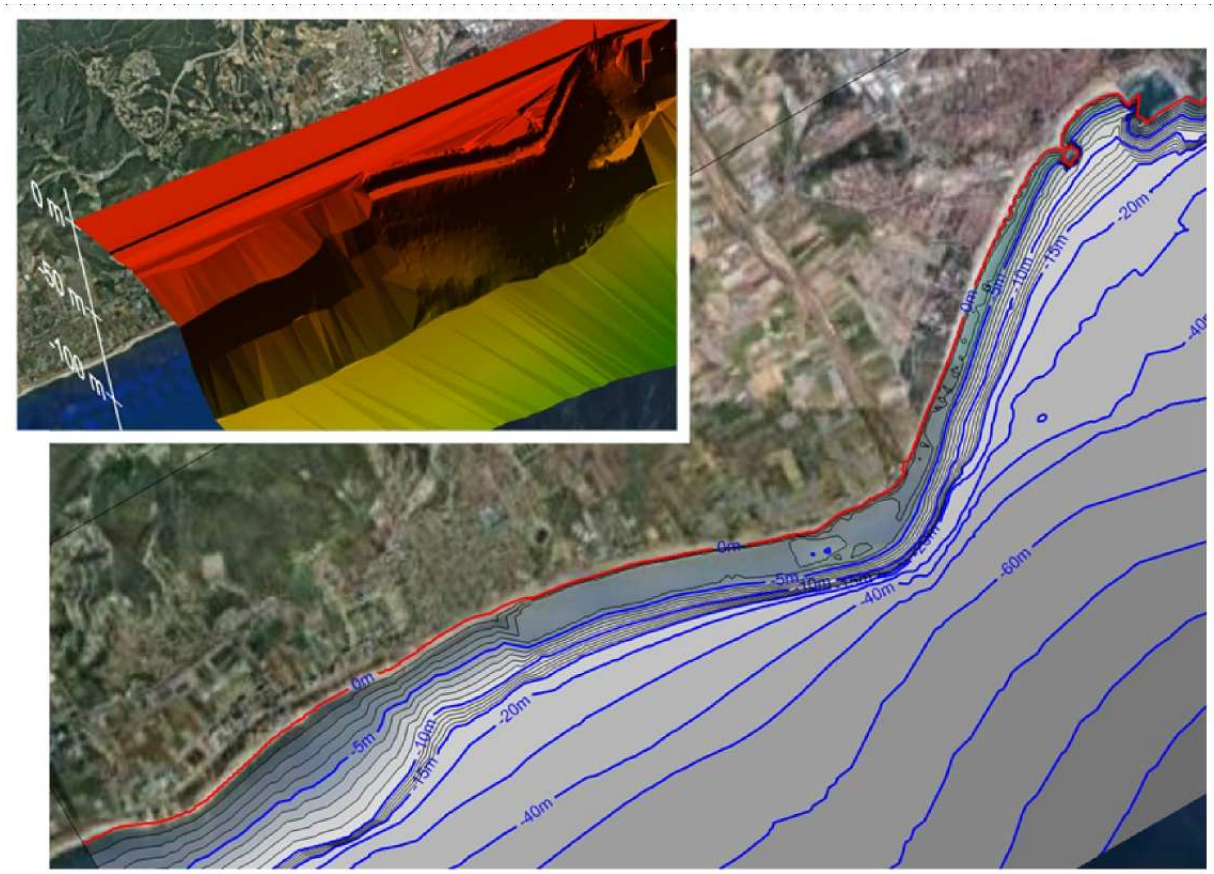

Figure 3.12. Bathymetry of the study area.

As shown on Figure 3.12, the resolution of the bathymetry around the river mouth is higher than in the southern part of Malgrat. This fact explains the sudden change on the contour levels that takes place in front of the town of Malgrat: the underwater slope is constant on the south, while the north there is a flat sea bottom stretch at approximately 5 metres of depth.

Mike 21 runs one wave simulation at a time, using a unique representative deep-water wave. For this reason, the storm characteristics given by the hourly wave data have been transformed into a simplified storm defined by six significant points (Figure 3.13 and Table 3.6).

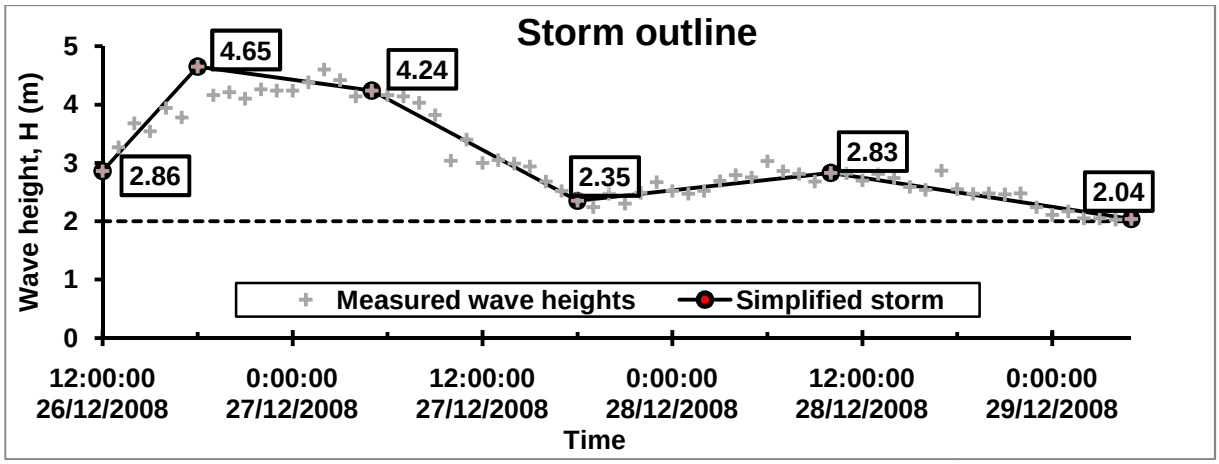

Figure 3.13. Storm outline and wave characteristics at the vertices.

Table 3.6. Storm outline and wave characteristics at the vertices.

DATE	TIME	SIGNIFICANT WAVE HEIGHT, H_{m0} (m)	WAVE DIRECTION (ºN)	PEAK PERIOD, T_p (s)	MEAN PERIOD, T_m(s)
26/12/2012	12:00:00	2.86	89	10.0	6.9
26/12/2012	18:00:00	4.65	91	11.8	8.0
27/12/2012	05:00:00	4.24	89	10.5	7.5
27/12/2012	18:00:00	2.35	91	9.1	6.1
28/12/2012	10:00:00	2.83	83	10.5	6.2
29/12/2012	05:00:00	2.04	86	8.3	6.1

The simulations were made twice: a first time using peak periods and a second time using mean periods. The output data files were converted and transferred to SURFER 9 for data processing.

3.5.3 Results

Figure 3.14 shows an example of the graphical results of the simulation corresponding to the wave heights at the peak of the storm.

Figure 3.14. Propagated wave heights at the peak of the storm (26/12/2012, 18:00) using the mean period.

The initial wave heights were unevenly modified by the bathymetry. The lines representing wave elevations are much tighter against the shoreline in S'Abanell than in Malgrat. The initial wave directions were also modified unevenly, resulting in varying incidence angles when the waves hit the coast. In S'Abanell the waves were practically left unchanged (in terms of direction), while in Malgrat there was a general reorientation.

The observed behaviour is the same for the six moments studied; it is only the intensity of the processes that varies. This is consistent with the physical processes described in section 3.5.1. Shoaling and wave breaking could be similar north and south of the river mouth, but refraction is different. The waves, which come from the East, suffer great changes on their way to Malgrat because the coast and bathymetry orientation has an angle of 55-850 to North. On their way to S'Abanell, refraction is not very pronounced.

Peak periods are always significantly higher than mean periods, and this increase (of around 40-50%) affects the results of the simulation. An example of the divergence of the results is shown on Figure 3.15:

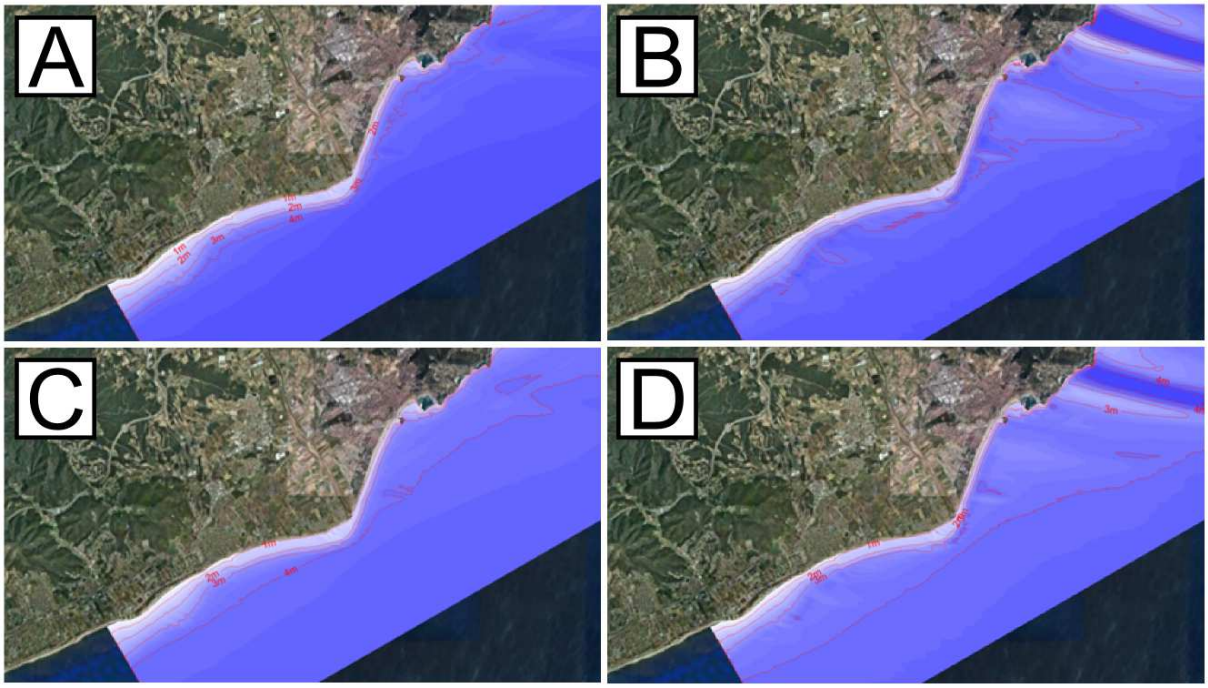

Figure 3.15. Propagated wave heights using mean periods (left) and peak periods (right). Results corresponding to 26/12/2012 at 18:00 (top) and to 27/12/2012 at 05:00 (bottom).

Wave heights modelled using peak periods seem to be much more dependent on the irregularities of the bathymetry than the ones obtained using mean periods. The effects of Blanes Canyon (at the northeast of the study area) are clearly visible.

The results show that the storm characteristics north and south of the river mouth were quite different. However, the variability exists also along each of the two zones. Figure 3.16 shows the position of three transects cast parallel to the shoreline and the significant wave heights and water depths along them.

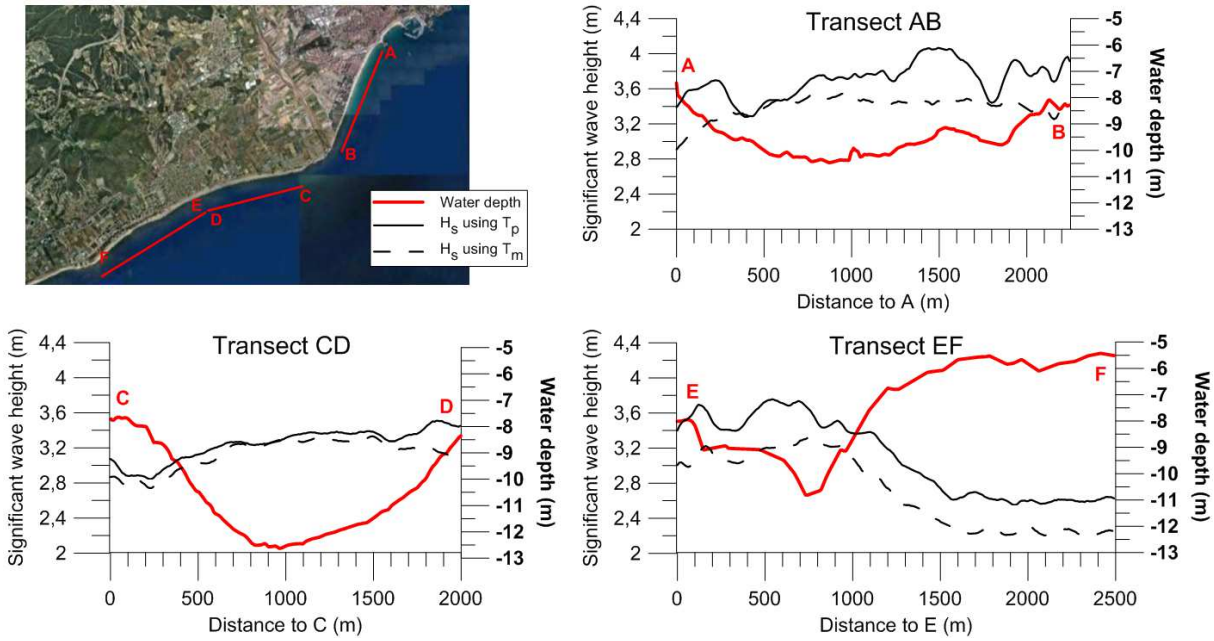

Figure 3.16. Wave height variations along the coast (27/12/2008, 05:00 a.m.).

In S'Abanell (transect AB), the waves in front of the central part of the beach were higher than at both ends. There is a depression of the sea bottom towards the centre of the beach, with depths ranging from 7-8 metres in the extremes to 10-11 metres in the middle. In this northern side of the river mouth, the variations linked to the election of the wave period are quite important: waves heights differ by 0.5 metres in some places.

The two transects cast parallel to the beach of Malgrat (CD and EF) show that the bathymetry is much more irregular than in S'Abanell. However, the irregularities are partly explained by the fact that transects are rectilinear, while the shoreline has changing orientations. The results do not depend on the wave period used as much as in the previous case, and they seem less affected by slight bathymetry variations.

3.6 Expected beach response

Before the analysis of the measured beach changes induced by the storm, it is interesting to describe the morphological response that could be expected from the beach.

During storms, the prevailing process is erosion of the beach profile (Figure 3.17, left). The storm boosts the beach evolution from its summer profile, characterized by a wide and smooth berm, towards a winter profile with and eroded berm. The eroded material is then usually deposited in an underwater bar parallel to the shoreline.

However, the high runup and overtopping values obtained in the previous section may have produce overwash (Figure 3.17, right). If this was the case, then not all the eroded sand was transported to the bar; a fraction was deposited in the backshore.

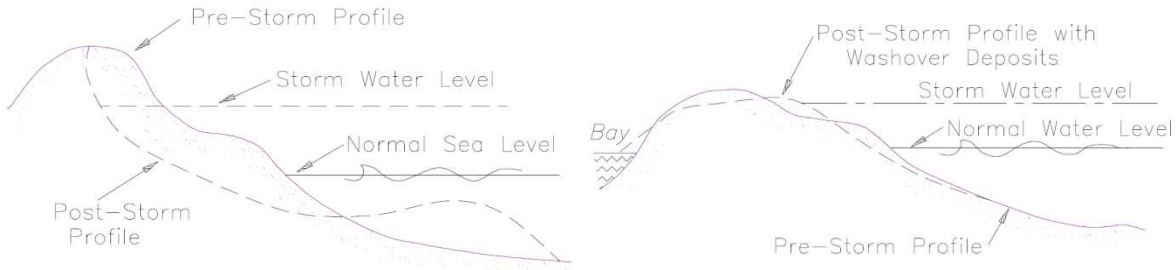

Figure 3.17. Expected beach response to storms: Left: Erosion. Right: Overwash. Coastal Engineering Manual, 1998.

The two previous processes are driven by shore-normal sediment transport, which is the dominant transport mechanism during storms. However, the oblique angle with which the waves reached the beaches of Malgrat could have cause important longshore sediment transport.

Chapter 4

LIDAR-BASED ANALYSIS OF THE COAST MORPHOLOGICAL EVOLUTION

4.1 Available datasets and methodology

The data used in this chapter has been provided by the Institut Cartogràfic de Catalunya (ICC). There are two kinds of data:

LIDAR elevation data from three different surveys:

- October 2008, representative of the pre-storm situation
- January 2009, representative of the post-storm situation
- August 2009, which shows the recovery after the storm

Ortophotos: Aerial photographs geometrically corrected.

- May 2008, pre-storm situation
- January 2009, post-storm situation
- June 2009, recovery after the storm

Even though the aerial photographs were not taken at exactly the same time as the LIDAR surveys were made, they have been used to provide spatial references to the viewer. In addition, they have been superposed to the LIDAR data to establish the buffer zone around the beach in where the storm-induced changes were registered, thus reducing the study area. As a result it has not been necessary to work with the complete aerial photographs, making the manipulation of the data a much easier and faster process.

The data processing has been made using ArcGIS 9.3. The first step was to “clean” the LIDAR elevation data eliminating the parts corresponding to the sea and interpolating the missing values. Once the elevation dataset was consistent, the sediment balance was obtained calculating the elevation difference between two consecutive elevation layers. In addition, shore-normal beach profiles spaced every 100-200 metres alongshore were cast on the three datasets. These profiles are used throughout this work, from the runup and overtopping studies (Chapter 3) to the erosion modelling (Chapter 5).

The sediment balances, shore-normal profiles and ortophotos have been analysed jointly to draw a picture of the storm-induced changes on the beaches of the study area. This comprehensive approach has made it possible to establish the areas where the behaviour of the beach can be considered homogeneous.

However, it is of utmost importance to keep in mind that this part of the study describes exclusively the behaviour of the emerged part of the beach, because the topographic LIDAR data does not provide information about the submerged areas. Complementary studies are carried out in subsequent chapters to overcome this limitation.

4.2. Morphological response to the storm

This section compares the situation existing before the storm of Sant Esteve 2008 with the one just after it. The LIDAR data used are from the surveys of October 2008 and January 2009. For all the figures, sediment loss is represented in red and sediment gain in blue.

4.2.1. Global response and homogeneous areas

Even where the storm characteristics can be considered homogeneous, within the storm-impact zone some areas may experience severe dune erosion and overwash while adjacent areas may appear unaffected (Stockdon et al., 2007). Amongst the many factors that may affect shoreline response there are shelf geology, shoreline morphology, and variations on the angle between the incident waves and the orientation of the shoreline.

Figure 4.1 shows the impact of the storm on the study area in terms of elevation difference. Figure 4.2 simplifies the results by splitting them in only two categories: erosion areas and accretion areas.

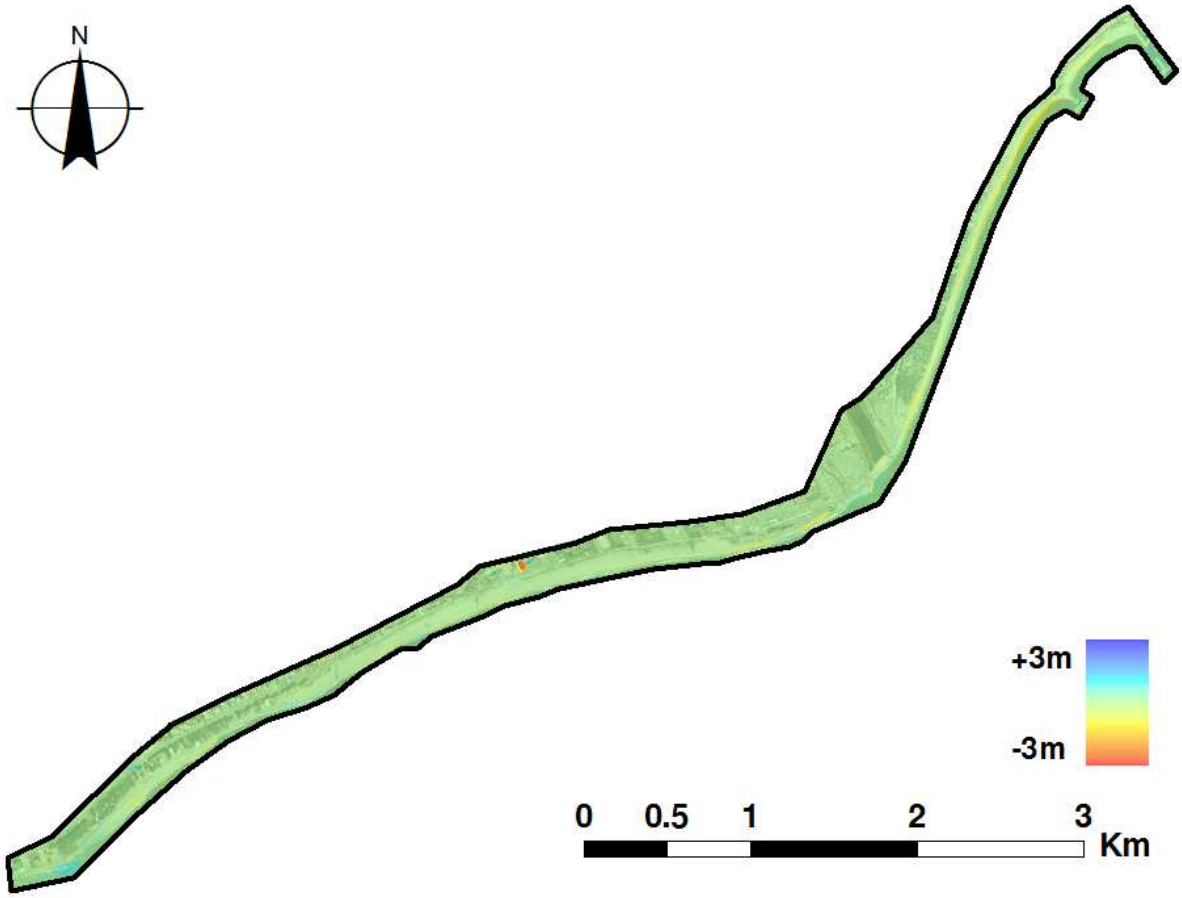

Figure 4.1. Morphological response to the storm: Elevation difference between the pre-storm and post- storm situations.

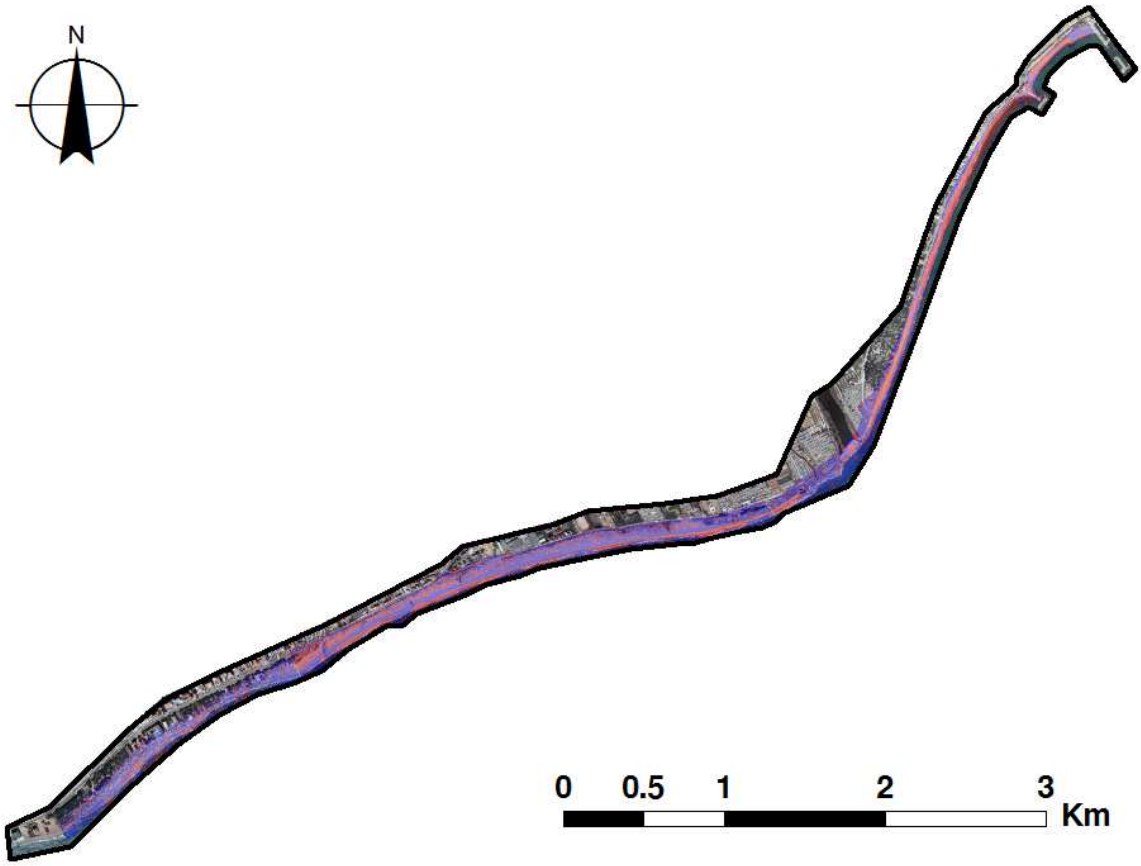

Figure 4.2. Morphological response to the storm: Areas of erosion (red) and accretion (blue).

A deeper analysis of these views and the shore-normal profiles (provided later for each zone), allows identifying six areas where the beach response to the event was quite homogeneous (Figure 4.3).

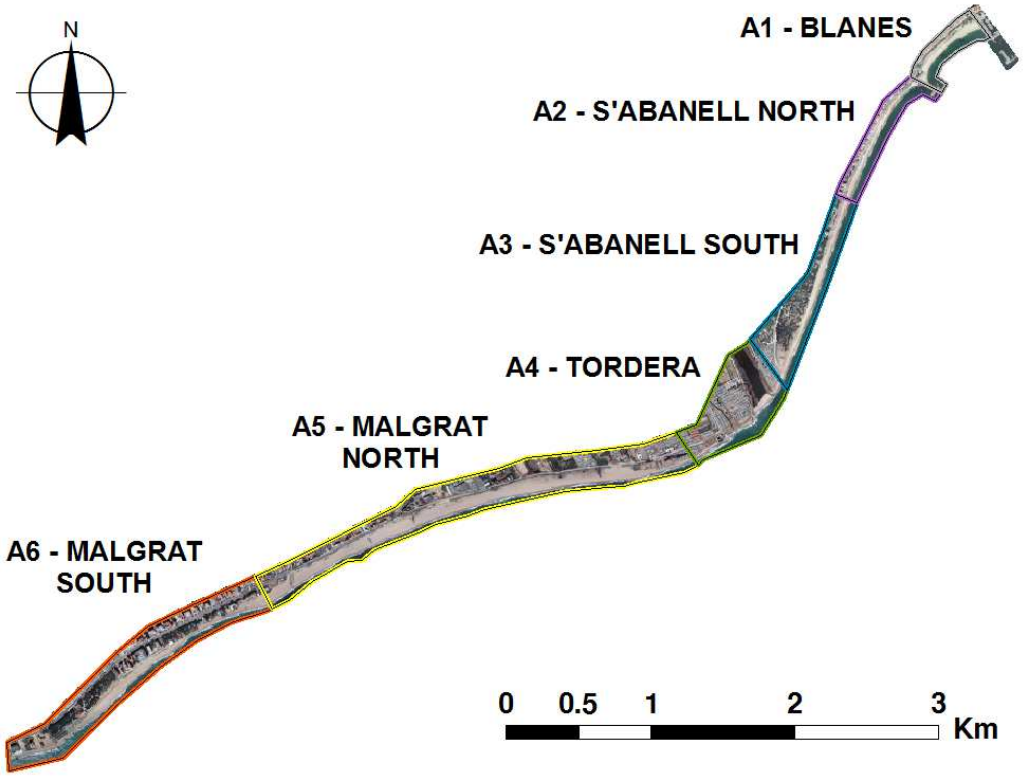

Figure 4.3. Areas of homogeneous response to the storm.

The first area is the pocket beach of the Bay of Blanes. The response of pocket beaches to deep-water wave conditions is different from the response of open ones and hence the bay has to be treated separately from the rest of the study area. In the same manner, the area surrounding the mouth of the Tordera is also a distinct area because its evolution depends partly on the river dynamics. The division of the beach of S'Abanell roughly corresponds to the limits of the village, but the delimitation has been established using the beach profiles. The same goes for Malgrat de Mar.

This division could be improved by subdividing it in even more areas, but the proposed solution is convenient to the goal of this study, which is to determine the storm-induced changes in the area. A more detailed partition that would allow studying local morphodynamic processes originated by irregularities could be the object of future research.

4.2.2. Area 1: Blanes

The first area is the Bay of Blanes. Nestled between the harbour at the north and the headland of Sa Palomera at the south, the beach is 600 metres long and divided in 1/3 and 2/3 by a small rock groyne. The beach is mainly touristic, and backed by a maritime promenade. There is a small park area at the north, and at the south a construction in the sand.

Figure 4.4 shows that the response of the beach to the storm of Sant Esteve 2008 was not homogeneous: erosion occurred at the centre of the beach, whereas the north and south ends were subject to accretion. The maritime promenade was not destroyed by the extreme wave conditions.

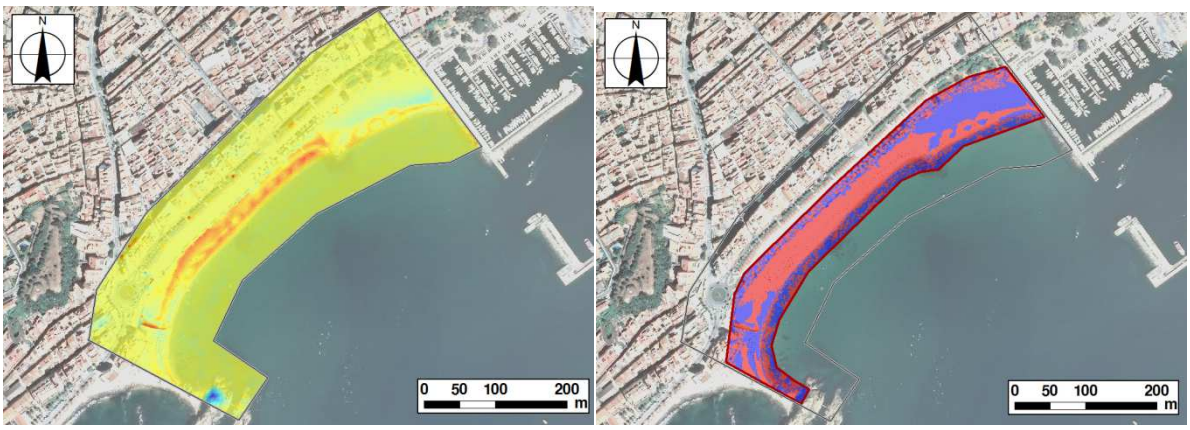

Figure 4.4. Area 1: Left: elevation difference between pre-storm and post-storm situations. Right: areas of erosion (red) and accretion (red).

Table 4.1. Area 1: Volumetric sediment balance.

	VOLUMETRIC SEDIMENT BALANCE	**-5580 m³**
A1	Gain	4372 m³
	Loss	-9952 m³

As it has been said, this area is treated as a unit because its behaviour cannot be compared to the behaviour of an open beach. However, the volumetric sediment balance on Table 4.1 suggests that the global sediment loss caused by the storm in the central area was not compensated by the gain of material in both ends. The sub-division of the area in three sub-areas (Figure 4.5) reinforces this observation.

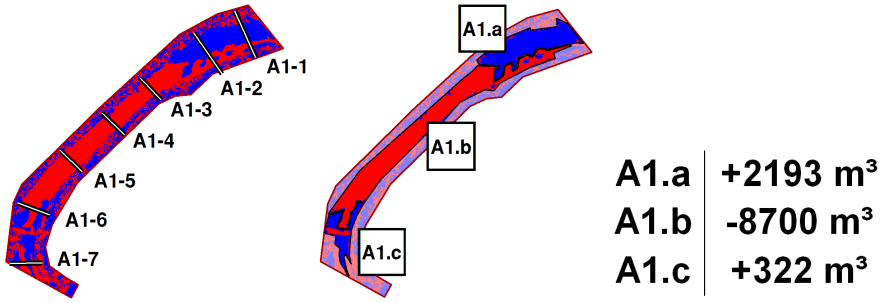

Figure 4.5. Area 1: Sub-areas and location of the shore-normal beach profiles.

The small erosion spot on sub-area A1.c is caused by a drain, a local disturbance quite frequent all along the study area and not directly related to the storm itself.

The cross-sections made and the resulting emerged beach profiles before and after the storm (Figure 4.6) add complementary information: the shoreline at both ends of the beach was almost left unchanged, and the accretion corresponds to sand deposits located on the backshore. This overwash material is most visible at the northern end of the area, where the beach is wider.

The data shows no accretion on the promenade and beyond. Nevertheless, according to local experience, media coverage and photographic archives, the waves reached the promenade and left it buried under a layer of sand. This inconsistency might be caused by the time lapse between the storm and the post-storm LIDAR surveys. The post-storm survey took place three weeks after the event, a period short enough to overlook many natural recovery processes but not human activities. By the time the LIDAR measures were made, the promenade had been restored to normal conditions by the municipality.

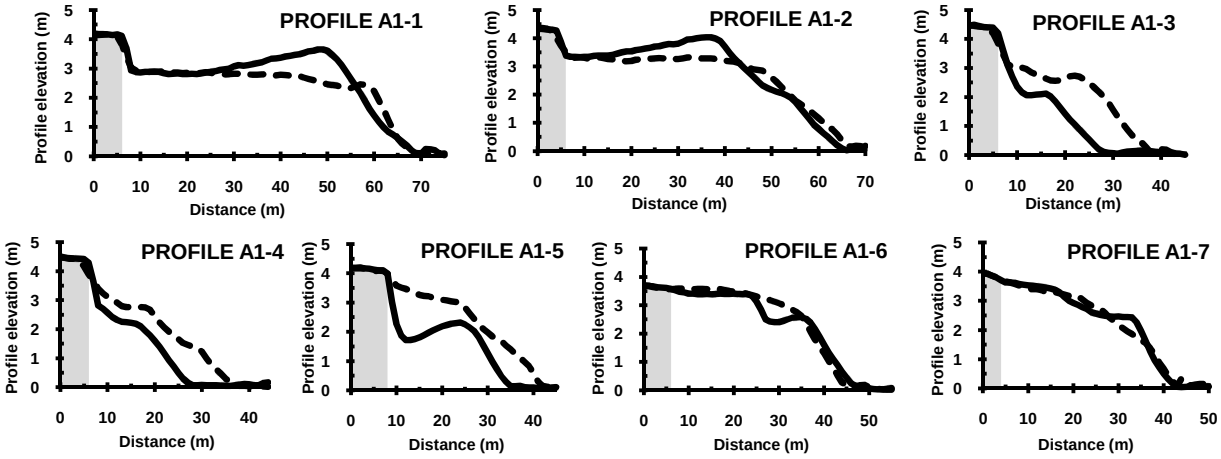

Figure 4.6. Area 1: Shore-normal beach profiles (dashed line = pre-storm; continuous line = post-storm). The grey area represents the location of the maritime promenade.

Without additional information, at this point it is not possible to establish if the lost sand from the central area remained in the bay or was lost off-shore. Bathymetric information would allow estimating the amount of sediment that was deposited in the submerged part of the beach, and consequently the amounts of sand that leaved the bay.

The erosion models used later in this work (Chapter 5) cannot be accurately applied to this area, because they are two dimensional models which do not account for strong alongshore processes that may occur in pocket beaches. However, and taking into consideration that the

Bay of Blanes was not artificially nourished after the event, the analysis of the LIDAR elevation data of summer 2009 could allow coming to some additional conclusions.

4.2.3. Area 2: S'Abanell North

In the case of S'Abanell the aerial photograph can lead to confusion, because it does not show the artificial beach nourishment that took place before the pre-storm lidar flight. The beach has been divided into two areas. In the northern part (Area 2) the beach profile was markedly modified by the storm, while in the south (Area 3) the changes were less significant. From north to south, the division roughly corresponds to the place where the town of Blanes ends and the camping sites and forest start.

Figure 4.7 shows the storm-induced changes in Area 2.

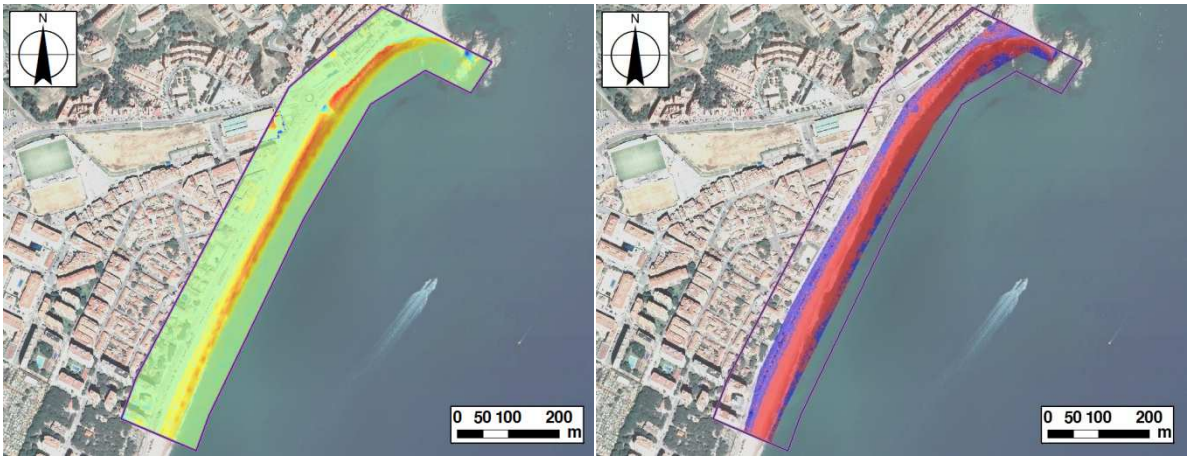

Figure 4.7. Area 2: Left: elevation difference between pre-storm and post-storm situations. Right: areas of erosion (red) and accretion (red).

Table 4.2. Area 2: Volumetric sediment balance.

	VOLUMETRIC SEDIMENT BALANCE	**-46603 m³**
A2	Gain	1709 m³
	Loss	-48313 m³

There was a general sediment loss in the entire area. The material of the artificial nourishment corresponding to the emerged part of the beach was lost almost entirely. The nourishment took place before summer 2008 in order to obtain a beach wide enough to meet the conditions for a touristic and recreational use. It cost 1.2 million euro and covered the northernmost 700 metres of S'Abanell. 165000 m^3 of sand were used, but by the time that the storm struck some of the sediment had already been lost. An average storm which struck the beach in May 2008 took around 10-15% of the sediment.

The results of the volumetric balance (Table 4.2) allow establishing that the general erosion rate for the entire area was about 53 m^3/m. However, the analysis of the shore-normal profiles (Figure 4.8) strongly suggests that the erosion rate was not constant along the area. The profiles show that the erosion was more intense in the north, and decreased towards the south. The southernmost profiles, where the beach berm was the least developed, were notably less eroded. The original beach width decreased from north to south, and this variation could account for part of the observed irregular sediment loss.

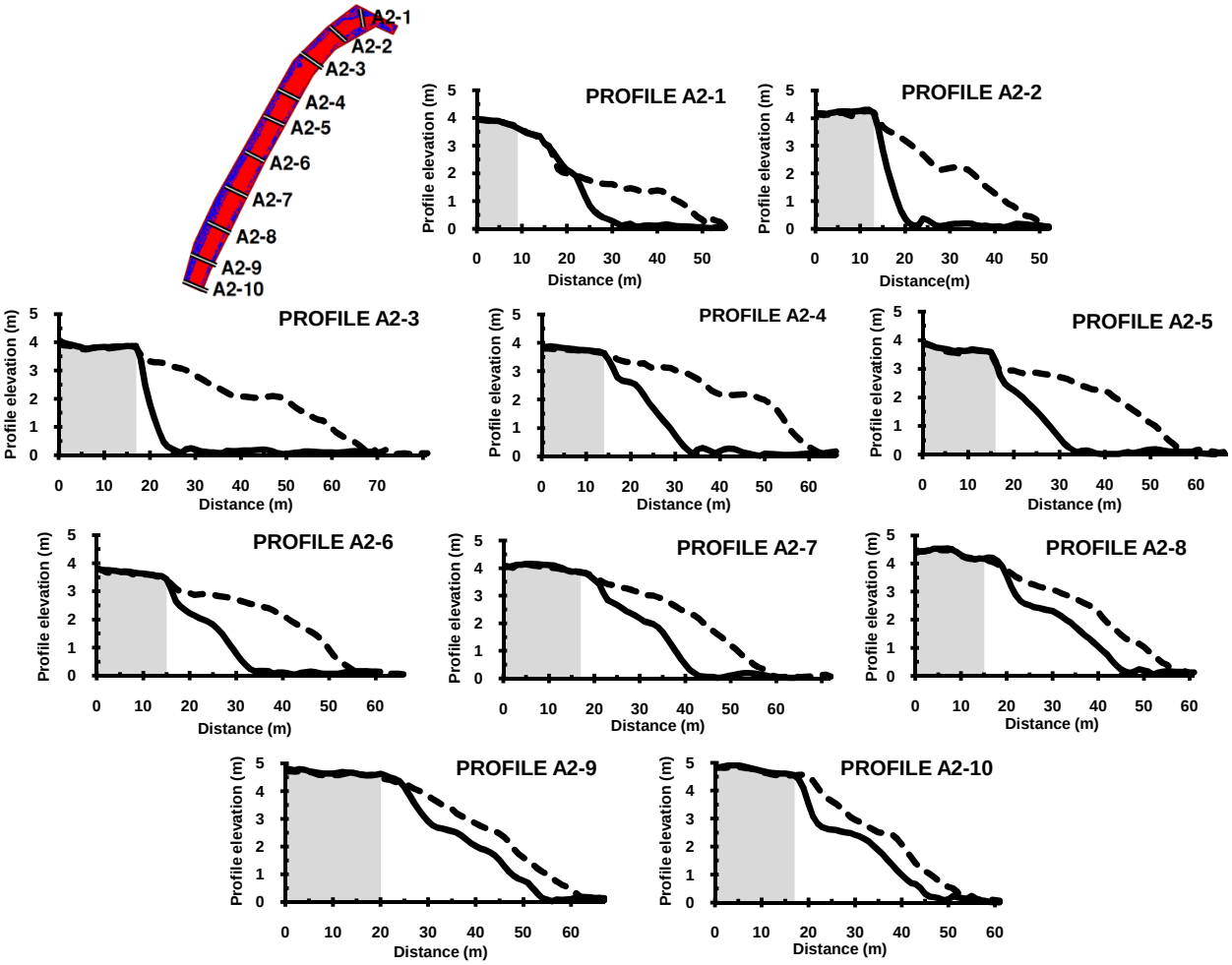

Figure 4.8. Area 2: Shore-normal beach profiles (dashed line = pre-storm; continuous line = post-storm). The grey area represents the location of the maritime promenade.

The measured sediment gain was about only 5% of the sediment loss and was located in the part closest to the village. However, the accretion values may be underestimated for the same reason than in the Bay of Blanes. If the storm transported overwash material to the promenade and the streets, it had surely been cleaned up and moved back to the beach by the time the LIDAR survey took place. Therefore, no accurate estimate can be made about the gain on the backshore, which was clearly smaller than the erosion rate.

The observations of this section concern exclusively the emerged part of the profile, because there is no bathymetric data available. In order to complement these results and fully analyse the storm-induced changes in S'Abanell and their origin, Chapter 5 will deal with the modelling of the beach response.

4.2.4. Area 3: S'Abanell South

As explained in the previous section, Area 3 corresponds to the southern part of the beach of S'Abanell.

Figure 4.9 shows that the response of this area to the storm was qualitatively the same than in the previous one: erosion occurred along the entire beach. However, the sedimentary balance (Table 4.3) suggests that the sediment volumes involved in the process in the south of S'Abanell were much smaller than in the north.

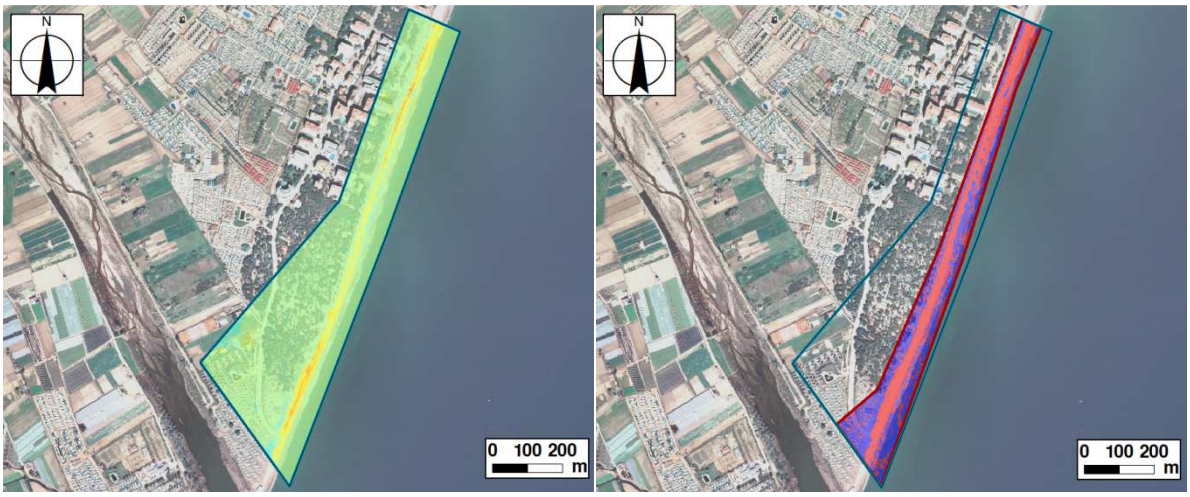

Figure 4.9. Area 3: Left: elevation difference between pre-storm and post-storm situations. Right: areas of erosion (red) and accretion (red).

Table 4.3. Area 3: Volumetric sediment balance.

	VOLUMETRIC SEDIMENT BALANCE	**-19319 m³**
A3	Gain	4990 m³
	Loss	-24310 m³

The general erosion rate for the entire area was approximately 20 m^3/m. In this case, the shore-normal beach profiles cast along the beach (Figure 4.10) reflect that this rate was much more constant than in S'Abanell North. They also show that in the north of the area the promenade was reached and destroyed by the waves. The southernmost end of S'Abanell, where the beach is wider, seems to have undergone more intense erosion.

As for the previous area, in order to explain the behaviour of S'Abanell South properly and account for the changes in the submerged part of the beach, its response to the storm is modelled in Chapter 5. The combination of the LIDAR-based observations and modelled response are then analysed jointly in Chapter 6.

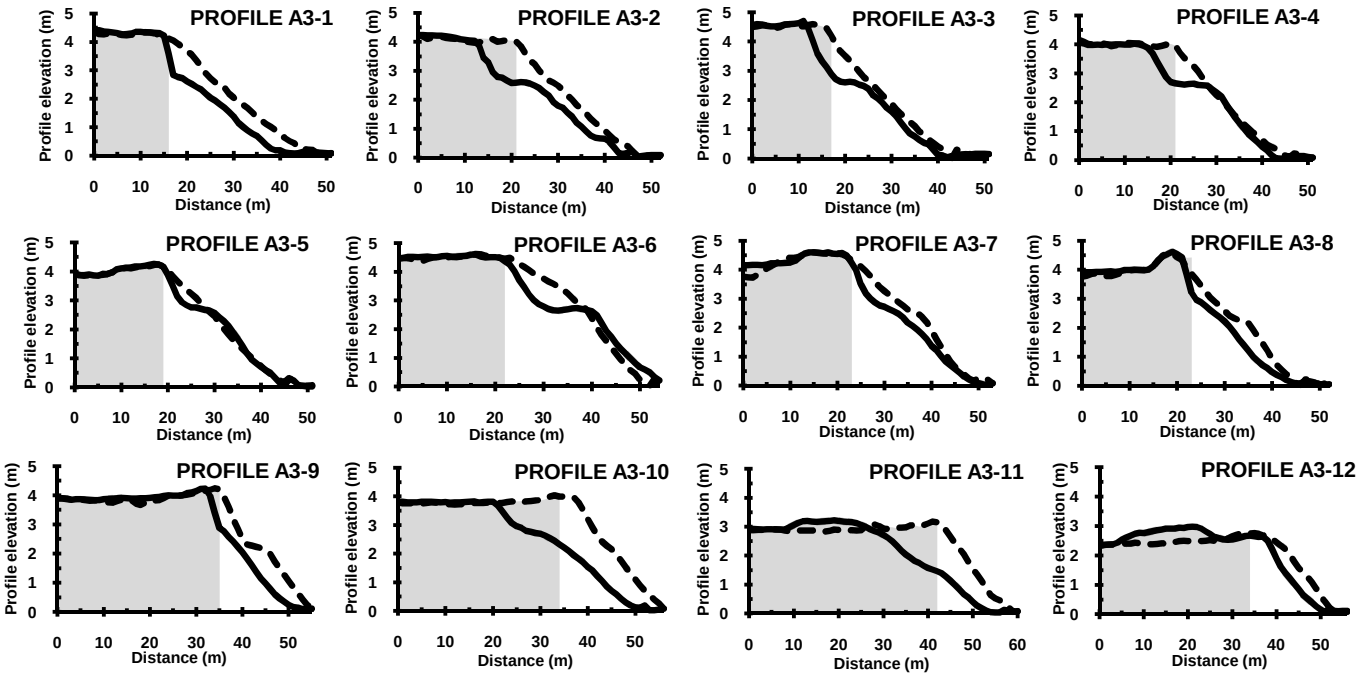

Figure 4.10. Area 3: Shore-normal beach profiles (dashed line = pre-storm; continuous= post-storm). The grey area represents the location of the maritime promenade for profiles A3-1 to A3-8, and the location of the fences bordering the camping sites for the rest.

The accretion in Area 3 is once again located at the inner part of the beach. For the same reasons than in the previous areas, LIDAR data do not reflect sand deposits in the profiles A3-1 to A3-5. The measured profiles A3-6 to A3-9 are also to be handled with care, because the LIDAR elevation data corresponding to the backshore might be inaccurate due to the presence of trees. The southernmost profiles (A3-10 to A3-12) are located in the stretch of beach closest to the river mouth and backed by camping sites. Extensive but low sand deposits are visible in these last profiles, possible because camping sites are bare sandy areas that cannot be restored back to normal as fast as the town streets.

A sub-area drawn around these last profiles allows making an estimate of the reach of the accretion. Figure 4.11 shows that the total sediment gain was about 1218 m^3, which represents an accretion rate on the backshore of 6 m^3/m. This rate is significantly lower than the erosion rate, suggesting that not all the eroded sediment was moved landward.

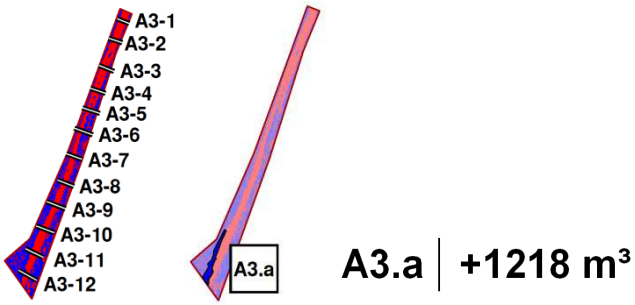

Figure 4.11. Area 3: Sub area with measurable accretion and location of the shore-normal beach profiles.

4.2.5. Area 4: Tordera

Figure 4.12 shows the difference between the pre and post storm situations at the mouth of the river Tordera and in its surrounding area.

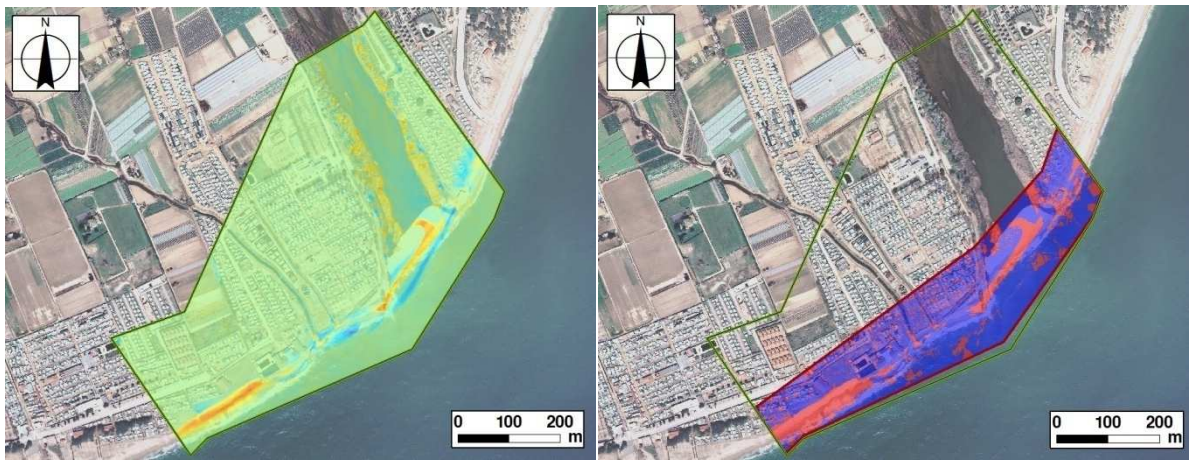

Figure 4.12. Area 4: Left: elevation difference between pre-storm and post-storm situations. Right: areas of erosion (red) and accretion (red).

Table 4.4. Area 4: Volumetric sediment balance.

	VOLUMETRIC SEDIMENT BALANCE	**3912 m³**
A4	Gain	18248 m³
	Loss	-14336 m³

The global volumetric balance (Table 4.4) was small, but this does not mean that there was little sediment movement. The sediment bar blocking the river mouth was pierced, and there was accretion in the northeast and erosion in the southwest. Figure 4.13 shows the sediment balances for each of these sub-areas.

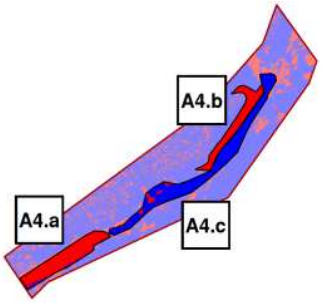

A4.a	**-7166 m³**
A4.b	**-4406 m³**
A4.c	**+6771 m³**

Figure 4.13. Area 4: Sub areas.

Given that the storm waves came from the East, it is unlikely that the sand deposits of the river mouth were originated by the eroded material of the southwest. Area 5 is a special case that has to be treated differently from the rest of the study area for two reasons. In one hand, In addition, the morphodynamics of river mouths are affected by the river flow and sediment transport capacity. On the other hand, the mouth of the Tordera corresponds to the location where the coast orientation starts to change. Taking these remarks into account, the storm-induced changes on Area 5 are treated again in Chapter 6.

4.2.6. Area 5: Malgrat North

Malgrat beach has been divided into two areas. Area 5 covers the northern 2400 metres. In this part the coastline is quite rectilinear, but its orientation starts to shift at two thirds of its length.

The beach of Malgrat is much wider than S'Abanell and has a well developed berm, and the additional sand width forms a buffer zone that acts as a natural protection. For this reason, the human built structures were less affected by the storm of Sant Esteve 2008.

Figure 4.14 shows the impact of the storm along the area.

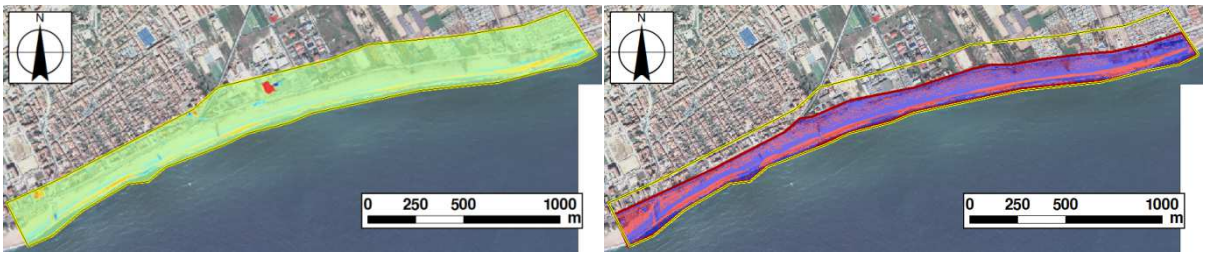

Figure 4.14. Area 5: Left: elevation difference between pre-storm and post-storm situations. Right: areas of erosion (red) and accretion (red).

Table 4.5. Area 5: Volumetric sediment balance.

	VOLUMETRIC SEDIMENT BALANCE	**5215 m³**
A5	Gain	36915 m³
	Loss	-31700 m³

The LIDAR data show that the storm only affected the stretch of the beach closest to the shoreline. The backshore was virtually left unchanged. The morphological response on the affected part follows a longitudinal pattern: the shore was eroded, and there was accretion on the central strip of the beach. The gain and loss values of the sediment balance (Table 4.5) give a first idea of the extent of the process. However, the erosion along the shoreline is uneven, and at some locations interrupted by accretion spots.

For a better understanding of the area, it has been divided into two longitudinal sub-areas and a third one accounting for the small accretion spots (Figure 4.15). The sub-areas give more accurate volume values because they do not take into consideration the backshore, where LIDAR data show a mix of erosion and accretion.

The absolute value of the sediment loss is higher than the sediment gain in the central strip, but they have the same order of magnitude (around 20000 m^3). The lineal rates are about 7.5 m^3/m for the accretion on the central strip of the beach and 10 m^3/m for the erosion on the shore.

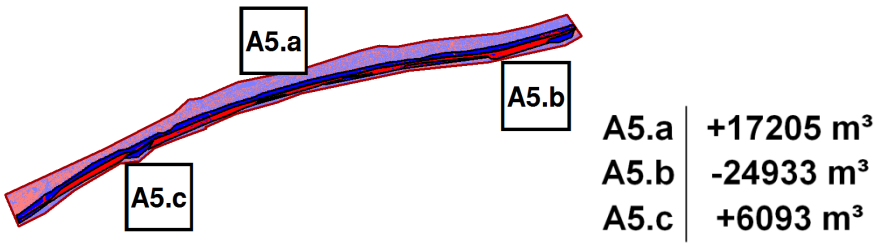

Figure 4.15. Area 5: Sub-areas.

The sub-division shows that the accretion spots, which seemed almost negligible at first, add up to more than 6000 m^3. They can be also be perceived on the shore-normal profiles (see Fig. 4.16). Moreover, the profiles show that except for some spots as A5-12, the position of the shoreline did not change much under the forcing conditions of the storm.

Lastly, as Malgrat is wider than S'Abanell the overwash material did not leave the beach and can be perceived in the profiles. The accretion of the central strip of the beach consists on an increase of the berm height rather than in deposits extensive deposits as it was the case in S'Abanell. However, at this point no conclusion can be reached about these deposits because the data about the overwash in S'Abanell are too scarce.

The global behaviour of the emerged part of Malgrat North was thus similar to the one of S'Abanell, but presented some additional aspects as the accretion spots on the shoreline.

The characterization of the storm made on Chapter 3 showed that the waves reaching both beaches were different due to shoaling, refraction, and other propagation processes. The runup and overtopping also presented local variations. In order to better assess the storm-induced changes in Malgrat, the effects of the wave conditions will be modelled in Chapter 5.

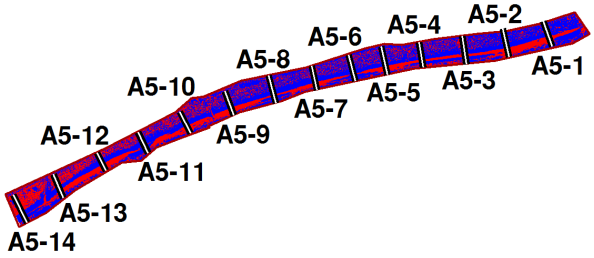

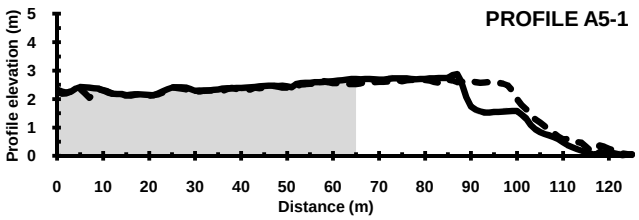

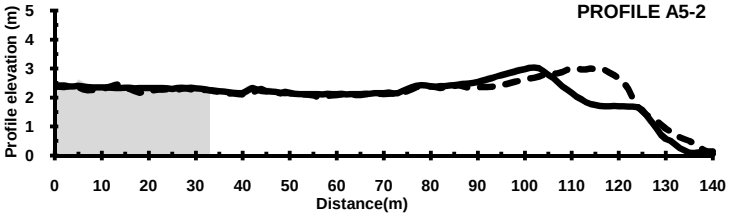

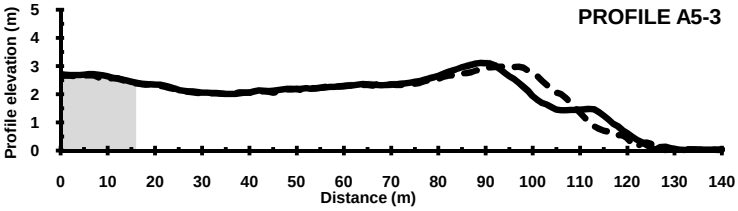

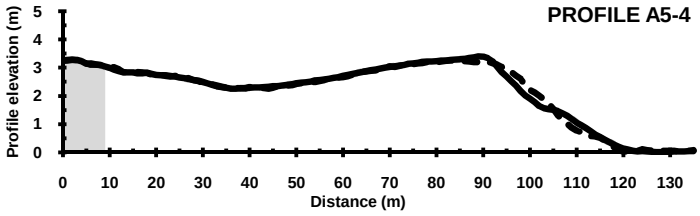

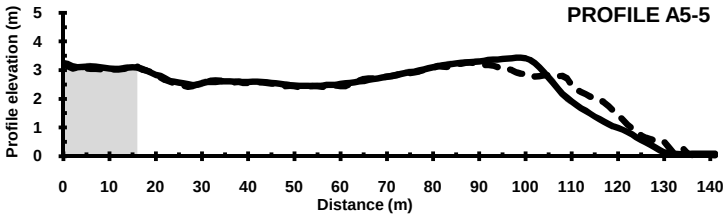

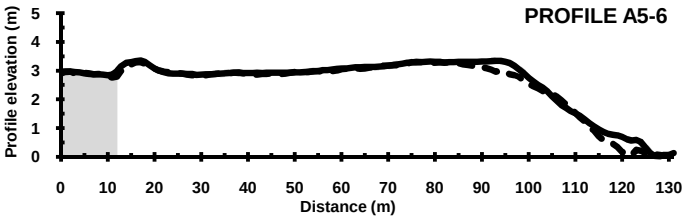

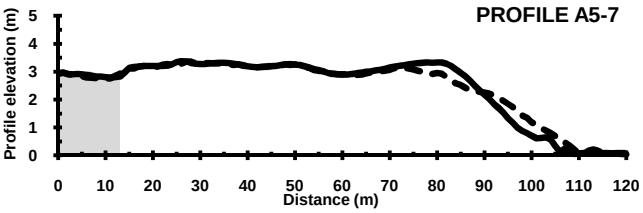

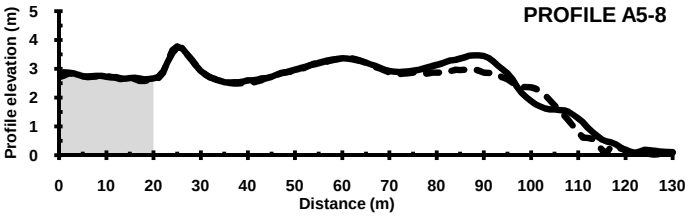

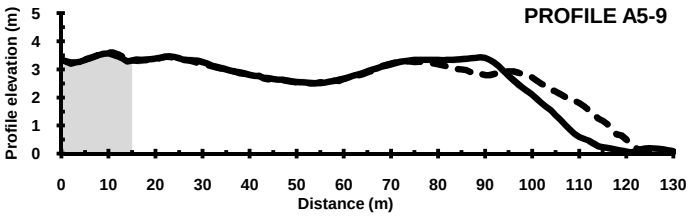

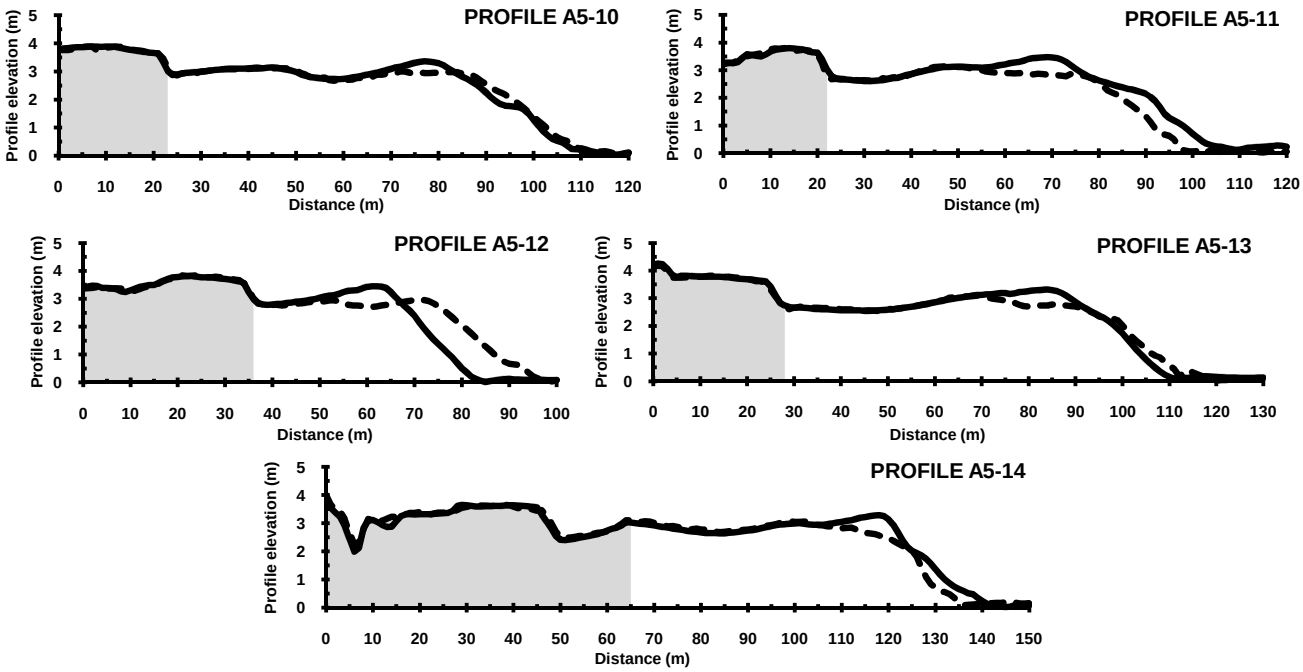

Figure 4.16. Area 5: Shore-normal beach profiles (dashed line = pre-storm; continuous line = post-storm). The grey area represents the location of houses in profiles A5-1, A5-2 and A5-14 and the location of the road/promenade for the rest.

4.2.7. Area 6: Malgrat South

The last area (Area 6) covers the last 1500 metres of the beach of Malgrat. This part of the beach is not straight, although some dominant directions can be perceived. In Malgrat South the berm is almost as well developed as in Malgrat North, but the beach is narrower. Figure 4.17 shows the changes induced by the storm of Sant Esteve 2008 in this part of the study area.

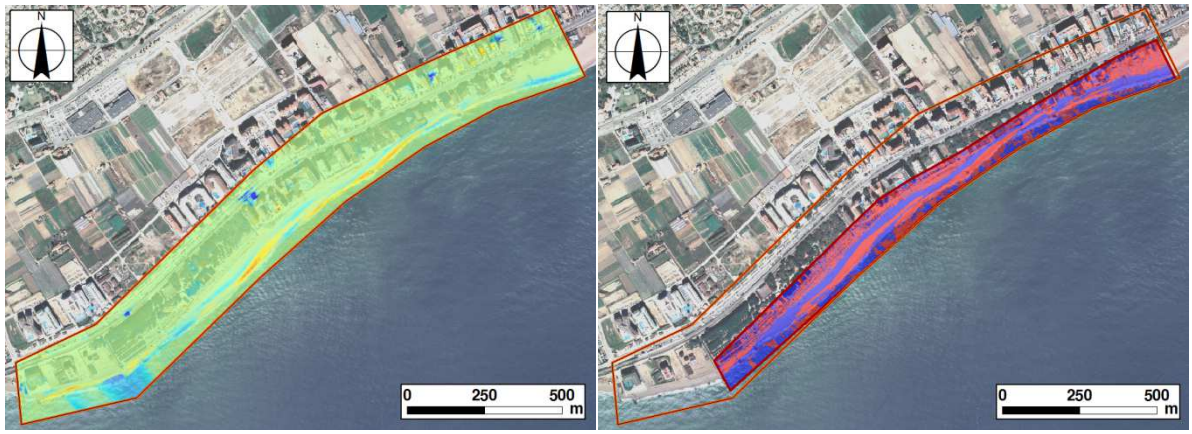

Figure 4.17. Area 6: Left: elevation difference between pre-storm and post-storm situations. Right: areas of erosion (red) and accretion (red).

Table 4.6. Area 6: Volumetric sediment balance.

	VOLUMETRIC SEDIMENT BALANCE	**8360 m³**
A6	Gain	27200 m³
	Loss	-18838 m³

The response of this area to the storm seems less regular than in Malgrat North, but there was once again a marked accretion strip on the central part of the beach. The strip closest to the shoreline presents an unclear behaviour. Erosion was the dominant process as in Malgrat North, but it was more tightly mixed with accretion zones.

Figure 4.18 shows the delimitation of the accretion of the central strip (A6.a), where the accretion rate on was about 11 m^3/m. The part corresponding to the erosion of the shore has also been transformed into a sub-area, but the resulting sediment balance is not accurate because of the intricate pattern it formed with the accretion areas. The sediment volumes involved (Table 4.6) in the processes were smaller than in Malgrat North.

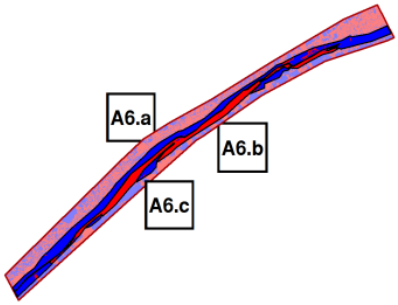

A6.a	+164405 m³
A6.b	-12929 m³
A6.c	+4289 m³

Figure 4.18. Area 6: Sub-areas.

The shore-normal profiles reflect the described irregularities of the beach response. On the southern end of Malgrat there are some rock groynes, shore-normal coastal protection structures that affect the sediment movement and that have been taken as the southern limit of the study area.

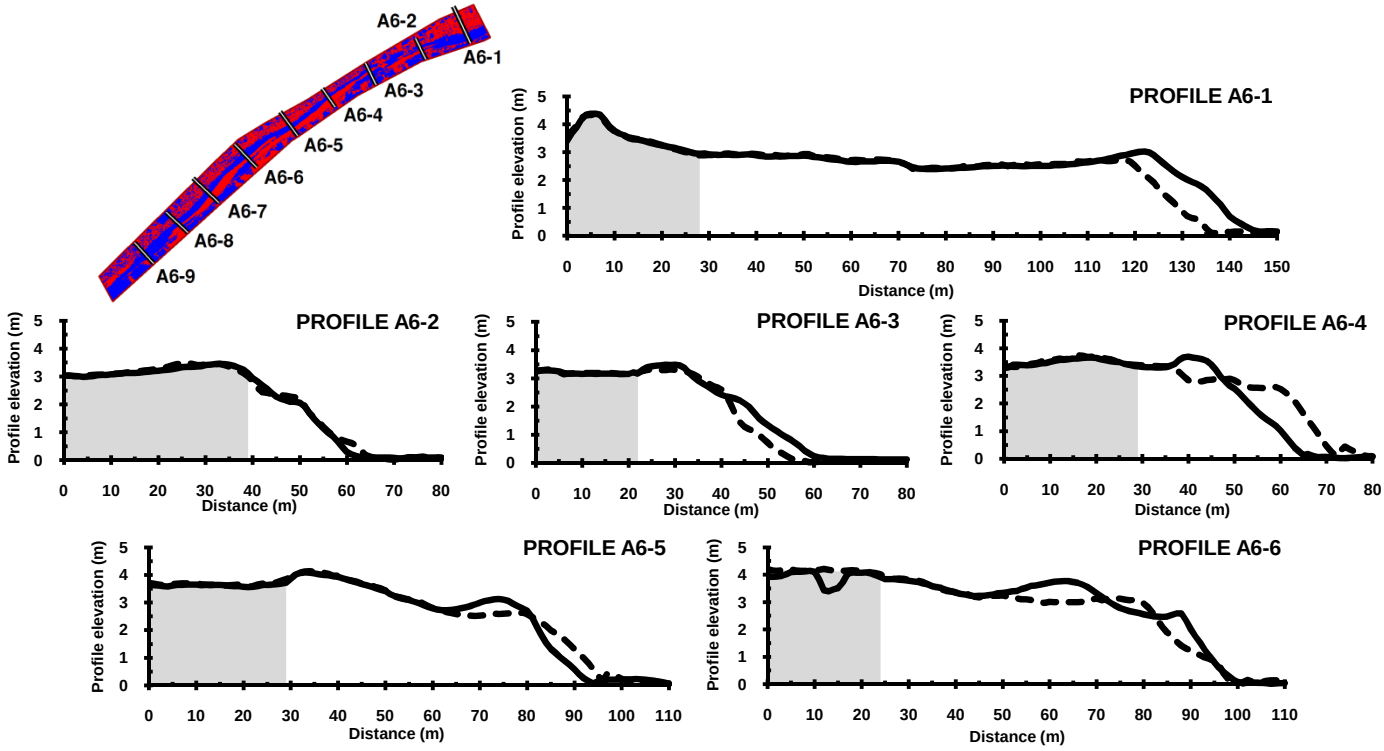

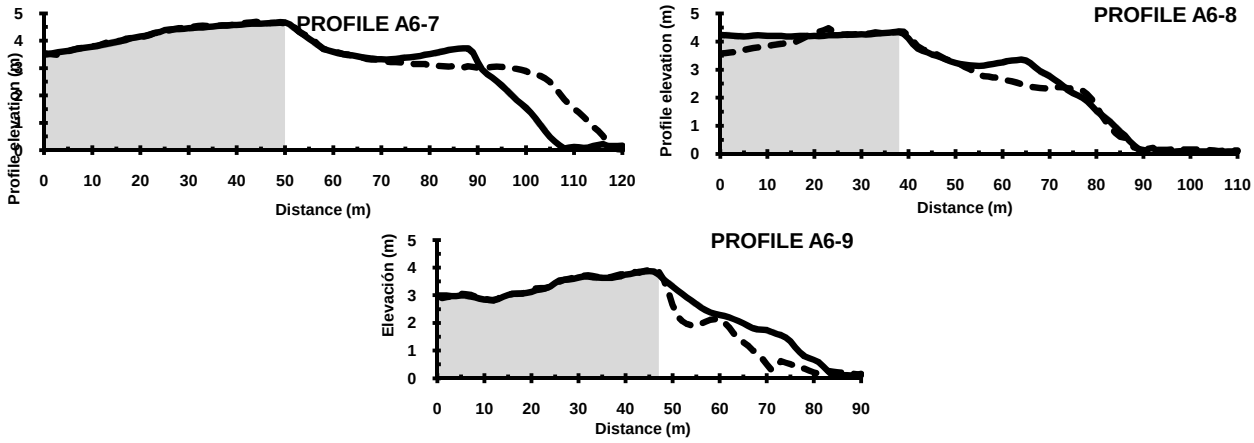

Figure 4.19. Area 6: Shore-normal beach profiles (dashed line = pre-storm; continuous line = post-storm). The grey area represents the location of houses built on the sand except for the profile A6-1, where it represents the location of the road.

The changes in the emerged part of Malgrat South could have been caused by the same factors than in Malgrat North: wave characteristics and beach orientation, added to the presence of the groynes. However, before coming to conclusions in Chapter 6, the response of the area will be modelled in Chapter 5 to account for the submerged part of the beach.

4.3. Morphological recovery after the storm

This section compares the situation existing just after the storm with the one of summer 2009. The LIDAR data used are from January and August 2009, and the aerial photograph used to give spatial references to the viewer was taken on July 2009. For all the figures, sediment loss is represented in red and sediment gain in blue.

4.3.1. Global response and homogeneous areas

Only a few hours are required to induce significant morphological changes on the coast during a high energy storm, but post-storm recovery occurs at longer time scales (Maspataud et al., 2009). The period needed to recover the former morphology can reach several years. After some extreme events, the whole coastal dynamics are modified and the beach does not recover its pre-storm characteristics and behaviour.

Along the storm-impact zone, post-storm beach recovery at individual sites can be highly variable depending on numerous factors ranging from beach orientation to interactions with shoals or artificial coastal structures.

Morton et al. (1994) described the dominant processes during four stages of recovery as follows: (1) rapid forebeach accretion, (2) backbeach aggradation, (3) dune formation, and (4) dune expansion and vegetation recolonization. It has been observed that developed beaches can reach stage 2, but additional recovery is usually prevented because beach widths seaward of the man-made structures (promenades, houses, etc) are too narrow to permit eolian transport and construction of dunes.

The post-storm recovery of a beach is generally brought by cross-shore sediment exchange between the offshore bar, which grows under storm conditions, and the upper beach (Komar, 1998).

In the study area of this work, the recovery six months after the storm of Sant Esteve was not complete. Moreover, the response was not equal along the coast. The following sections analyse the recovery in each of the areas defined in Section 4.2 and use the same shore-normal profiles.

4.3.2. Area 1: Blanes

Figure 4.20 shows the recovery of the Bay of Blanes. The morphodynamic behaviour of the beach after the storm was the opposite of the behaviour during the event. During the recovery period, sand was eroded from both sides of the bay, and the central area underwent an accretion process. As the beach is located in a dense urban area and has an important touristic role, the state of the beach in summer 2009 might be partially originated by human intervention and redistribution of the sand. However, the beach was not artificially nourished.

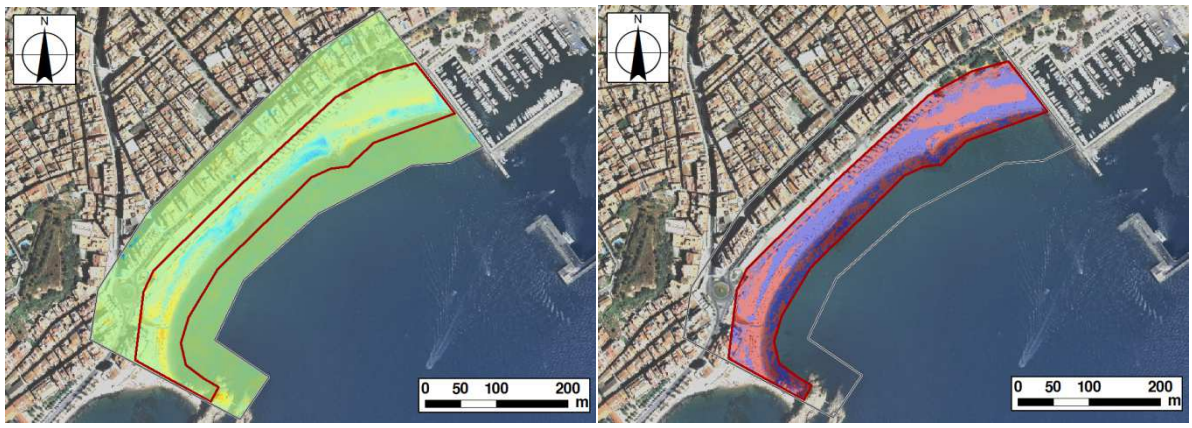

Figure 4.20. Area 1: Left: elevation difference between post-storm and summer 2009 situations. Right: areas of erosion (red) and accretion (red).

Table 4.7. Area 1: Volumetric sediment balance.

	VOLUMETRIC SEDIMENT BALANCE	**1453 m³**
A1	Gain	5575 m³
	Loss	-4122 m³

The volumetric sediment balance (Table 4.7) shows that the amount of sediment gained in the central area was higher than the loss at both ends of the beach. Besides, there was an additional accretion zone at the northeast. The variations can be seen on detail in the sub-areas defined in Figure 4.21.

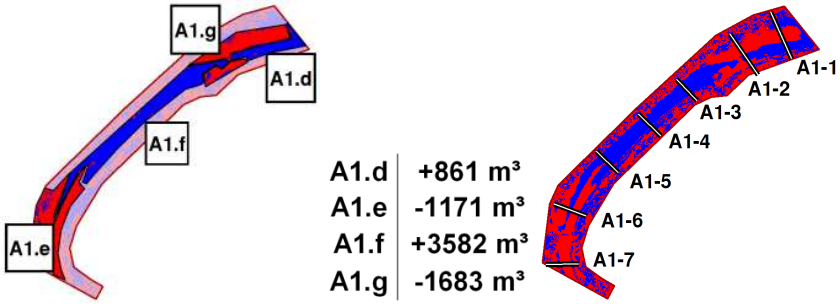

Figure 4.21. Area 1: Sub-areas.

However, the difference between the erosion and accretion absolute values was not as marked as during the event of Sant Esteve 2008. The emerged accretion caused by the

storm represented about 30% of the eroded volume (see Section 4.2.1). The absolute eroded volume (above the sea level) between the event and July 2009 was approximately 65% of the accretion.

In addition, the sediment volume displaced during the recovery was significantly smaller than the volume moved during the storm. In the central area, the storm eroded almost 9000 m^3 of sand, of which about only 4000 m^3 had been recovered by July 2009. By contrast, the 2500 m^3 of sand gained on the ends of the beach had been totally compensated (by about 2800 m^3). However, the sand of the ends of the beach was in summer 2009 distributed differently than before the storm: the gain in the south was slightly higher than in the north, while during the storm the north had been more eroded. The behaviour of the central part of the bay suggests that the recovery was not complete by July 2009.

The fact that the central area of the Bay of Blanes had not recovered its original aspect by July 2009 could have two explanations: 1) there was not enough sediment available in the submerged part of the profile or 2) the recovery was potentially possible, but the speed of the process was not high enough to have finished by summer 2009. There are no available bathymetry evolution data to accept or rejected either of the two scenarios.

The variations on the ends of the beach (profiles A1-1 and A1-7, Figure 4.22) could be explained by longshore transport (see Chapter 6), which is the prevailing sediment transport mechanism during non-storm conditions. There were no additional extreme events between the storm of Sant Esteve 2008 and July 2009.

As the bay is a closed or partially closed system, the sedimentary budget for longshore transport has to be close to zero. Depending on the wave conditions, the sediment moves from north to south or from south to north. The gain of sediment in the sub-area A1-E could be partially caused by dominant wave directions towards the southwest during the first half of 2009.

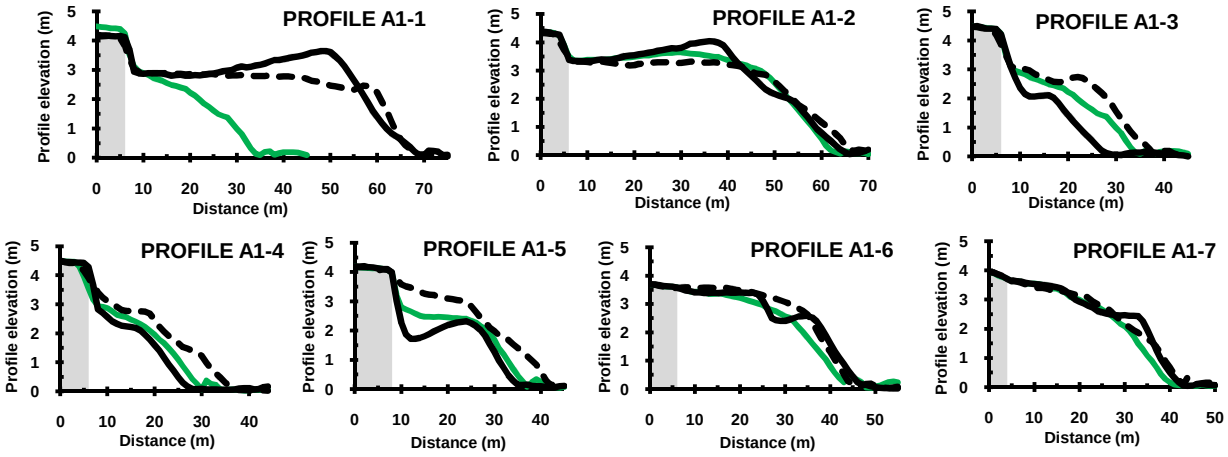

Figure 4.22. Area 1: Shore-normal beach profiles (dashed line = pre-storm; continuous black line = post-storm; green line = summer 2009). The grey area represents the location of promenade.

4.3.3. Area 2: S'Abanell North

In the northern part of S'Abanell the morphological changes after the storm were opposed to the changes during the storm, as in the Bay of Blanes (Figure 4.23).

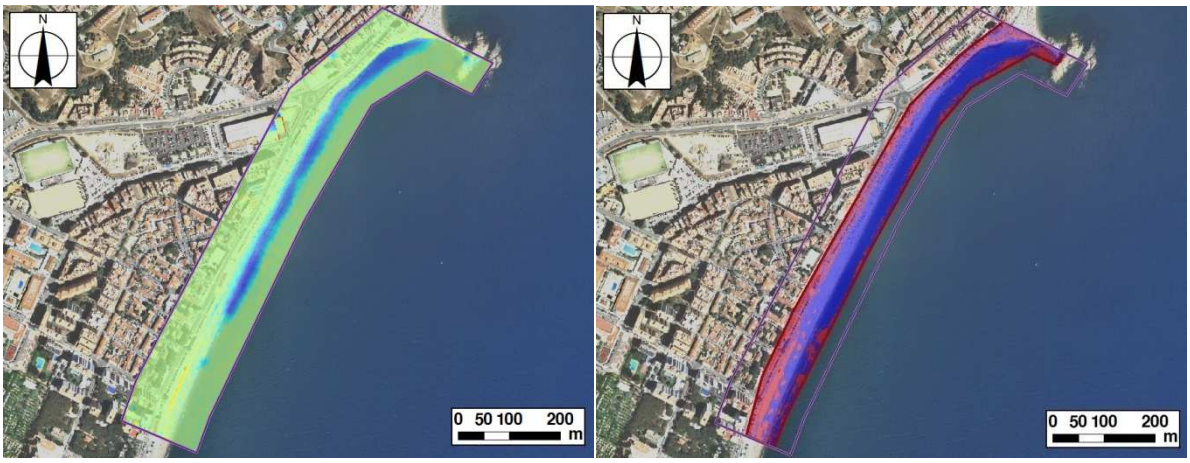

Figure 4.23. Area 2: Left: elevation difference between post-storm and summer 2009 situations. Right: areas of erosion (red) and accretion (red).

Table 4.8. Area 2: Volumetric sediment balance.

	VOLUMETRIC SEDIMENT BALANCE	**39010 m³**
A2	Gain	41109 m³
	Loss	-2098 m³

The volumetric balance (Table 4.8) shows that the prevailing tendency was accretion, and that up to 85% of the emerged lost sand had been recovered. The profiles show that this is only true on the northern half of the profiles (Figure 4.24), where in summer 2009 there was even more sand than before the storm. However, this recovery was not natural: a second artificial nourishment took place during the first week of August 2009, shortly before the LIDAR survey. This time, 250000 m^3 of sand were used to nourish the beach between the profiles A2-1 to A2-7. For the rest of the beach, the post-storm and summer profiles are almost identical: the natural recovery was almost non-existent.

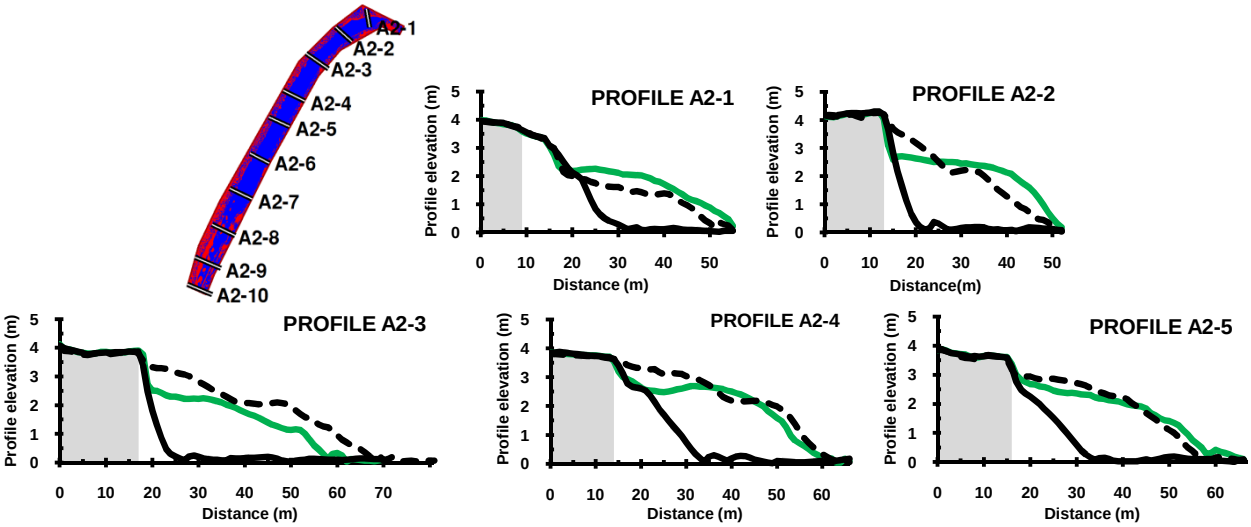

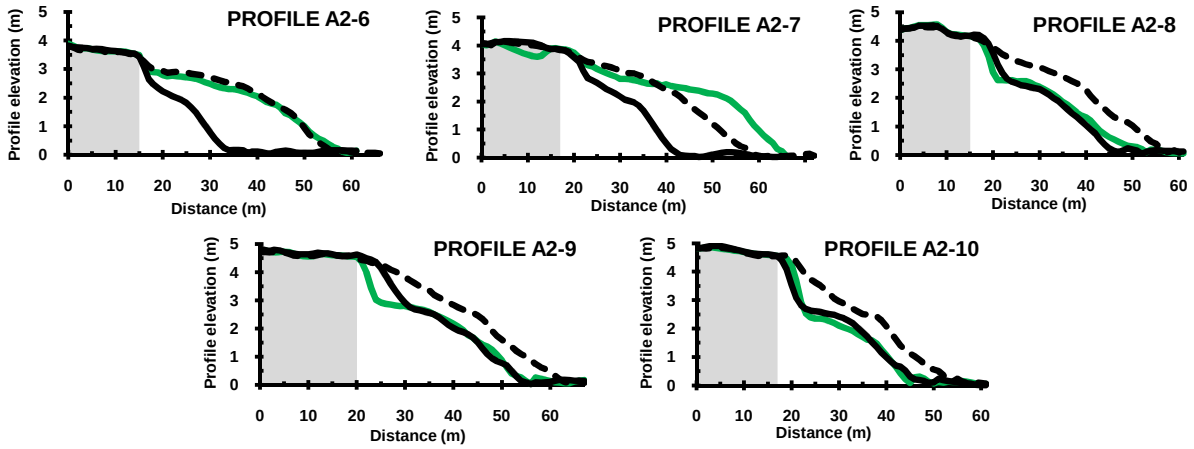

Figure 4.24. Area 2: Shore-normal beach profiles (dashed line = pre-storm; continuous black line = post-storm; green line = summer 2009). The grey area represents the location of promenade.

4.3.4. Area 3: S'Abanell South

The recovery of the southernmost part of S'Abanell (A3) is shown on Figure 4.25.

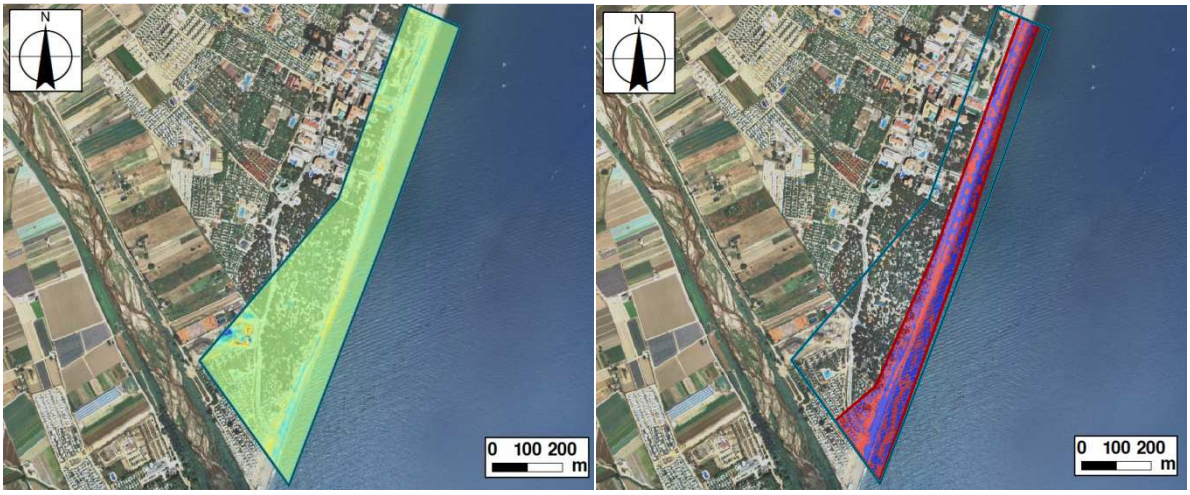

Figure 4.25. Area 3: Left: elevation difference between post-storm and summer 2009 situations. Right: areas of erosion (red) and accretion (red).

Table 4.9. Area 3: Volumetric sediment balance.

	VOLUMETRIC SEDIMENT BALANCE	**1783m³**
A3	Gain	8832 m³
	Loss	-7049 m³

Except for the southern part, only occupied by camping sites, the recovery does not show a clear pattern along emerged part of the area. This uneven behaviour is confirmed by the shore-normal profiles (Figure 4.26), which show that there were only slight changes on the beach shape. The total gain and loss values (Table 4.9) were very similar and probably caused by local variations or by human intervention and redistribution of the sand.

On area closest to the mouth of the River Tordera (profiles A3-10 and A3-12, Figure 4.26), during the storm the sand was moved to the backbeach. The LIDAR survey of summer 2009 shows that the tendency was reversed during the recovery period. The recovery of this part of Area 3 might have been partly produced by the artificial displacement of the overwash material back to the shore.

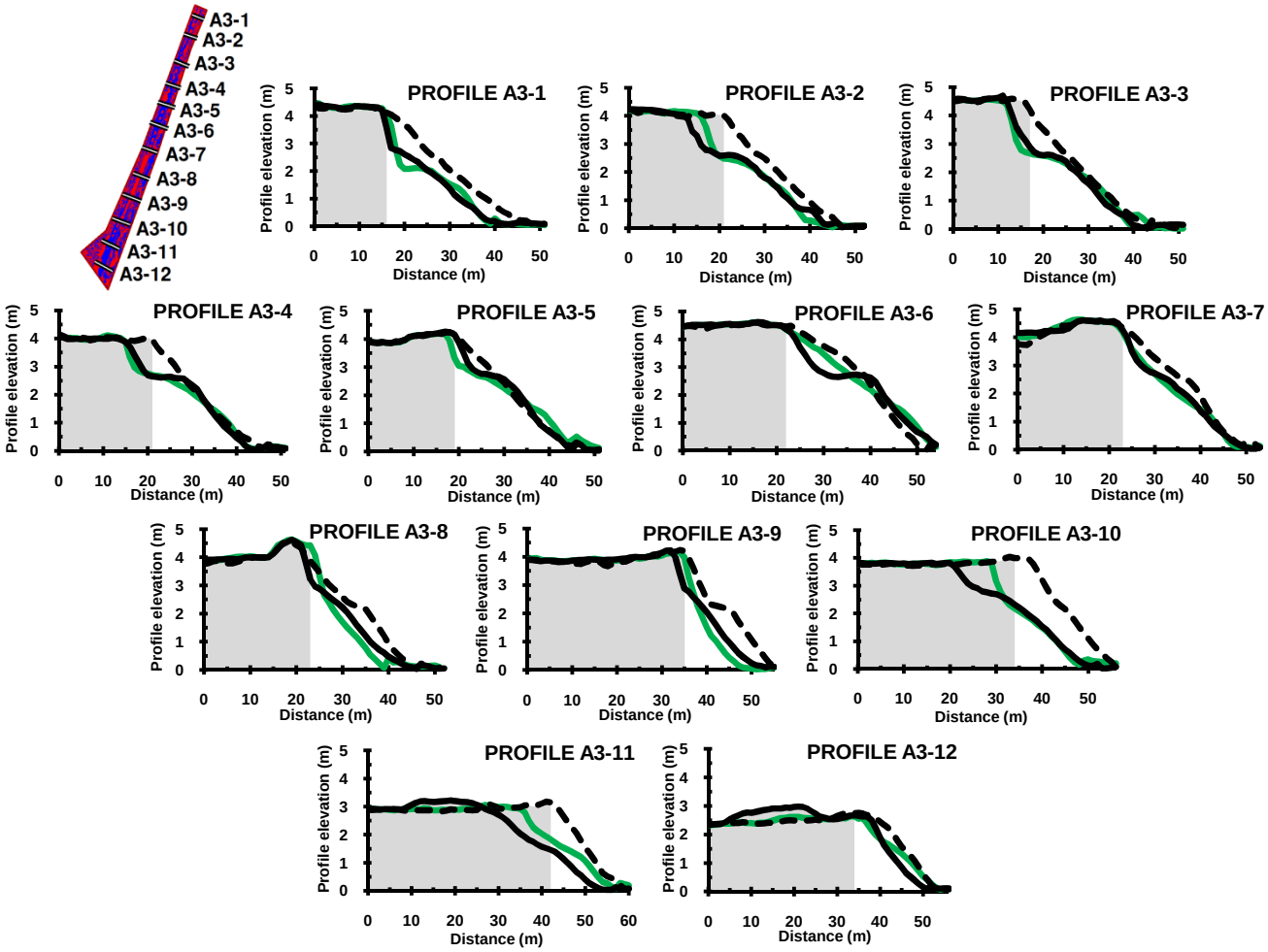

Figure 4.26. Area 3: Shore-normal beach profiles (dashed line = pre-storm; continuous black line = post-storm; green line = summer 2009). The grey area represents the location of the maritime prome- nade for profiles A3-1 to A3-8, and the location of the fences bordering the camping sites for the rest.

4.3.5. Area 4: Tordera

Figure 4.27 show the evolution of the mouth of the Tordera and its surrounding area during the recovery period. There were no torrential events in the period between the storm and the summer LIDAR survey, so it can be assumed that the observed changes were caused primarily by the sea waves.

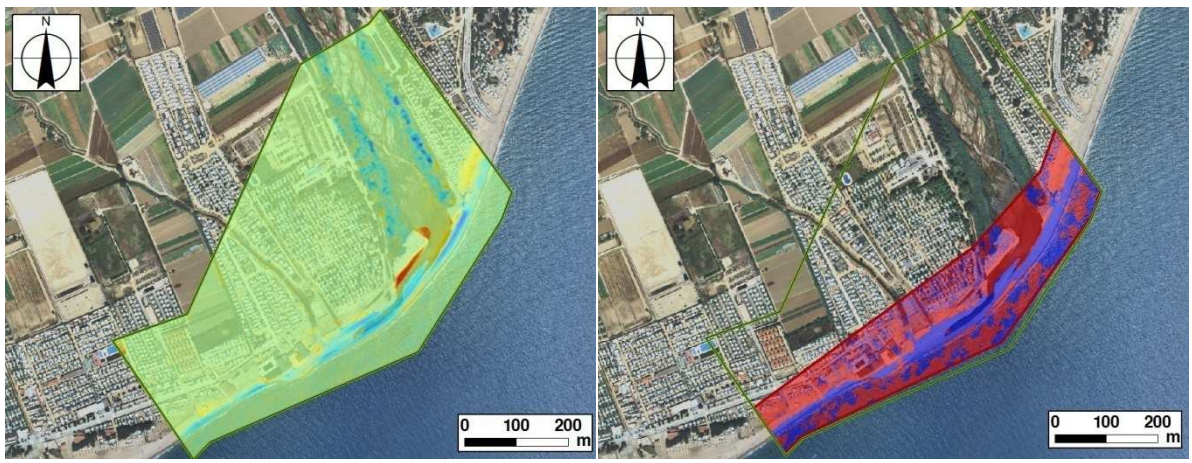

Figure 4.27. Area 4: Left: elevation difference between post-storm and summer 2009 situations. Right: areas of erosion (red) and accretion (red).

Table 4.10. Area 4: Volumetric sediment balance.

	VOLUMETRIC SEDIMENT BALANCE	**-724 m³**
A4	Gain	13685 m³
	Loss	-14410 m³

The global volumetric balance (Table 4.10) is even smaller than it was during the storm, but once again this does not mean that there was little sediment movement. The gain and loss values are more adequate to describe the situation. Both the gain and the loss were about 15000 m^3. This is the same order of magnitude than during the storm, which implies that the storm conditions had enough energy to move the same amount of sediment in a few hours than the normal waves in six months.

The river mouth did not experiment a marked recovery. The pierced sand barrier was not reconstructed, and the accretion of the eastern part continued. This accretion formed, to a certain degree, a new sand bar. The western part of the area surrounding the river mouth, which was severely eroded during the storm, does show some recovery. In Chapter 6 the behaviour of Area 5 will be studied again.

4.3.6. Area 5: Malgrat North

As noted on the previous section, the beach of Malgrat is wider than S'Abanell. Besides, the storm-induced overwash reached the backbeach, not the town. The shoreline did not experience a significant migration during the storm, and although the general trend was erosion there were accretion spots along the beach. Figure 4.28 shows the recovery of the area between the storm of Sant Esteve and July 2009.

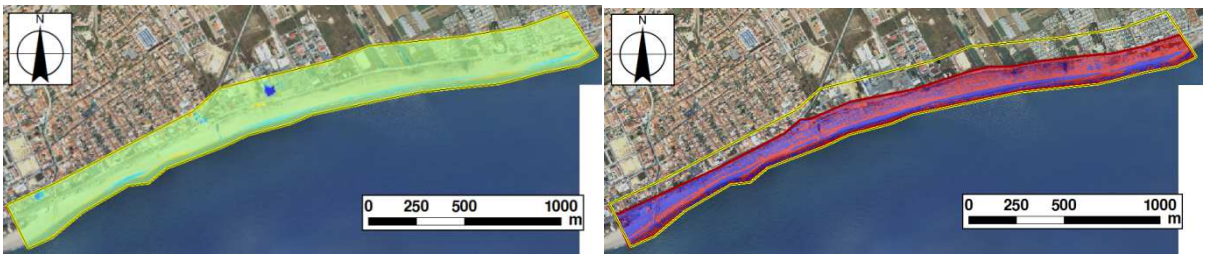

Figure 4.28. Area 5: On the left, elevation difference between post-storm and summer situations. On the right, areas of erosion and areas of accretion.

Table 4.11. Area 5: Volumetric sediment balance.

	VOLUMETRIC SEDIMENT BALANCE	**8374 m³**
A5	Gain	28925 m³
	Loss	-20550 m³

The absolute values of sediment moved are lower than during the storm (Table 4.11). This fact suggests that the recovery was not complete by summer 2009. However, the behaviour of this area is better analysed through the shore-normal beach profiles (Figure 4.29).

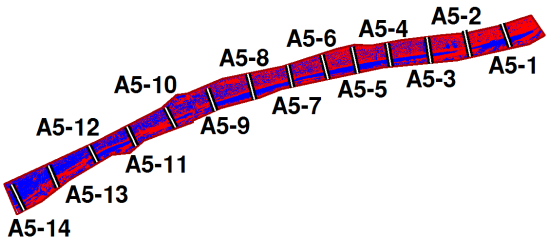
A5-1
A5-2
A5-3
A5-4
A5-5
A5-6
A5-7
A5-8
A5-9
A5-10
A5-11
A5-12
A5-13
A5-14

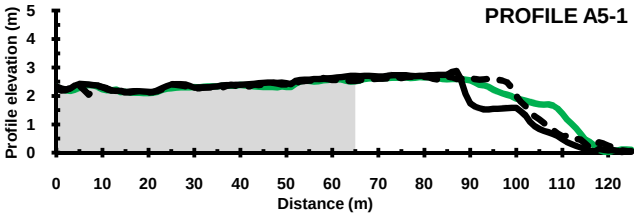
PROFILE A5-1
Profile elevation (m)
Distance (m)

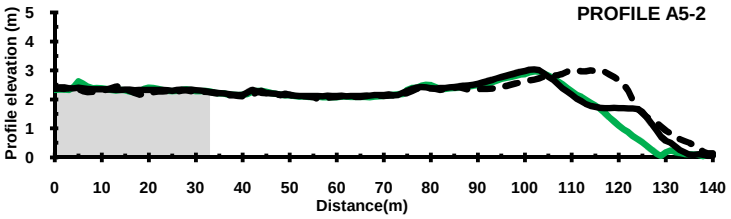
PROFILE A5-2
Profile elevation (m)
Distance(m)

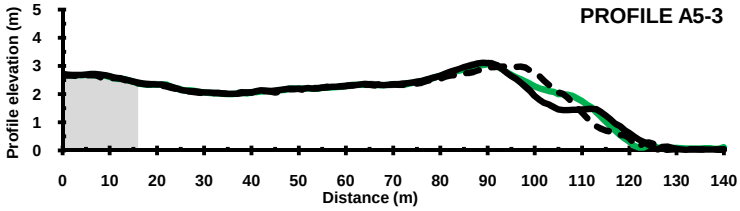
PROFILE A5-3
Profile elevation (m)
Distance (m)

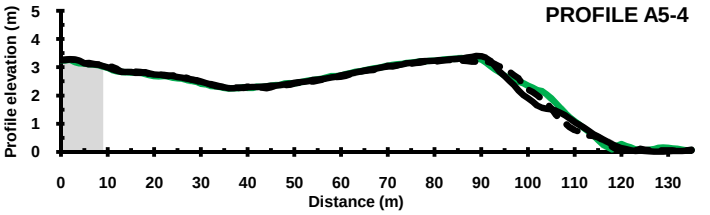
PROFILE A5-4
Profile elevation (m)
Distance (m)

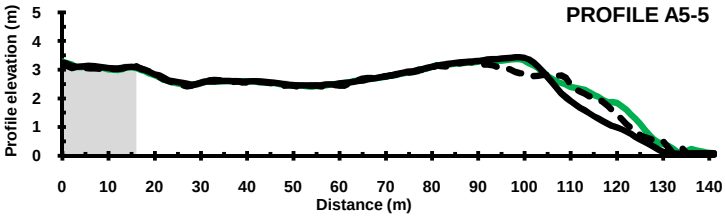
PROFILE A5-5
Profile elevation (m)
Distance (m)

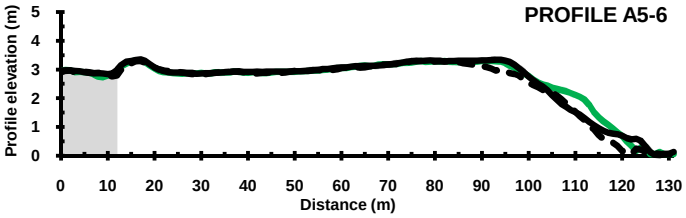
PROFILE A5-6
Profile elevation (m)
Distance (m)

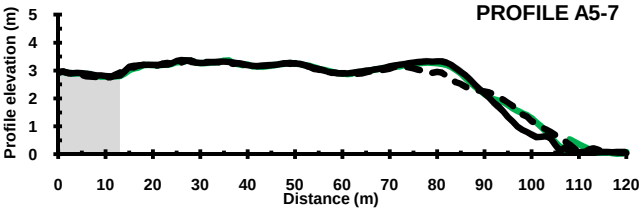
PROFILE A5-7
Profile elevation (m)
Distance (m)

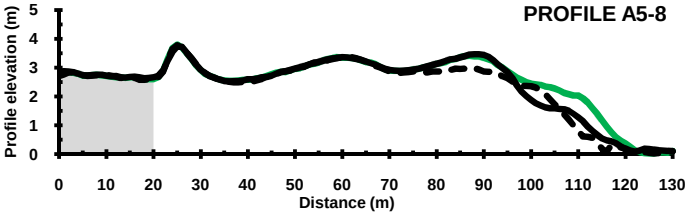
PROFILE A5-8
Profile elevation (m)
Distance (m)

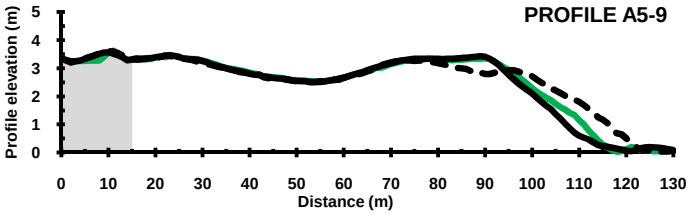
PROFILE A5-9
Profile elevation (m)
Distance (m)

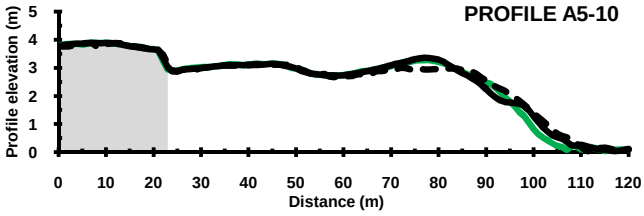
PROFILE A5-10
Profile elevation (m)
Distance (m)

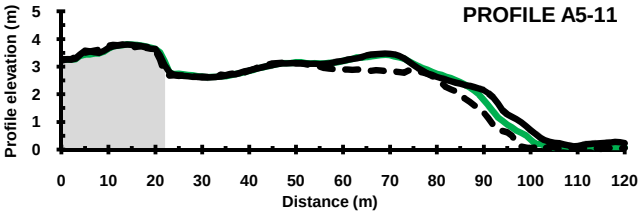
PROFILE A5-11
Profile elevation (m)
Distance (m)

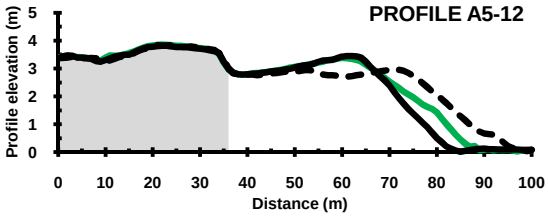
PROFILE A5-12
Profile elevation (m)
Distance (m)

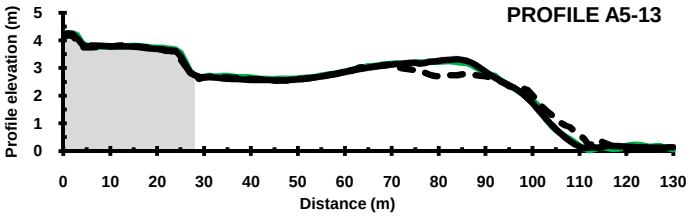
PROFILE A5-13
Profile elevation (m)
Distance (m)

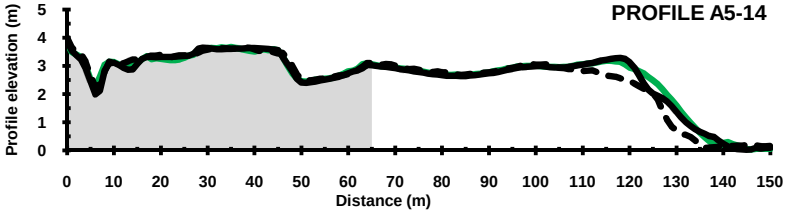
PROFILE A5-14
Profile elevation (m)
Distance (m)

Figure 4.29. Area 5: Shore-normal beach profiles (dashed line = pre-storm; continuous black line = post-storm; green line = summer 2009). The grey area represents the location of houses in profiles A5-1 to A5- and A5-14 and the location of the road/promenade for the rest.

Two parts of each beach profile can be distinguished: the sloping face and the berm. The berm in July was almost exactly the same than just after the storm, it had not returned to its original lower elevation. By contrast, the sloping face of the beach was modified in the recovery period, but unevenly: in some parts the beach totally recovered its pre-storm situation (A5-5), or recovered partially (A5-12), and in other areas the beach evolution was in the same direction as during the storm (A5-14).

4.3.7. Malgrat South

The recovery of Area 6 is shown on Figure 4.30.

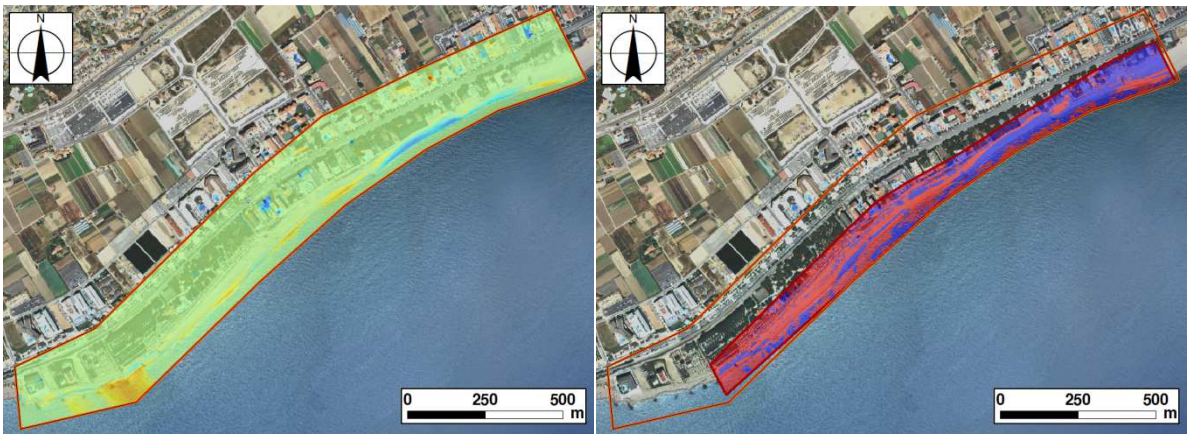

Figure 4.30. Area 6: Left: elevation difference between post-storm and summer 2009 situations. Right: areas of erosion (red) and accretion (red).

Table 4.12. Area 6: Volumetric sediment balance.

	VOLUMETRIC SEDIMENT BALANCE	**-4128 m³**
A6	Gain	17603 m³
	Loss	-21730 m³

Once again, the global volumetric sediment balance (Table 4.12) is inadequate to fully understand the recovery state of the beach, because the process affects the area in very different ways. On the contrary, the shore-normal beach profiles (Figure 4.31) provide important insights on the situation.

The profiles show that the northern part of Malgrat South recovered from the erosion that occurred during the storm, and in many places it accumulated more sediments than before the storm. By contrast, the central and south part of Area 6 did not recover their original state. In some parts, and as in Malgrat North, the beach morphodynamics after the storm were in the same direction that during the event.

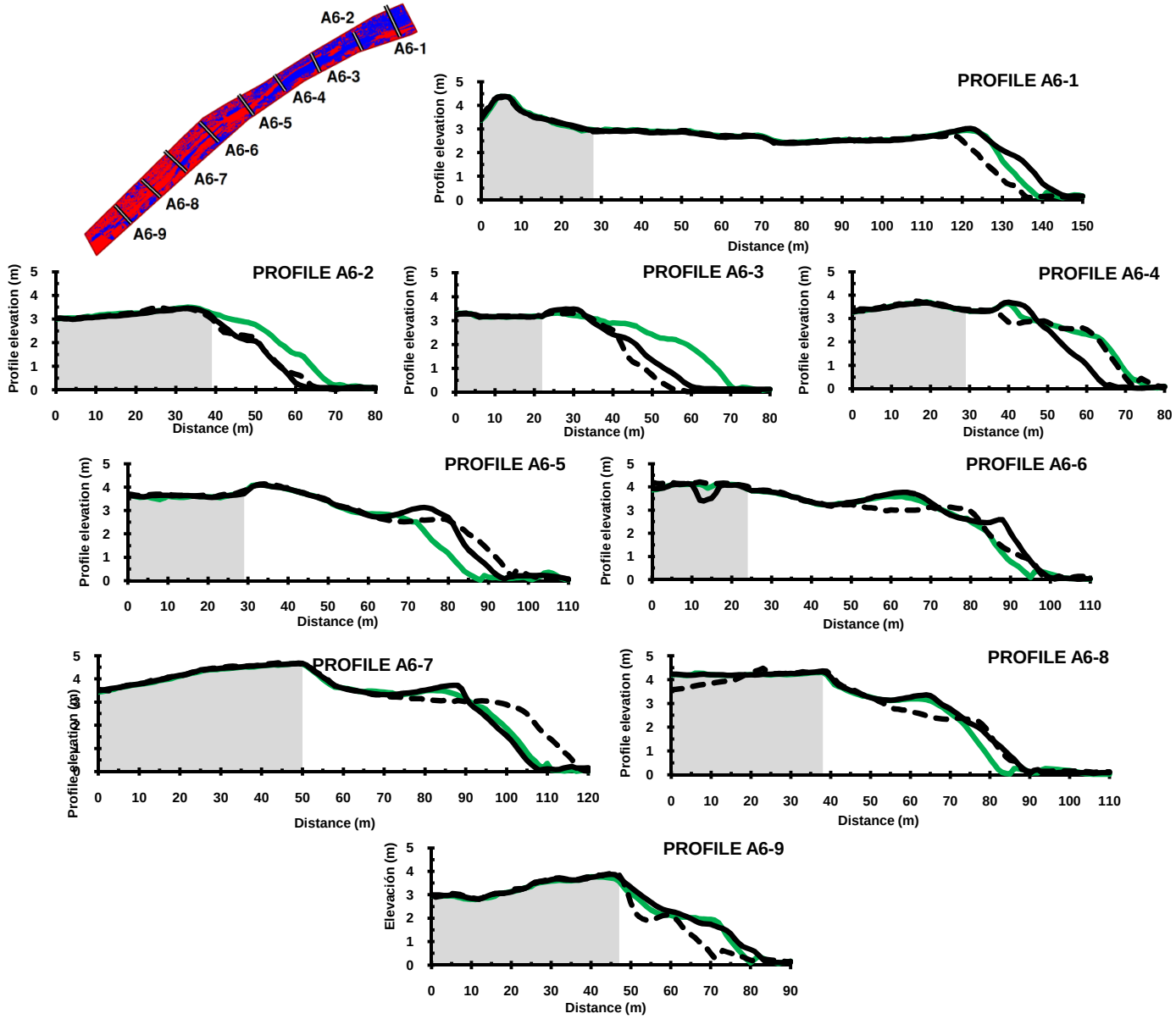

Figure 4.31. Area 6: Shore-normal beach profiles (dashed line = pre-storm; continuous black line = post-storm; green line = summer 2009). The grey area represents the location of houses built on the sand except for the profile A6-1, where it represents the location of the road.

4.4. Summary

In this chapter, the ICC LIDAR elevation datasets have been used to describe the morphological changes induced by the storm of Sant Esteve 2008 in the Catalan beaches of Blanes and Malgrat de Mar.

The characteristics of the beach response to the event were:

- General erosion of the beach, especially in S'Abanell and in the Bay of Blanes.
- Erosion rates ranging from 10 m^3/m to 50 m^3/m. These values are lower than the 60-65 m^3/m predicted Mendoza et al. (2011, see Chapter 3). However, the predicted values are potential values which do not take into considerations factors as the beach characteristics or the incidence angle of the swell.
- Overwash along the entire study area. This is consistent with the results of the runup estimation of Chapter 3 which showed that overtopping occurred in all the beach profiles.
- Accretion spots and irregular beach response in Malgrat, particularly on the south.

The topographic LIDAR data used in this work does not provide any information about the submerged part of the beach, making the analysis of the impact of the storm incomplete. In order to overcome this limitation, Chapter 5 will deal with the modelling of the beach response to the event. Once the results are obtained, they will be analysed together with the LIDAR-based observations (Chapter 6).

Chapter 5

MODELLED EROSION

The main limitation of LIDAR elevation data is that it lacks bathymetric information. When bathymetric LIDAR is not available, the underwater beach response to storms has to be quantified by other means.

Many analytical and numerical models for storm-induced beach change have been developed over the years (e.g. Larson and Kraus, 1989; Dibajnia et al., 1994; Kriebel, 1986; Eagleson et al., 1958). Field data measured all around the world have allowed to improve the models and to consolidate them as an efficient way to obtain realistic and accurate beach response results. However, the enormous variability of beach morphology and storm characteristics around the globe usually limits a given model application to specific conditions. Very simple models, which try to overcome these limitations by being as general as possible, tend to perform poorly in beaches with complex morphology.

In the specific case study of this work, LIDAR topographic data have made it possible to measure with high accuracy the erosion caused by the event of Sant Esteve 2008 on the emerged part of the beach between Blanes and Malgrat de Mar. Valid models for the case study conditions will be those whose results match the observed response. In addition, any model which shows the correct qualitative behaviour could be calibrated using the LIDAR data.

The goal of the present chapter is to combine LIDAR data and modelling tools to make an accurate estimate of the total eroded sand volumes (m^3/m) of each of the shore-normal beach profiles cast along S'Abanell and Malgrat, defined in the previous chapters. The chosen modelling tools are the Convolution Method, which gives a simple analytical solution for approximating the time-dependent beach–profile response to severe storms, and the numerical model SBEACH.

5.1 Methodology

Figure 5.1 shows the volumetric change of the emerged part (ΔV_{+0}) of each profile along the study area measured using LIDAR.

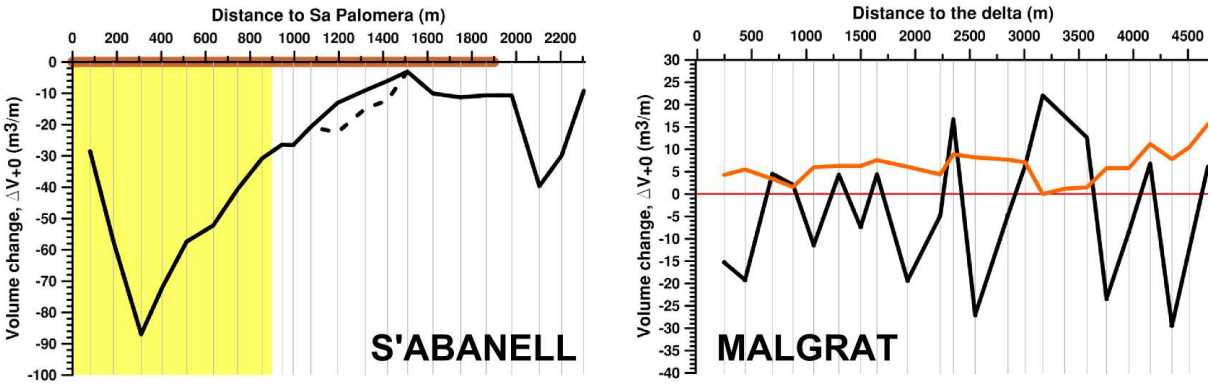

Figure 5.1. Volumetric change along the study area measured using LIDAR in S'Abanell (left) and Malgrat (right). The grey lines mark the position of the shore-normal beach profiles, the yellow area the extend of the artificial nourishment and the brown line the maritime promenade. The orange line represents the accretion on the central strip of Malgrat (overwash material).

S'Abanell is a very rectilinear beach, but its characteristics vary alongshore and make it necessary to set four different groups:

- Artificially nourished beach limited by the maritime promenade: profiles A2-1 to A2-8.
- Narrow beach (not artificially nourished) limited by the maritime promenade: profiles A2-9 and A3-1.
- Very narrow beach (absence of a developed berm) limited by the maritime promenade: profiles A3-2 to A3-9.
- Wide beach without landward limitations (only camping sites): profiles A3-10 to A3-12.

The qualitative behaviour of each of these groups can be represented by one characteristic profile for each case (profiles A2-5, A3-1, A3-3 and A3-10).

The methodology consists of four steps:

1) Application of the two models to the characteristic profiles defining each group.
2) Calibration of the models to match the observed results on the emerged part (ΔV_{+0})
3) Determination of the modelled total volumetric change of the characteristic profiles ($\Delta V_T = \Delta V_{+0} + \Delta V_{-0}$).
4) Extrapolation of the results to the complete set of profiles.

The case of Malgrat is more delicate, because the beach response to the event was not the same all along the beach: erosion and accretion areas appeared, forming beach cusps (see Chapter 4). However, erosion was the prevailing behaviour in terms of quantity. Using the same methodology than in S'Abanell, the submerged parts of the erosion profiles can be obtained. The characteristic profiles are in this case A5-9 (Malgrat North) and A6-4 (Malgrat South). The beach cusps or accretion profiles are studied in Chapter 6.

The Bay of Blanes and the mouth River Tordera are not treated in this chapter, because the chosen models cannot be applied in areas with varying longshore characteristics and behaviour. Lastly, it has to be noted that the selected models to not account properly for the overwash process. These aspects will be dealt with in Chapter 6.

5.2 Convolution method

5.2.1 Model overview

The convolution method was developed by Kriebel and Dean (1993) and is based on the observation that beach response to steady-state forcing conditions is approximately exponential in time. It approximates the response of any depth contour as in (Eq. 5.1).

$$R(t) = R_\infty\left(1 - e^{-t/T_S}\right) \quad \text{(Eq. 5.1)}$$

R_∞ is the maximum potential response of the contour (advance or retreat) that occurs after the system reaches equilibrium, and T_S is the characteristic time scale of the exponential response. As a result, the differential equation governing the problem is (Eq. 5.2).

$$\frac{dR(t)}{dt} = \frac{1}{T_S}[R_\infty - R(t)] \quad \text{(Eq. 5.2)}$$

$R(t)$ and R_∞ are most conveniently described as the erosion or retreat of the top of the berm. Figure 5.2 illustrates the situation described by the previous equations.

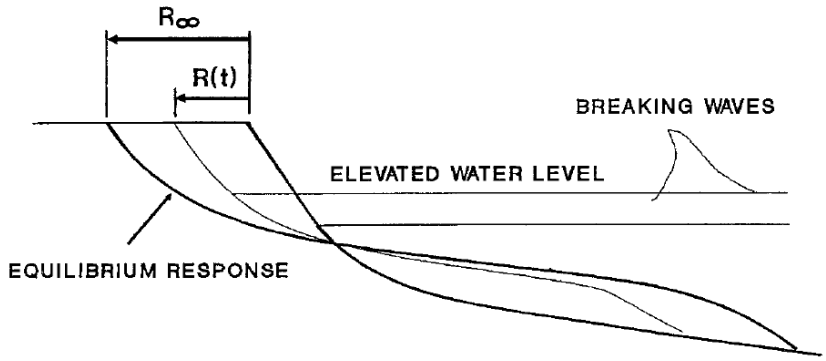

Figure 5.2. Definition sketch for beach profile response (Kriebel and Dean, 1993).

The erosion-forcing function may be expressed as R_∞ times as unit-amplitude function of time, $f(t)$, as shown on (Eq. 5.3).

$$\frac{dR(t)}{dt} + \alpha R(t) = \alpha R_\infty f(t) \quad \text{(Eq. 5.3)}$$

Where $\alpha = \frac{1}{T_S}$ is the characteristic rate parameter of the system.

The solution to differential equations of this kind can be formally obtained by the method of Laplace transforms. However, it can be more simply found by the convolution of the time-dependent forcing and the characteristic solution for steady forcing, in this case an exponential function. As a result, the response of the profile may be expressed in the form of a convolution integral defined by (Eq. 5.4) and (Eq. 5.5).

$$R(t) = \frac{R(t)}{T_S}\int_0^t f(\tau)e^{-(t-\tau)/T_S}d\tau \quad \text{(Eq. 5.4)}$$

$$R(t) = \alpha R_\infty \int_0^t f(\tau)e^{-\alpha(t-\tau)}d\tau \quad \text{(Eq. 5.5)}$$

Where τ is the time lag.

The sand volumes needed for this work can be connected to the recession of the profile if the hypothesis is made that all elevation contours erode at the same relative rate. This implies that the dimensionless erosion, $\frac{R(t)}{R_\infty}$, is the same everywhere. The relative volume eroded is then the same as the relative retreat (Eq. 5.6).

$$\frac{V(t)}{V_\infty} = \frac{R(t)}{R_\infty} \quad \text{(Eq. 5.6)}$$

Where $V(t)$ is the time-dependent sediment volume eroded above the surge level, and V_∞ the equilibrium eroded volume or potential erosion. The original convolution integral is thus transformed into (Eq. 5.7) and (Eq. 5.9).

$$\frac{V(t)}{V_\infty} = \frac{R(t)}{R_\infty} \quad \text{(Eq. 5.7)}$$

$$V(t) = \frac{V(t)}{T_S}\int_0^t f(\tau)e^{-(t-\tau)/T_S}d\tau \quad \text{(Eq. 5.8)}$$

$$V(t) = \alpha V_\infty \int_0^t f(\tau)e^{-\alpha(t-\tau)}d\tau \quad \text{(Eq. 5.9)}$$

However, Kriebel and Dean suggest a simplified approach to the problem. Using an idealized storm surge, it is possible to obtain a closed-form solution for beach response. The water-level rise and fall are approximated by the sine-squared function as in (Eq. 5.10).

$$f(t) = (\sin \sigma t)^2 \; for \; 0 < t < T_D \quad \text{(Eq. 5.10)}$$

Where $\sigma = \pi/T_D$ and T_D is the duration of the storm. For the event of Sant Esteve 2008, $T_D = 66$ hours (see Chapter 3).

Substituting $f(t)$ into the convolution integral and integrating the resulting expression, the solution to the beach response (Eq. 5.11) is then a function of just one parameter, β.

$$\frac{R(t)}{R_\infty} = \frac{1}{2}\left\{1 - \frac{\beta^2}{1+\beta^2}exp\left(-\frac{2\sigma t}{\beta}\right) - \frac{1}{1+\beta^2}[\cos(2\sigma t) + \beta \sin(2\sigma t)]\right\} \quad \text{(Eq. 5.11)}$$

Where β is the ratio of the erosion time scale to the storm duration (Eq. 5.12).

$$\beta = 2\pi\frac{T_S}{T_D} \quad \text{(Eq. 5.12)}$$

Figure 5.3 shows an example of profile response using this methodology.

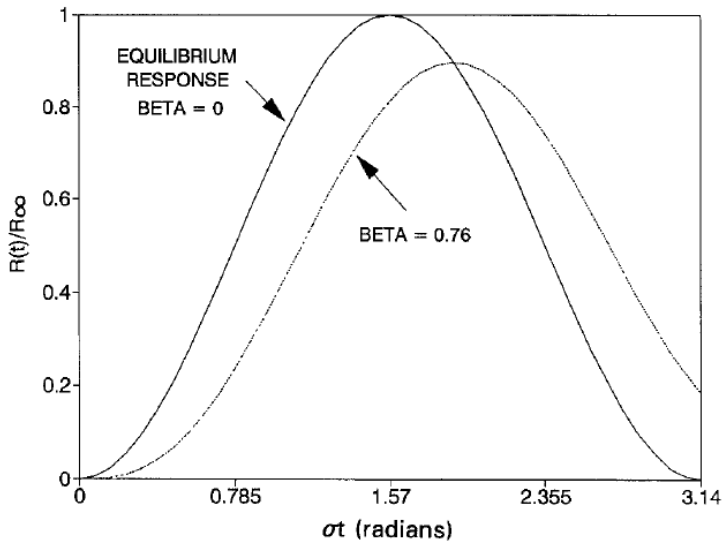

Figure 5.3. Example of profile beach response obtained using the idealized storm surge simplification and the Convolution Method, (Kriebel and Dean, 1993).

For the purpose of this study an additional simplification can be made, because the time-dependent response of the beach is not needed. For this reason, it is only necessary to evaluate $R(t)$ at the end of the storm. If the duration of the storm is not long enough, not all the potential beach retreat R_∞ will occur. The maximum retreat R_{max} can be analytically obtained evaluating $\frac{R(t)}{R_\infty}$ at the time of maximum erosion, t_m. This time can be found by setting the time derivative of (Eq. 5.3) to zero. This results in an equation that has to be solved iteratively and then t_m has to be substituted in (Eq. 5.5) to find the value of the ratio $\frac{R_{max}}{R_\infty}$.

In this work the graphical solution for $\frac{R_{max}}{R_\infty}$ proposed by Ferreira et al. (1995) has been preferred over the analytical solution. The graphical method consists on, once β has been obtained, reversing (Eq.11) to obtain a function as the ones shown on Figure 5.4.

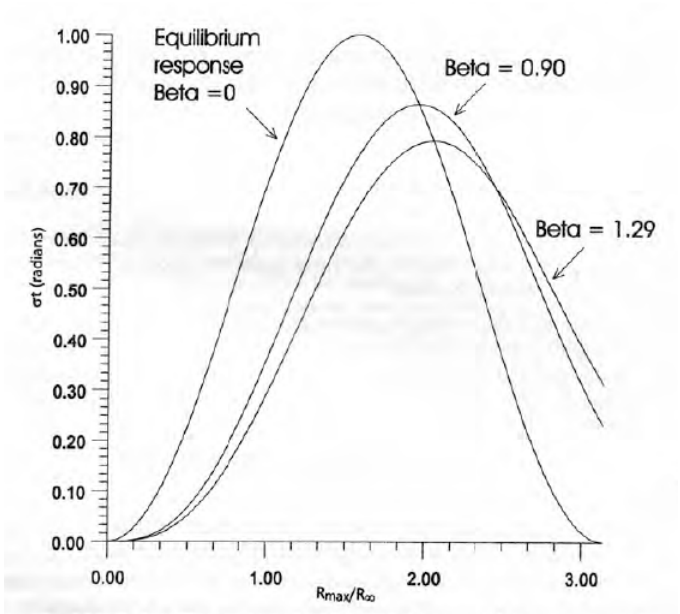

Figure 5.4. Graphical solution of $\frac{R_{max}}{R_\infty}$, (Ferreira et al., 1995).

From this figure $\frac{R_{max}}{R_\infty}$ is obtained as the maximum value of the function.

To sum up, in order to predict the response and eroded volume of any given beach profile using the Convolution Method it is first necessary to obtain two values: R_∞ and T_S.

Kriebel et al. define the maximum potential response R_∞ as a function of the geometrical characteristics of the simplified equilibrium beach profile derived by Bruun (1954) and Dean (1976, 1977, 1991) for open-coast beaches.

Dean's theory states that the profile shape is given by a power-law curve (Eq. 5.13).

$$h = Ax^{2/3} \; or \; x = \left(\frac{h}{A}\right)^{3/2} \quad \text{(Eq. 5.13)}$$

h is the water depth at a distance x offshore from the still-water level and A is a parameter that governs the steepness of the profile and varies primarily with the sediment grain size. The determination of parameter A and its variations with sediment characteristics and wave height has been subject of abundant research (Moore, 1982; Dean et al., 1994; Türker and Kabdas, 2006). The empirical expression proposed by Kriebel and Dean to determine A is (Eq. 5.14).

$$A = 2.25\left(\frac{\omega^2}{g}\right)^{1/3} \quad \text{(Eq. 5.14)}$$

This expression is valid for sediment sizes ranging from 0.1 mm to 0.4 mm. In this work an empirical expression adjusted for coarser sediment has been used (Eq. 5.15) to estimate A directly from the sediment size:

$$A = 0.23D_{50}^{0,44}(mm) \quad \text{(Eq. 5.15)}$$

Dean's original equilibrium profile, Figure 5.5 (a), imposes an infinite slope at the shoreline and a square berm form. To improve this unrealistic approximation, the usual approach is to include a linearly sloping beach face from the berm crest to a point where the beach slope is tangent to the concave equilibrium profile form Figure 5.5 (b). With this change,

$$x = x_0 + \left(\frac{h}{A}\right)^{3/2} \quad \text{(Eq. 5.16)}$$

Where x_0 is the distance from the still-water shoreline to the virtual origin of the concave equilibrium profile form.

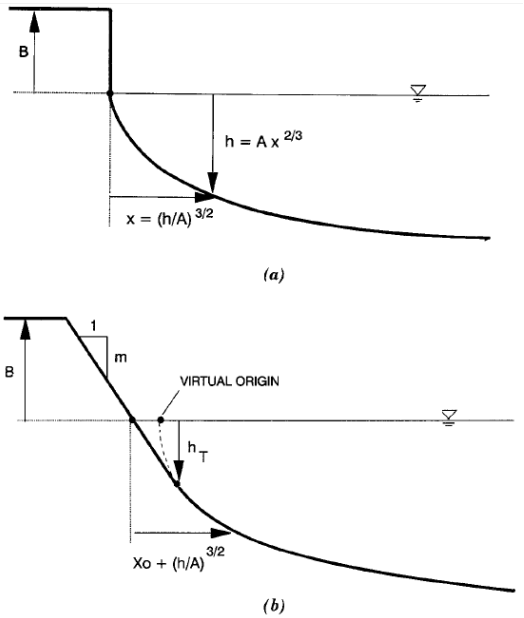

Figure 5.5. Idealized equilibrium profile forms. (a) Square-berm profile with infinite foreshore slope; (b) Equilibrium profile with linear foreshore slope, (Kriebel and Dean, 1993).

It has to be noted that two hypotheses are made in the Convolution Method that are not always true for the event studied in this work.

The first one is that the beach face erodes without changing its slope. This is true in the northern half of the beach of Malgrat and in the central areas of S'Abanell, but Figure 3.6 (Chapter 3) shows that in many other places the pre-storm and post-storm slopes where fairly different. However, the extreme variations are for the Bay of Blanes, which is not being treated in this chapter. Thus, the theoretical error made can be overlooked for a preliminary calculation.

The second hypothesis is that there is conservation of sand on the profile: the sand eroded from the emerged part of the profile is the same than the sand that is accumulated in the submerged part. This is false in the studied event, because according to the results of Chapter 3 and Chapter 4 the overtopping process was intense, moving a fraction of the sand towards the backbeach (overwash). In the previous section it has been stated that overtopping occurs around the peak runup values, generally on the night of 26th December 2008. This concentration of the overtopping on a short period of time comparing to the total duration of the storm makes it possible to use the Convolution Method, but the results will have to been handled with care: they might be correct for almost the entire duration of the storm, but not for the periods were the overtopping occurs.

Figure 5.6 illustrates the two hypotheses of the method and the geometry used:

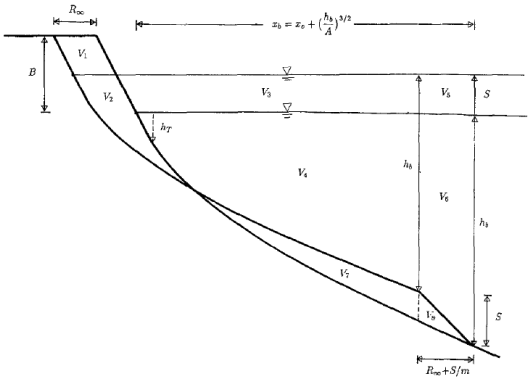

Figure 5.6. Maximum potential response of modified equilibrium profile to water level rise, (Kriebel and Dean, 1993).

The proposed expression for the maximum potential response is:

$$R_\infty = \frac{S\left(x_b - \frac{h_b}{m}\right)}{B + h_b - \frac{S}{2}} \qquad \text{(Eq. 5.17)}$$

B is the berm height, S the water level rise, m the profile foreshore slope and h_b the breaking depth. In the method, h_b and the breaking wave height H_b can be used interchangeably and it is assumed that $H_b = 0{,}78h_b$. Finally, $x_b = x_0 + \left(\frac{h_b}{A}\right)^{3/2}$. For severe storm conditions x_0 is generally small in comparison to the second term and it can be neglected for simplicity.

Once R_∞ is estimated, the potential eroded volume can be obtained. The geometrical relation between the potential berm retreat and the potential eroded volume above the peak storm-surge level is:

$$V_{S\infty} = R_\infty(B - S) \qquad \text{(Eq. 5.18)}$$

Equation (Eq. 5.18) can be problematic when $B = S$. An alternate measure of the storm erosion is the volume eroded from above the original mean sea level, given by (Eq. 5.19).

$$V_{M\infty} = R_\infty B + \frac{S^2}{2m} - \frac{2}{5}\frac{S^{5/2}}{A^{3/2}} \qquad \text{(Eq. 5.19)}$$

This second alternative is more convenient for this work, because the model results have to be compared to the LIDAR measures, which correspond to the volume eroded above the original mean sea level.

The last parameter that has to be obtained is the time scale of the profile response, T_S. The authors of the method state that this parameter seemingly cannot be found from a simple geometrical comparison of pre and post storm equilibrium profiles. Furthermore, at present there is no available analytical estimate for T_S, and field data are too limited to allow meaningful empirical relationships to be developed. The empirical estimate proposed by Kriebel and Dean (Eq. 5.20) is based on numerical experiments. The authors of the method found that T_S is most strongly dependent on the breaking wave height and on the sediment size.

$$T_S = C_1 \frac{H_b^{3/2}}{g^{1/2} A^3} \left(1 + \frac{h_b}{B} + \frac{m x_b}{h_b}\right)^{-1} \quad \text{(Eq. 5.20)}$$

The recommended value of the empirical coefficient C_1 for practical determination of the erosion time scale is $C_1 = 320$.

5.2.2 Application to the studied event

i) Parameter determination and additional hypothesis

The shore-normal profiles used in this section are composed by two different datasets. The emerged parts are the same than in the previous chapters, LIDAR elevation data of the pre-storm situation. The formulation of the method imposes that the underwater part of the profiles follows Dean's geometry.

The initial parameters of each of the profiles are summarized in Table 5.1.

Table 5.1. Convolution Method: Geometrical parameters of the characteristic profiles.

PROFILE	B (m)	m	D_{50} (mm)
A2-5	3.0	0.14	1.4
A3-1	4.0	0.12	1.3
A3-3	4.5	0.14	1.3
A3-10	3.5	0.16	1.2
A5-9	3.0	0.14	1.3
A6-4	2.5	0.16	1.8

Slopes and berm heights have been determined for each profile fitting the real topography to the ideal profile as much as possible. Figure 5.7 displays two examples of the simplifications made. It can be seen that the accuracy of the fit varies, which has important implications on the results because the method is very depending on the berm height. The post-storm measured profile has been added to show in which cases the hypothesis of the method are far from been fulfilled.

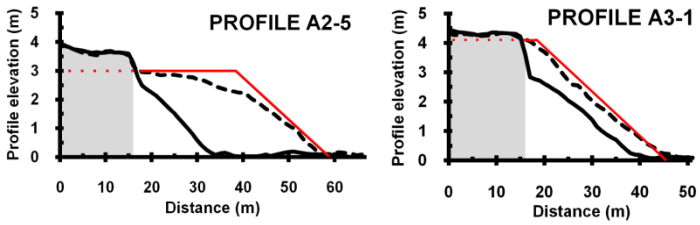

Figure 5.7. Examples of the profile simplified geometry used in the Convolution Method. The grey area represents the maritime promenade.

The breaking wave characteristics at the studied profiles in Table 5.1 have been estimated from the propagated storm data obtained using Mike 21 (see Chapter 3, Section 3.5). The breaking point is located where the propagated wave heights start to decrease abruptly. The water depth h_B and the distance to the shoreline at the breaking point x_B have been calculated using Dean's expressions. Lastly, the surge has been set to 0.5 metres to represent the extreme conditions.

However, the direct application of the method causes problems because the real profiles around the river delta are significantly different to the equilibrium profile (see Fig. 5.8). The sediment transported by the river through the years accumulates and forms a flat land stretch (see Chapter 3, Figure 3.12). The wave propagation made is based on the real bathymetry of the area. For this reason, there is a significant discrepancy between the distances to the wave breaking point given by Dean's formulas and the values obtained from the propagated storm. The erosion is very dependent on x_B, and it has been preferred to the propagated values because they are closer to the real situation.

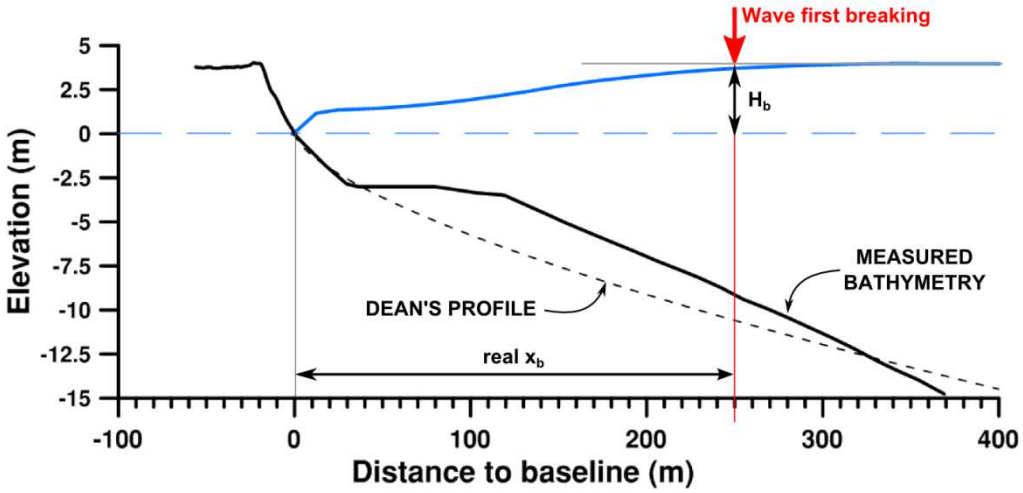

Figure 5.8. Wave characteristics used by the Convolution Method. Profile A3-10.

A second problem related to the bathymetry is that the resolution of the data of profile A6-4 is lower than in the rest of the area, and it does not reflect the flat stretch of sea bottom. To overcome this situation, the distance to the breaking point has been established equal to the adjacent profile (A5-9).

Table 5.2. Convolution Method: Wave characteristics at the breaking point for the characteristic profiles.

PROFILE	H_b (m)	h_b (m)	x_b (m)
A2-5	3.5	4.5	185
A3-1	4.0	5.1	250
A3-3	4.0	5.1	250
A3-10	3.9	5.0	250
A5-9	4.0	5.1	230
A6-4	3.5	4.5	230

ii) Results

The potential beach retreat values obtained calculated using the Convolution Method, R_{max}, are shown on Table 5.3. For the profiles A3-1 and A3-3 the modelled retreat is bigger than the initial beach width, so the maximum possible retreat (R'_{max}), of the beach has been set to equal this initial width.

Table 5.3. Convolution Method: Potential (R_{max}) and maximum possible (R'_{max}) beach retreat for the characteristic profiles.

PROFILE	R_{max} (m)	Berm initial width (m)	R'_{max} (m)
A2-5	10.5	20	11.5
A3-1	11.6	5	5

A3-3	11.3	1*	1*
A3-10	13.2	**	13.2
A5-9	12.3	80	12.3
A6-4	15.0	31	15.0

*The berm initial width of profile A3-3 is practically zero, but it has been set to the minimum value 1 metre to apply the method. **The profile A3-10 is not physically limited landward, it is located in the camping site area).

Using the maximum possible retreat values R'_{max}, the corresponding eroded volumes for the emerged part of the profiles are:

Table 5.4. Convolution Method: Eroded volumes above mean sea level for the characteristic profiles.

PROFILE	ΔV_{+0}^{CONV} (m^3/m)	ΔV_{+0}^{LIDAR} (m^3/m)
A2-5	32.0	57.3
A3-1	20.4	20.7
A3-3	4.8	14.9
A3-10	46.4	39.6
A5-9	37.1	19.4
A6-4	37.9	23.4

5.3 SBEACH numerical model

5.3.1 Model overview

SBEACH (Storm-induced BEAch Change) numerical simulation model was developed at the U.S. Army Waterways Experiment Station, Coastal Engineering Research Center (CERC), to calculate beach and dune erosion under storm wave action. The original version by Larson and Kraus (1989) has been modified and over the years, including additional coastal processes and improving its calibrations with more field experiments. SBEACH is an operational model that has been used in many applied and fundamental studies.

SBEACH is empirically based, and its fundamental assumption is that profile change is produced solely by cross-shore processes, resulting in a redistribution of sediment across the profile with no net gain or loss of material. This approach, that neglects alongshore processes, is expected to be valid for short-term storm-induced profile response on open coasts away from tidal inlets and coastal structures.

The input data required by the model concerns both the storm and the beach characteristics. The essential input data needed to characterize the storm include time series of wave height, wave period, and total water elevation (tide and surge). The beach is characterized by pre- and post-storm beach profiles (survey data) and median sediment grain size. Optionally, wave direction and wind speed and direction can also be specified. In this work wave direction is known and can be included in the model, but wind is overlooked.

The main advantage of the SBEACH model over the Convolution Method is that the former has the capability to deal with real and irregular beach profiles. It does not require simplifying the bathymetry to an idealised equilibrium profile. In addition, SBEACH can mathematically model overwash caused by elevated water elevation and wave runup.

As it has been previously noted, the high runup peaks that occurred during the storm of Sant Esteve resulted in overtopping along almost the entire study area. The overtopping did not

last for the entire duration of the storm, but in some places it covered fairly long periods of time (up to almost a day). Sand deposits on the backshore have indeed been detected on the LIDAR-based analysis of the beach morphological adaptation to the storm conditions (Chapter 4).

Figure 5.9 shows the two kinds of overwash that exist: overwash by runup and overwash by overflow. The former occurs when the storm tide water level is lower than the berm crest or freeboard value, but some waves overtop the beach. The latter occurs when the storm tide is higher than the freeboard. The SBEACH model can only predict values for overwash by runup, generally underestimating the resulting sand deposits.

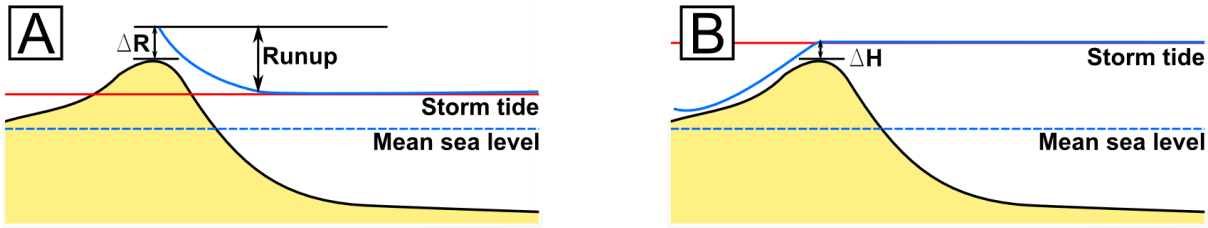

Figure 5.9. Definition sketches showing the cross-section of a beach subject to overwash by wave runup (A) and overwash by overflow (B). Adapted from the Regional Sediment Management Demonstration Program Technical Note 14, US Army Corps of Engineers, 2004.

5.3.2 Application to the studied event

i) Input data and calibration

The storm and beach characteristics needed to run the SBEACH model are already known, but they have to be adapted to meet SBEACH formal requirements.

Storms

The input wave height and direction data series for each of the six profiles studied have been obtained from the propagation of the simplified storm using the same methodology than the one used to obtain H_B and θ_B in the Convolution Method (see Figure 5.8), but choosing the values at a water depth of 20 metres and not at the breaking point. As the propagated storm is a simplified version of the real one with only six data points, the rest of the data has been obtained interpolating linearly between those values. The period and wave elevation data are known hourly, and they are common to all the reaches.

SBEACH requires wave directions to be established with reference to the coast orientation. Table 5.5 shows the coast orientation angles used to transform the data.

Table 5.5. Orientation of the characteristic beach profiles.

PROFILE	º N to the coastline
A2-5	23
A3-1	23
A3-3	23
A3-10	23
A5-9	70
A6-4	55

There are two sets of input storm data for each reach: one using the mean period T_m and one using the peak period T_p. The propagated wave heights and directions series

corresponding to T_m are smooth; those obtained using T_p have peaks and hollows at each step (see Fig. 5.10). The propagated wave characteristics' sensitivity to bathymetric irregularities increases when periods increase. As peak period values are always considerably higher than mean values, the resulting wave heights and directions corresponding to T_p reflect almost instantaneously the irregularities of the sea bottom.

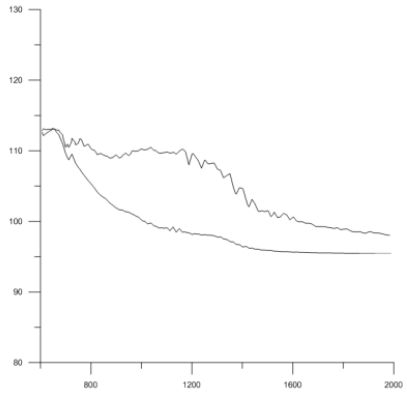

Figure 5.10. Sketch of the difference between wave directions using T_p (above) and using T_m (below).

Reaches

Unlike for the Convolution Method, SBEACH can work with real and complex measured beach profiles. The emerged parts are once again the same than in previous chapters, LIDAR elevation data of the pre-storm situation. The underwater part of each profile has been obtained from transects cast in the available bathymetry.

A seawall has been defined in all reaches except in A3-10 (camping site area) to limit the modelled erosion to the initial beach width. The avalanching angle has been set to 17º, a common value for this area of the Catalan coast.

Finally, the sediment grain size D_{50} should be set to the real known values, but the experience using the SBEACH model on the Catalan beaches has shown that using the real values results in unrealistic model outputs. Moreover, the simulation software does not accept values greater than 1mm. The common and experience-validated approach adopted by researchers is to set the sizes to 0.5-0.7 mm. As in this work the real erosion of the emerged part of the profile is known, the more convenient values of D_{50} have been determined by calibration to the observed results.

Finally, the bathymetry of profile A6-4 has been substituted by its corresponding Dean profile because the resolution of the measured bathymetry is too low to reflect the real situation.

The calibration for each one of the 12 reach-storm combinations has been made varying the sediment transport parameters and the effective grain size. An example is given in Figure 5.11.

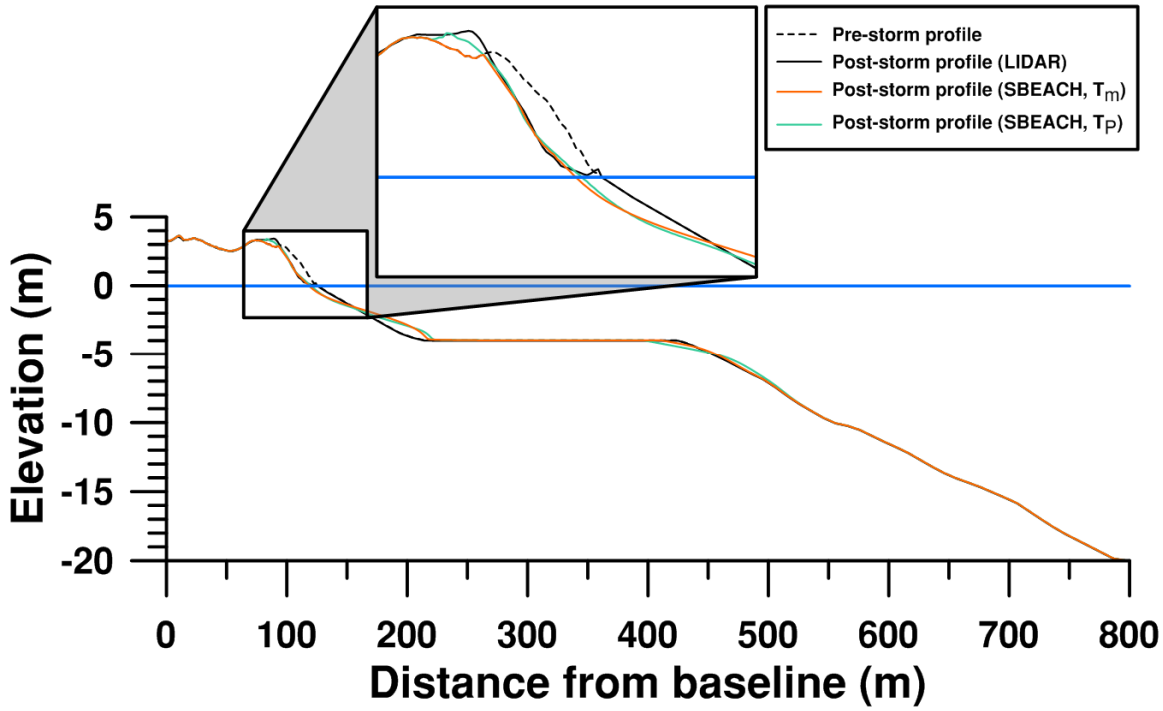

Figure 5.11. Example of SBEACH results. Profile A5-9.

The modelled results are closer to the measured values when the mean period is used, but in this case the overwash material is not reflected. The results obtained using peak periods do reflect some accretion of the backbeach. However, the accretion results are quite poor in S'Abanell, where there is no real data. In addition, the is no need to model the sand deposits in Malgrat, because as they are in the emerged part of the profiles they can be accurately evaluated using the LIDAR elevation data. For this reason, it has been decided to work with the results corresponding to mean period values.

ii) Results

Table 5.6 gives the modelled eroded volumes for the emerged part of the profiles.

Table 5.6. SBEACH: Eroded volumes for the characteristic profiles.

PROFILE	ΔV_{+0}^{SBEACH} (m^3/m)	ΔV_{+0}^{LIDAR} (m^3/m)
A2-5	45.6	57.3
A3-1	23.3	20.7
A3-3	16.7	14.9
A3-10	44.5	39.6
A5-9	23.8	19.4
A6-4	29.5	23.4

5.4 Model comparison and total erosion

5.4.1 Model comparison and validation

Figure 5.12 shows the measured volume variation for the emerged part of each one of the entire set of profiles together with the modelled values using SBEACH and the Convolution Method. The divergence between measured and modelled values is quantified in Table 5.7.

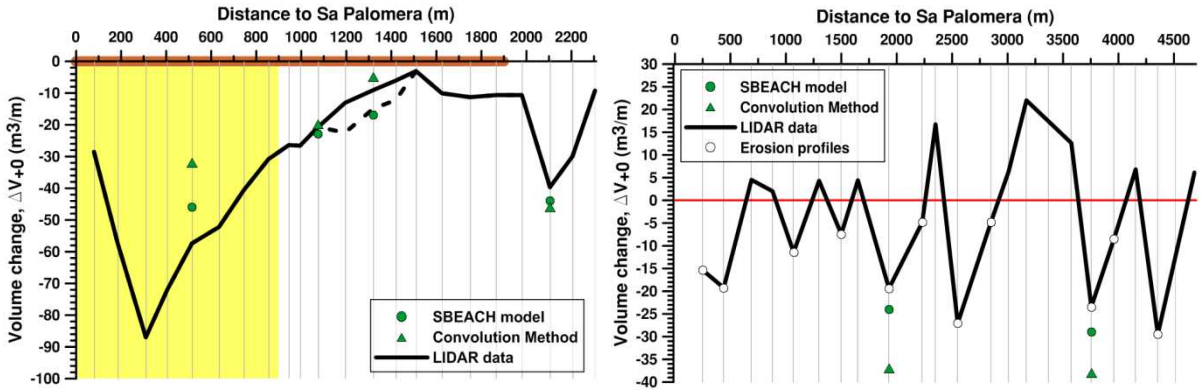

Figure 5.12. Measured and modelled emerged volume variations along S'Abanell (left) and Malgrat (right). The grey lines mark the position of the shore-normal beach profiles, the yellow area the extend of the artificial nourishment and the brown line the maritime promenade.

Table 5.7. Measured and modelled emerged volume variations at the characteristic profiles.

PROFILE	ΔV_{+0}^{LIDAR} (m^3/m)	ΔV_{+0}^{SBEACH} (m^3/m)	$K_1 = \frac{\Delta V_{+0}^{LIDAR}}{\Delta V_{+0}^{SBEACH}}$	ΔV_{+0}^{CONV} (m^3/m)	$K_2 = \frac{\Delta V_{+0}^{LIDAR}}{\Delta V_{+0}^{CONV}}$
A2-5	57.3	45.6	1.26	32.0	1.79
A3-1	20.7	23.3	0.89	20.4	1.01
*A3-3**	14.9	16.7	0.89	4.8*	1.88*
A3-10	39.6	44.5	0.89	46.4	0.85
A5-9	19.4	23.8	0.81	37.1	0.52
A6-4	23.4	29.5	0.81	37.9	0.62

*The geometry of the Convolution Method cannot be adapted to the case in which the promenade fails, as it was the case in this profile. For this reason, the modelled value has been compared to the erosion observed only on the original beach (approximately 9 m^3/m).

It can be seen that in all but one of the profiles (A3-1), the values modelled by SBEACH are more accurate than the ones modelled by the Convolution Method.

Leaving aside profile A2-5, SBEACH results have approximately a 10-20% deviation from the measured values. This deviation is quite constant between profiles and generally an underestimation. In contrast, the Convolution Method has very good results in some cases (A3-1, 3%; A3-10, 14%) but very deficient ones in some others (up to almost 50% in Malgrat). In addition, this second method does not show a clear tendency towards underestimation or overestimation.

Thus, SBEACH results seem to be more robust than the Convolution Method results. This could be caused by the difficulties of fitting the real initial beach profiles to the Convolution idealized geometry and to the marked difference between the real bathymetry and Dean' equilibrium profiles.

Taking into consideration the comments above, SBEACH results are be the ones used for the rest of this analysis.

The case of the artificially nourished part of S'Abanell (profile A2-5) is special: both methods show results significantly lower than the LIDAR measures. The real emerged erosion cannot be obtained with SBEACH without setting unrealistic sediment transport parameters. At the light of the results, it seems sensible to think that some additional hypothesis has to be made in this area. This issue will be addressed later in this work.

5.4.2 Estimation of the total erosion values

The goal of this section is to estimate the total eroded volumes for the entire set of profiles the profiles. Table 5.8 summarizes the erosion results obtained by SBEACH model for the six characteristic profiles. The geometry of the problem is depicted in Figure 5.13.

Table 5.8. Storm-induced erosion for the six characteristic profiles modelled using SBEACH.

PROFILE	ΔV_{+0}^{SBEACH} (m^3/m)	ΔV_{T}^{SBEACH} (m^3/m)	$K_3 = \frac{\Delta V_{+0}^{SBEACH}}{\Delta V_{T}^{SBEACH}}$
A2-5	45.6	59.3	0.76
A3-1	23.3	24.7	0.93
A3-3	16.7	16.9	0.98
A3-10	44.5	46.7	0.95
A5-9	23.8	32.3	0.75
A6-4	29.5	44.0	0.66

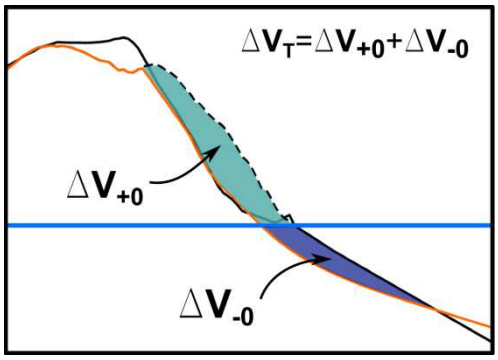

Figure 5.13. Sketch of the emerged, submerged and total erosion of a beach profile.

These results can be extrapolated to the rest of profiles of each of the six zones if the additional hypothesis of (Eq. 5.21) is made in each of those zones.

$$\frac{Emerged\ erosion}{Total\ erosion} = constant = \frac{\Delta V_{+0}^{SBEACH}}{\Delta V_{T}^{SBEACH}} = K_3 \qquad \text{(Eq. 5.21)}$$

This hypothesis is based on the consideration that in each zone there are no longshore significant variations. The limitations of this approach in Malgrat will be addressed later in Chapter 6.

As the measured erosion (ΔV_{+0}^{LIDAR}) in the emerged part of all the profiles is known, the real total erosion ΔV_{T}^{REAL} can be obtained using the following expression:

$$\Delta V_{T}^{REAL} = \frac{1}{K_3} \Delta V_{+0}^{LIDAR} \qquad \text{(Eq. 5.22)}$$

The results for the complete set of profiles of S'Abanell are given in Table 5.9.

Table 5.9. Storm-induced erosion for the entire set of profiles of S'Abanell estimated combining LIDAR data and SBEACH modelling.

PROFILE	ZONE	K_3	ΔV_{+0}^{LIDAR} (m^3/m)	ΔV_T^{REAL} (m^3/m)
A2-1	*A2-5*	0.76	28.0	38.0
A2-2			57.0	76.3
A2-3			87.0	114.3
A2-4			72.0	94.7
A2-5			57.3	75.4
A2-6			52.1	68.6
A2-7			40.5	53.3
A2-8			30.7	40.4
A2-9			26.3	28.3
A2-10			26.5	28.4
A3-1	*A3-1*	0.93	20.7	22.2
A3-2			22.4	22.8
A3-3	*A3-3*	0.98	14.9	15.1
A3-4			12.1	12.4
A3-5			3.0	3.1
A3-6			10.0	10.2
A3-7			11.2	11.4
A3-8			10.6	10.8
A3-9			10.6	10.8
A3-10	*A3-10*	0.95	39.6	41.8
A3-11			29.8	31.5
A3-12			9.2	9.7

This approach cannot be directly applied to Malgrat, because the response to the storm was not the same along the beach. As it has been said in Chapter 3, some profiles suffered erosion and some others accretion. Between an eroded profile and one which suffered accretion, there was generally a zone which recorded very little changes or mixed erosion and accretion (see Fig. 5.14).

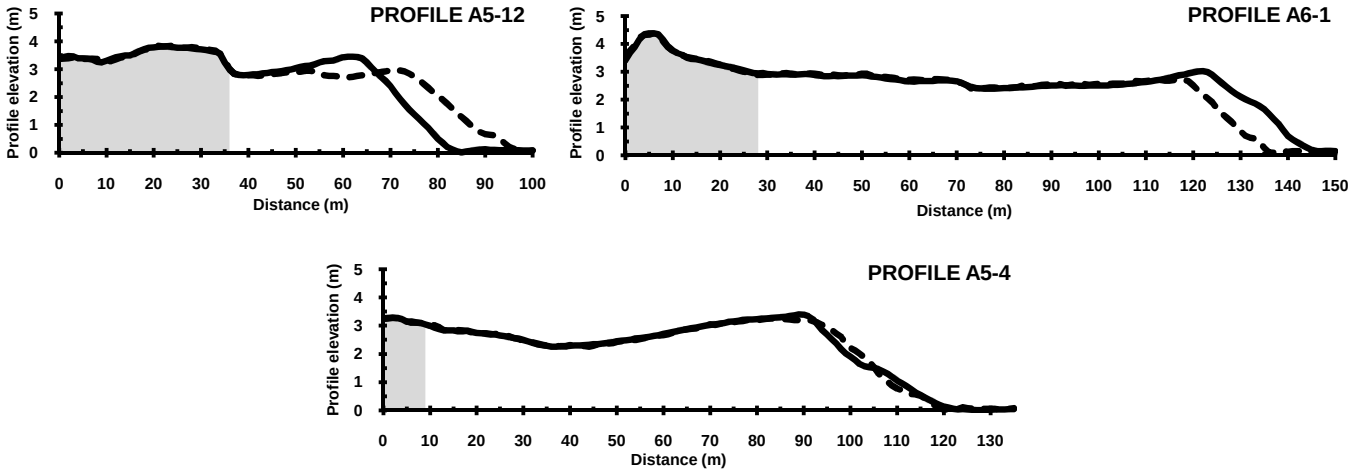

Figure 5.14. Different types of beach response to the storm conditions along the coast of Malgrat: Erosion profile (A5-12), Accretion profile (A6-1) and Mixed profile (A5-4). Dashed line: pre-storm profile. Black continuous line: post-storm profile.

The behaviour of the accretion and mixed profiles will be studied in Chapter 6. Table 5.10 shows the results for the erosion profiles, in which it is assumed that the approach of this chapter can be applied for a first estimation of the erosion rates.

Table 5.10. Storm-induced erosion for the erosion profiles of Malgrat estimated combining LIDAR data and SBEACH modelling.

PROFILE	ZONE	K_3	ΔV_{+0}^{LIDAR} (m^3/m)	ΔV_T^{REAL} (m^3/m)
A5-1	**A5-9**	0.75	15.4	20.5
A5-2	**A5-9**	0.75	19.2	25.6
A5-3			*Mixed profile*	
A5-4			*Mixed profile*	
A5-5	**A5-9**	0.75	11.5	15.3
A5-6			*Accretion profile*	
A5-7			*Accretion profile*	
A5-8			*Mixed profile*	
A5-9	**A5-9**	0.75	19.4	25.9
A5-10	**A5-9**	0.75	4.9	6.5
A5-11			*Accretion profile*	
A5-12	**A5-9**	0.75	27.1	-36.1
A5-13	**A5-9**	0.75	4.8	-6.4
A5-14			*Accretion profile*	
A6-1			*Accretion profile*	
A6-2			*Mixed profile*	
A6-3			*Accretion profile*	
A6-4	**A6-4**	0.66	23.4	-35.6
A6-5	**A6-4**	0.66	8.5	-12.9
A6-6			*Mixed profile*	
A6-7	**A6-4**	0.66	29.5	-44.7
A6-8			*Accretion profile*	
A6-9			*Accretion profile*	

This chapter has permitted to complete the data obtain from the LIDAR surveys. A noteworthy aspect of the results is that they show that, especially in S'Abanell, the storm-induced changes happened primarily on the emerged part of the profiles. This behaviour enhances the advantages of LIDAR as an operational tool for beach monitoring in the study area.

Chapter 6

BEACH RESPONSE TO THE EVENT

The aim of the present chapter is to combine the results obtained in the previous parts of this work. The joint analysis permits to overcome the limitations of each individual approach to the explanation of the studied event. Thus, a picture of the beach response to the storm of Sant Esteve 2008 can be drawn.

6.1 Storm-induced changes in S'Abanell

6.1.1 General behaviour

The beach of S'Abanell is a very rectilinear system with no man-made coastal defences. The beach is only limited in its northernmost end by the headland of Sa Palomera. In this part of the study area, the waves of storm of Sant Esteve 2008 reached the shore with an almost normal angle.

This regularity is to account for the qualitatively homogeneous response of the beach to the event (see Fig. 6.1), with erosion being the prevailing adaptation mechanism to the storm conditions. The erosion took place mainly on the emerged part of the beach, which is the behaviour usually associated with reflective beaches with important slopes.

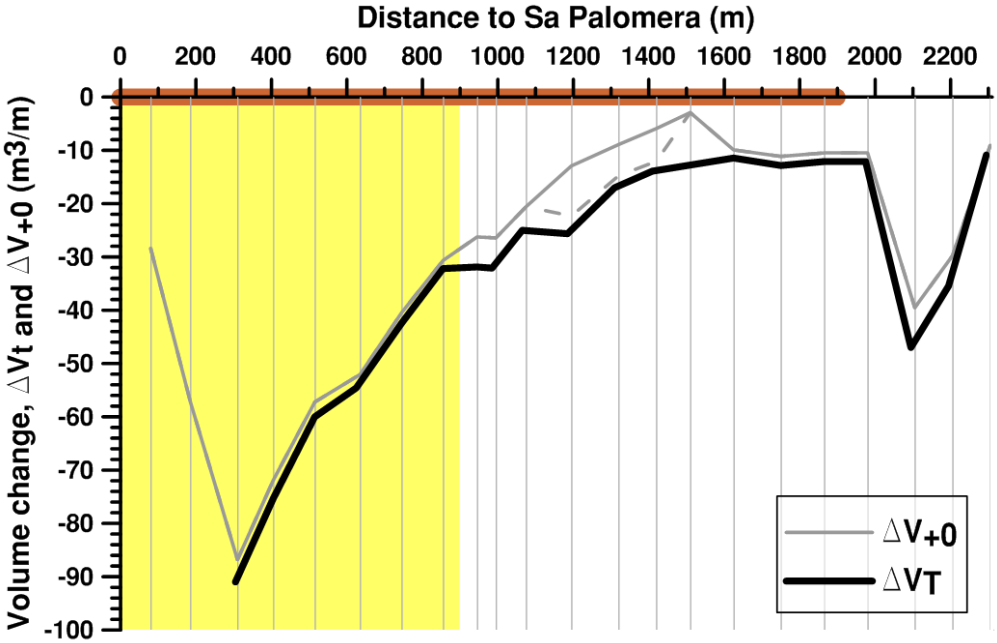

Figure 6.1. Storm-induced erosion along the beach of S'Abanell. The grey lines mark the position of the shore-normal beach profiles, the yellow area the extend of the artificial nourishment and the brown line the maritime promenade.

Nevertheless, the erosion rate was extremely variable along the beach of S'Abanell. Leaving aside the first 200 metres, where the processes had not been studied in detail due to the interference of Sa Palomera, the erosion rate decreased from north to south and ranged from 90 m^3/m to almost zero.

The higher erosion rates were recorded in the area of the artificial nourishment. There, the lidar-based analysis of beach elevations shows that the real erosion was much more significant than the values predicted by different modelling tools. This behaviour has been observed in other artificially nourished beaches, and it can be partly explained using Dean's equilibrium profile theory.

In order to be stable without contention structures, the equilibrium profile of a newly nourished beach has to intersect with the original one. Both profiles can be described by Dean's theory (see Chapter 5) as:

$$x = \left(\frac{h}{A}\right)^{3/2} \qquad \text{(Eq. 6.1)}$$

As the parameter A increases with grain size, coarser material produces steeper profiles. For this reason, artificial beach nourishments are usually done with material coarser than the one of the already existing beach. If the available material is smaller or very similar to the original sand, additional stability structures need to be build (see Fig. 6.2).

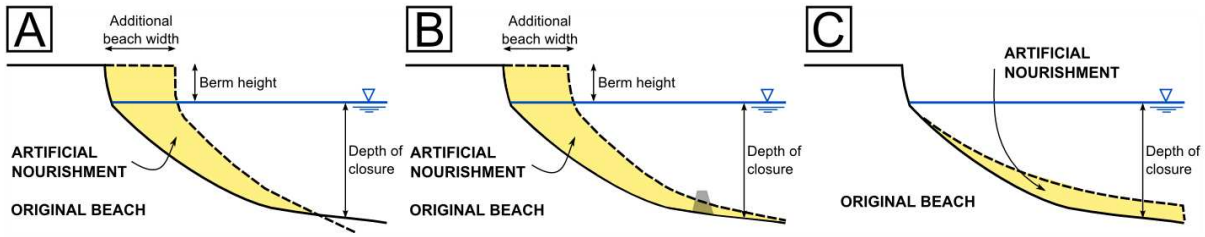

Figure 6.2. Three generic typed of nourished profiles. (A) intersecting, (B) nonintersecting and (C) submerged, (adapted from the Coastal Engineering Manual, U.S. Army Corps of Engineers, 1998).

The beach nourishment of S'Abanell (2008) of was done with 165000 m^3 of sand from the area of Tordera Delta, and therefore its granulometric characteristics were extremely similar to the already existing beach. Thus, the Dean parameter A and the resulting equilibrium profiles of the beach before and after the nourishment should have been very close. In addition, no underwater contention structures were constructed. The nourishment was stable mainly due to the construction slope.

Under the extreme wave conditions of events like the storm of Sant Esteve, the construction slope is destroyed and the new sand moved towards the bottom of the beach to reach the real equilibrium profile (Elko and Wang, 2007), accelerating the normal evolution of the nourished beach as shown on Figure 6.3.

Table 6.1 shows the eroded volumes in the shore-normal profiles studied in the area of the artificial nourishment, S'Abanell North. The last profiles were the transition towards the not-nourished part. Simplifying the beach real response to those representative points, the total eroded volume for the entire area is approximately 75000 m^3.

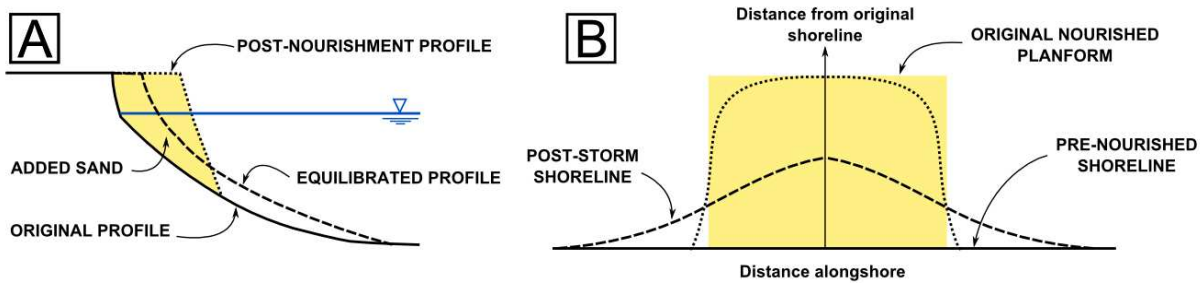

Figure 6.3. Evolution of a nourished beach profile: (A) Profile equilibration via cross-shore transport and (B) Planform adjustment via longshore transport, (modified from Dean, 2002).

The artificial nourishment used 165000 m^3. Given that by the time that the storm struck approximately 15-20% of the sediment had already been lost, the storm of Sant Esteve took away more than 55% of the nourishment.

Table 6.1. Total eroded volumes in the artificially nourished beach (S'Abanell North.

PROFILE	LENGTH (m)	ΔV_T^{REAL} (m^3/m)	ΔV_T^{REAL} (m^3)
A2-1	80	38.0	3039
A2-2	105	76.3	8013
A2-3	120	114.3	13721
A2-4	100	94.7	9469
A2-5	110	75.4	8294
A2-6	110	68.6	7545
A2-7	120	53.3	6402
A2-8	110	40.4	4449
A2-9	90	28.3	2543
A2-10	40	28.4	1138

In the central area of S'Abanell the erosion rates were moderate and constant at approximately 10-12 m^3/m (see Table 6.2). However, this is explained by the pre-storm situation rather than by the event extreme conditions. In this area, the original beach was very narrow with almost no developed berm. The storm eroded the beach until it reached the maritime promenade, which acted as a seawall. In many places (between the profiles A3-1 and A3-5), the energy of the storm destroyed the promenade.

Table 6.2. Total eroded volumes in S'Abanell South.

PROFILE	LENGTH (m)	ΔV_T^{REAL} (m^3/m)	ΔV_T^{REAL} (m^3)
A3-1	120	22.2	1773
A3-2	120	22.8	2737
A3-3	125	15.1	1890
A3-4	100	12.4	1236
A3-5	90	3.1	275
A3-6	115	10.2	1171
A3-7	125	11.4	1428
A3-8	115	10.8	1237
A3-9	110	10.8	1183
A3-10	120	41.8	5018
A3-11	100	31.5	3152
A3-12	100	9.7	967

However, the nourished area was not eroded evenly: the north was very severely eroded, and the erosion rate progressively decreased towards the south. This tendency continued in the stretch between the end of the nourishment and the camping sites. The last part of S'Abanell, the erosion rates locally increased again.

Given the orientation of the beach (approximately 23º to North), the wave directions (East) and the barrier of Sa Palomera at the north, this erosion gradient could be explained by longshore sediment transport.

6.1.1 Longshore sediment transport

Longshore sediment transport (LST) results of the combination of waves and currents in the nearshore, It is a process that occurs during both storm and non-storm conditions. It consists on the displacement of volumes of sediment (the littoral drift) parallel to the coast. The intensity and direction of this process may vary seasonally, resulting in gross and net transport rates (see Fig. 6.4).

Gross longshore transport is the total transport up and down the beach for the time studied. Net longshore transport is the summation of the movement under all wave trains arriving at the shore, and is generally significantly smaller than gross transport (Komar, 1998).

The potential longshore transport rate is usually expressed as an immersed-weight transport rate. I_l. As

$$I_l = KP_l \qquad \text{(Eq. 6.2)}$$

P_l represents wave conditions and K is a dimensionless proportionality coefficient. P_l is often referred as the longshore component of wave power and involves the wave energy flux per unit. $(ECn)_b$, converted to a unit-shoreline basis:

$$I_l = KP_l = K(ECn)_b \sin\alpha_b \cos\alpha_b \qquad \text{(Eq. 6.3)}$$

The energy flux is evaluated at the breaker line using the expressions

$$\begin{cases} Wave\ energy\ density: & E_b = \left(\frac{1}{8}\right)\rho g H_b^2 \\ Wave\ phase\ velocity: & C_b = \sqrt{g(h_b + H_b)} \end{cases} \qquad \text{(Eq. 6.4)}$$

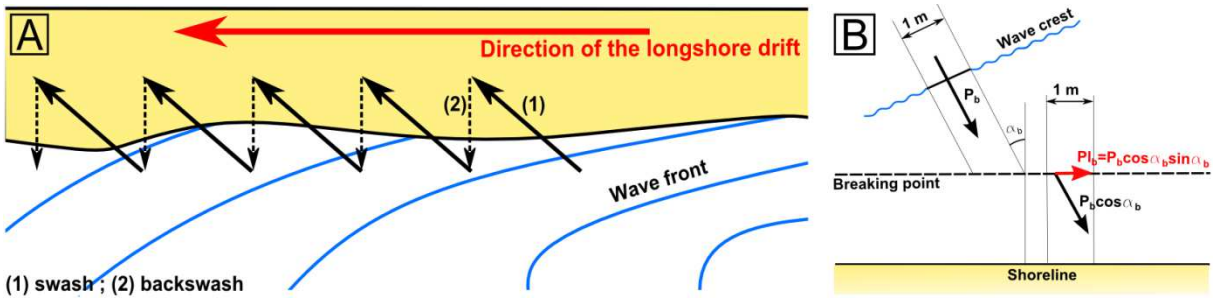

Figure 6.4. Longshore sediment transport: (A) Components of the longshore drift and (B) Wave energy flux.

Lonsghore sediment transport in the Catalan coast has been extensively studied, and the proportion of transport caused by storm conditions ($H_S > 2\ m$) has also been evaluated. This

section is based on the evaluation of the longshore sediment transport capacity at the Catalan coast made by Homar (2010). For the study area, Homar's estimations of the transport rates in an average year are given in Table 6.3.

Table 6.3. Longshore sediment transport estimation in average year: total, by wave direction and in storm conditions ($H_S > 2m$), (Homar ,2010).

Beach	Direction of Littoral Drift	Total LST (m3/year)	Wave direction			Hs	
			Wave direction	LST (m3/year)	%	LST (Hs>2m)	%
S'Abanell North	South	26396	ENE	8666	32.8	4392	50.7
			E	15651	59.3	9368	59.9
			ESE	2079	7.9	1268	61.0
	North	8074	ESE	209	2.6	137	65.6
			SE	3066	38.0	1206	39.3
			SSE	2311	28.6	366	15.8
			S	1813	22.5	379	20.9
			SSW	675	8.4	292	43.3
S'Abanell South	South	12544	ENE	4436	35.4	2196	49.5
			E	7167	57.1	4316	60.2
			ESE	941	7.5	584	62.1
	North	3587	ESE	91	2.5	63	69.2
			SE	1371	38.2	556	40.6
			SSE	1029	28.7	169	16.4
			S	805	22.4	175	21.7
			SSW	291	8.1	133	45.7
La Tordera	South	148139	ENE	60975	41.2	27715	45.5
			E	77052	52.0	46398	60.2
			ESE	10112	6.8	6280	62.1
	North	38573	ESE	979	2.5	676	69.1
			SE	14742	38.2	5974	40.5
			SSE	11068	28.7	1812	16.4
			S	8654	22.4	1877	21.7
			SSW	3130	8.1	1428	45.6
La Tordera - Arenys	South	168268	ENE	9643	5.7	5698	59.1
			E	65749	39.1	38108	58.0
			ESE	60999	36.3	26919	44.1
			SE	31216	18.6	12952	41.5
			SSE	661	0.4	144	21.8
	North	114825	SSE	1495	1.3	281	18.8
			S	15557	13.5	2833	18.2
			SSW	77843	67.8	16942	21.8
			SW	19785	17.2	2061	10.4
			WSW	145	0.1	35	24.1

In the study area the transport is more intense towards the south, and it can be seen that LST rates caused by waves coming from the east are the higher rates. They account for more than half of the littoral drift towards the south in S'Abanell (from 59.3% at the north to 52% at the south), and for some 40% in Malgrat.

Homar observed that the behaviour of S'Abanell had three different parts. A summary of the results of the study can be seen on Figure 6.5:

	1 S'Abanell North	2 S'Abanell South	3 Tordera
Gross LST(m^3/yr)	34 500	16 100	186 700
Net LST (m^3/yr)	18 300 (to South)	9 000 (to South)	109 600 (to South)

Figure 6.5. Longshore sediment transport in S'Abanell, (Homar, 2010).

Regarding LST under extreme wave conditions, it can be seen from Table 6.3 that storms have a greater influence on transport to the south direction. This is consistent, because as seen on Chapter 3 the most important storms hitting the study area come from the East, and waves in this direction usually produce transport towards the South. Transport towards the North is lower and generally caused by normal conditions.

In all cases, storms coming from the East (as Sant Esteve 2008 event) account for approximately 60% of the littoral drift associated to that direction. Thus, even though during a storm the prevailing transport process is usually cross-shore sediment transport, extreme events account for a very significant part of longshore transport. This reinforces the observations that major changes on beach morphology take place during storms.

Figure 6.5 shows the average annual behaviour of the beach, but given the direction of the Storm of Sant Esteve it can be assumed that the qualitative response during the event was the same. It can be seen that the area is closed to LST at the northern end, but open at the south. The sediment migration towards the south is more important on the north, gradually decreases towards the south and presents another peak at the limit with the mouth of the Tordera. This behaviour matches the fluctuations of the beach response to the storm (see Fig. 6.1).

Longshore transport implies that during the storm any given profile loses sediment moved off-shore by the waves, but at the same time it gains/loses sediment transported by the longshore component of the same waves. Given that the incidence angle of the waves in S'Abanell was close to normal, it could be thought that LST was not a major process. However, the abundant sediment available due to the nourishment gave to the northern part of S'Abanell had a high capacity to lose sediment, boosting LST. The sand from the nourishment moved southwards without being compensated by sand coming from the north, hence adding another factor to its accelerated erosion.

The sediment transported by LST moves until the forcing conditions stop or until it reaches an obstacle. As S'Abanell is a rectilinear beach without any artificial or natural barrier, sand freely moves until it reaches the Tordera. According to Homar, the river mouth does not represent a barrier for LST. However, in this location the beach orientation abruptly changes

The estimation of the littoral drift associated to the specific event of Sant Esteve 2008 could be the subject of further research. The sediment travelling parallel to the beach of S'Abanell is thus oriented towards an area in front of the river mouth.

The erosion increase observed at the southern end of the beach could be explained by the local wave conditions. The wave propagation showed that the waves reached that area were higher than the waves reaching the north of the beach (see Figure 3.16, Chapter 3).

The total amount of lost sediment in S'Abanell was approximately 97000 m^3.

6.1.2 Overwash

The lidar elevation data shows sand deposits on the camping areas of S'Abanell of approximately 6 m^3/m (see Chapter 4). There are no data about the rest of the study area, because the sand that reached the village was cleaned before the lidar flights. However, there is photographical evidence that there were sand deposits all along the beach (Figure 6.6). Given the regularity of the beach, it could be assumed that the rate was the same all along the beach. That would represent a total amount of overwash material of around 13000 m^3.

Figure 6.6. Overwash in S'Abanell.

However, this is a very rough estimate and certainly an overestimation. Overwash depends on the capacity of the waves to overtop the berm, and thus on the freeboard. The camping area, which is the only place where the sand deposits could be measured using lidar, are the lowest points of the beach and therefore surely suffered more overwash that the northern areas.

6.2 Storm-induced changes in the beaches of Malgrat

6.2.1 General behaviour

The analysis of the lidar data has shown that the response of the beach of Malgrat de Mar to the impact of the studied event was more complex than the response of S'Abanell. Even though some areas were eroded like S'Abanell, it was not a generalized behaviour. Figure 6.7 shows the spatial distribution of the areas of erosion and accretion (not considering the overwash of the backshore). In addition, the results obtained using SBEACH model match

the observed data of the emerged part of the profile with less accuracy than in S'Abanell (around a 20% deviation in Malgrat. and a 10% in S'Abanell). The Convolution Method has even poorer results, with predictions that double the observed values.

Figure 6.7. Spatial distribution of the areas of erosion and accretion along the beach of Malgrat (not considering the overwash of the backshore.

Taking the above observations into consideration, the response of the beach of Malgrat to the storm of Sant Esteve 2008 has to have been driven by additional processes which are not accounted for by the used models. Both the Convolution Method and the SBEACH model for storm-induced changes are based on the hypothesis of a homogeneous beach which can be represented by a shore-normal profile: they consider the beach to be a two-dimensional system and neglect alongshore variations. This simplification hypothesis, which can be applied to S'Abanell without a great accuracy loss, has to be revised in the case of Malgrat.

The main difference between the beaches of Malgrat and S'Abanell is their planform. Unlike S'Abanell, Malgrat is not rectilinear. Its orientation shifts slowly from almost 90ºNorth at the mouth of the river Tordera towards smaller angles at the south. This curvature gives the beach a concave planform. Moreover, there are some small groynes scattered along the beach. The combined effects of the curvature and the groynes make the beach a clearly three-dimensional system (see Fig. 6.8).

Given that the prevailing wave direction during the storm was east, the waves reached Malgrat with an oblique angle. Even though wave refraction due to the sea bottom tends to align wave crests with the bathymetry and thus to the shoreline, it does not so with such intensity as to make the waves reach the coast in a perfect normal angle. The incidence angle increased towards the south, reaching values similar to the ones of S'Abanell in the southern end.

Figure 6.8. Irregularities in the beach of Malgrat: groynes and changing orientations.

(Eq. 6.3) from the previous section implies that oblique wave incidence angles boosts longshore sediment transport. If in a given beach stretch there are no barriers to stop the migration of this sediment, it moves until the forcing conditions stop. This is the case in S'Abanell, where the beach is a rectilinear system not limited in its south-west end but closed at the north.

In his study of LST along the Catalan coast, Homar (2010) includes the beaches of Malgrat in a homogeneous unit that stretches from the Tordera to Arenys. The general behaviour of the unit can be seen on Figure 6.9.

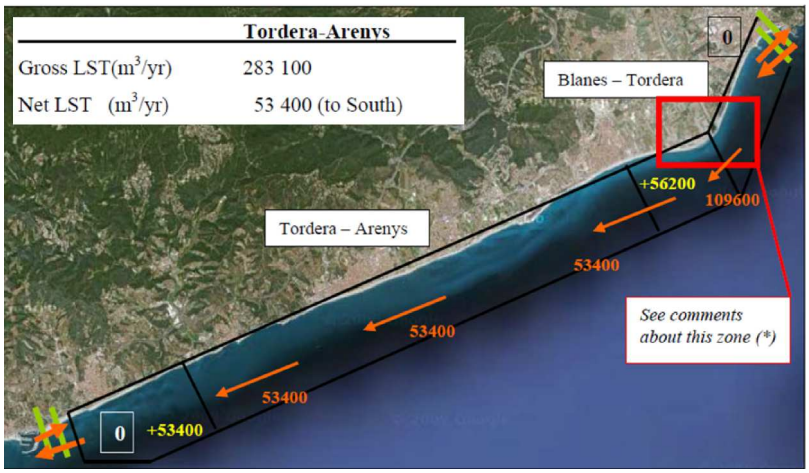

Figure 6.9. Evaluation of longshore sediment transport along the zone of La Tordera – Arenys, (Homar, 2010).

The unit considered by Homar is appropriate for the general study of the Catalan coast, but too much of a simplification for the analysis of the response of the beach of Malgrat to the storm of Sant Esteve. It is necessary to zoom in to the study area, maintaining the open boundary conditions. The orientation of the beach of Malgrat forms a concave layout, but it does not change at a constant rate: some major directions can be sensed where the coast is nearly strait (see Fig. 6.10).

Figure 6.10. Major beach orientations in Malgrat.

Comparing the response of the beach (Figure 6.10) to its geometrical properties (Figure 6.11), it can be seen that the accretion spots are not randomly located. They are generally located near the places where the beach orientation changes more abruptly or where there is a breakwater. It could be implied that the beach "vertices" and groynes act as sediment traps.

Figure 6.11. Location of the accretion spots in the beach of Malgrat and geometrical irregularities.

At the northeastern part of the beach the wave incidence angle is very oblique, and thus it can be assumed than alongshore transport was an intense process that eroded the river mouth significantly. This erosion due to longshore transport has to be added to the cross-shore sediment erosion normally associated to storms.

The first accretion spot is located where the beach orientation shifts quite significantly (from about 80ºN to about 65ºN). This vertex acted as a natural contention measure, trapping the

sediment. The sediment trapped moves the vertex upstream, accounting for the regressive accretion. Figure 12 (a) shows the proposed explanation for this mechanism.

The second major accretion spot can be explained by the same mechanism boosted by the presence of the groynes (see Fig. 12 (a) and (b)). The accretion in this second spot was more intense than in the previous one, with a peak of 22 m^3/m at the profile A6-1. This could be explained by the fact that there was more sediment that could potentially be trapped, because the first spot may not have been a total barrier.

The last stretch of the beach (profiles A6-4 to A6-7) is where the incidence angle of the waves was closer to normal. Thus, it can be thought that the importance of cross-shore sediment transport was greater than in the previous sections, and longshore transport less pronounced (but important still). This would account for the high erosion rates, 30 m^3/m in some parts.

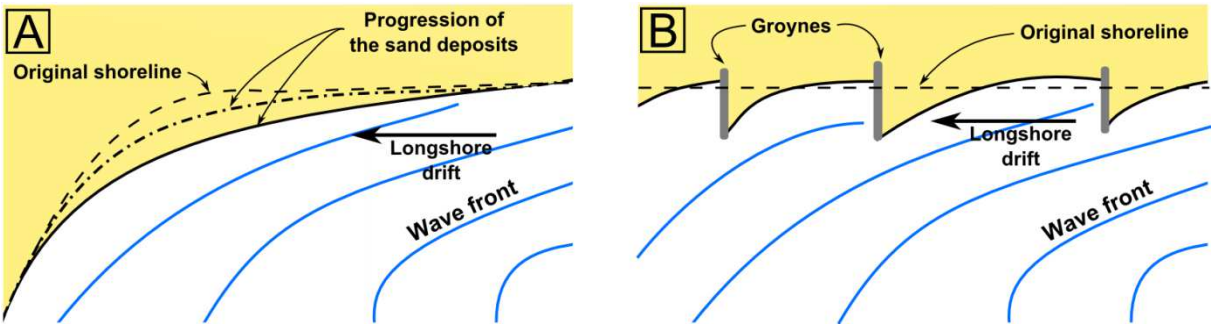

Figure 6.12. Barriers to longshore sediment transport: (A) Change in the beach orientation and (B) Presence of groynes.

Lastly, there was a very developed accretion stop at the south-west end of the study area. In this point the beach orientation shifts abruptly, but in the opposite direction than previously. According to Figure 6.13, this should translate in erosion and sediment loss. However, the area has many small groynes whose mission is to trap the sediment in non-storm conditions, when longshore transport is the prevailing mechanism. During this specific event, and due to the waves' incidence angle, the groynes were also very active during the storm. They trapped sediment until they were saturated, as it can be seen in Figure 6.13.

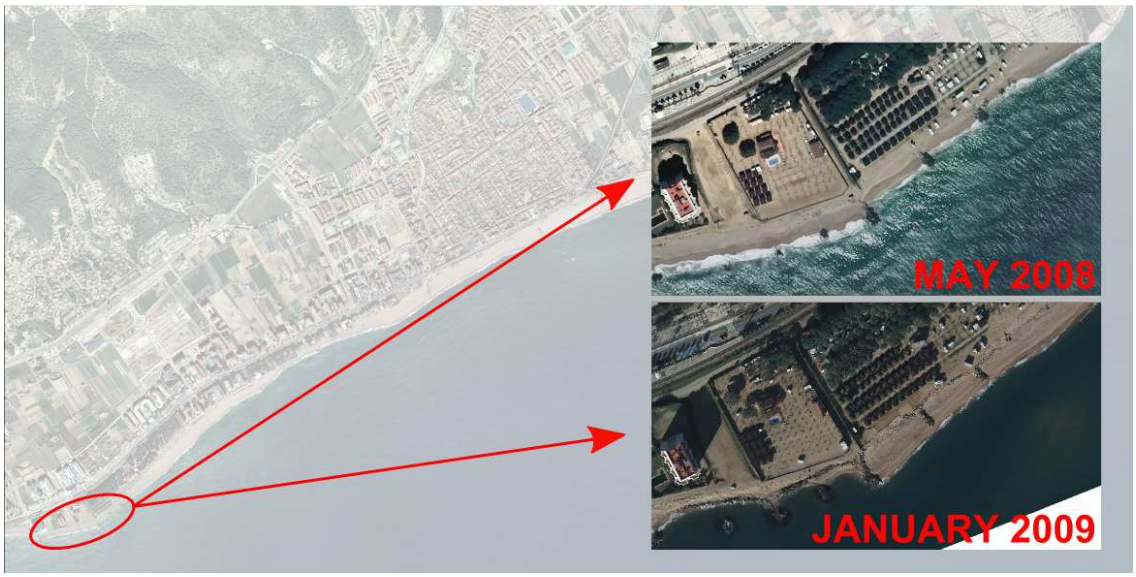

Figure 6.13. Saturation of the southernmost groynes of the beach of Malgrat.

At the light of these observations it can be induced that the response of the beach of Malgrat to the storm of Sant Esteve to 2008 was deeply affected by longshore sediment transport, not only by cross-shore sediment movements. The relative high importance of the first process is stressed by the fact that the shoreline did not suffer major changes except at located hot spots.

Moreover, there is a second aspect of the storm-induced changes in Malgrat that has to be studied. The shore-normal profiles show that, even in the eroded parts, there was accretion of the backshore.

6.2.1 Overwash

Figure 6.14 shows an example of the accretion measured in the backbeach of the shore-normal profiles cast in Malgrat. The hypothesis made to explain this behaviour is that, as it was the case in S'Abanell, the accretion is overwash material.

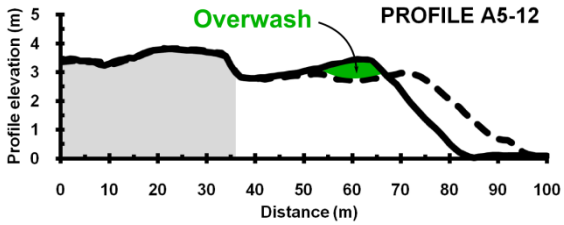

Figure 6.14. Example of overwash induced by the storm in the beach of Malgrat.

Given that overwash is dependent on the overtopping of waves because it is the discharged water that carries the sediment, a study of the overtopping at each profile has been made. The overtopping has been calculated using not the deep water wave conditions as in Chapter 3, but the local nearshore conditions of the propagated storm. In addition, the calculations were done using the values of freeboard and slope of each profile, not the medium values of the areas defined in Chapter.

Figure 6.15 shows the correlation between the estimated overtopping and the measured overwash. The graphical representation suggests that higher overtopping values are related to higher deposits, but the correlation is poor due to some of the highest overtopping peaks.

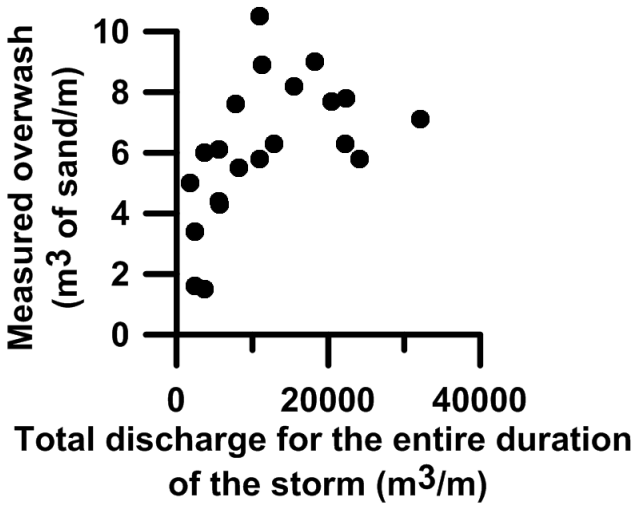

Figure 6.15. Correlation between the measured overwash and the estimated overtopping.

In addition, the shape of the backshore sand deposits is different in Malgrat and in S'Abanell: in Malgrat they are higher and sloped landwards. In S'Abanell, at least in the area where aerial photographs allow the analysis, the deposits are low and cover wide extensions of the backbeach (see Fig. 6.16 (b)). By contrast, in Malgrat they form a new, continuous and higher berm along the entire beach (see Fig. 6.16 (a)).

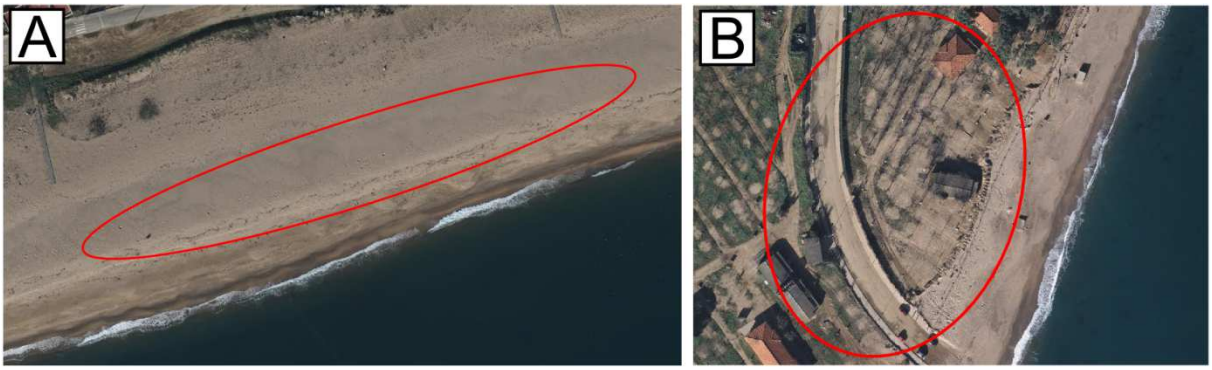

Figure 6.16. Location of the overwash in (A) Malgat and (B) S'Abanell.

This configurations hint that the deposits may have been formed in a slightly different way, even though both would be caused by overwash material. In the lowest areas of the study zone, like the south of S'Abanell (freeboard around 2.5 metres), many waves could overtop the berm and produce overwash. In the high zones as Malgrat, the overtopping was produced only by the very highest waves.

Waves that would produce overtopping if they reached a low profile may be only capable of reshaping a higher one (if the rest of the beach characteristics remain constant). The overwash observed in Malgrat would be in part the result of the reshaping of the beach profile under the storm wave conditions.

Bagnold (1940) demonstrated that the berm elevation depends on the wave run-up height on the sloping beach face, and thus in part on the wave height. The proposed relation is:

$$Berm\ elevation = b \cdot H \qquad \text{(Eq. 6.5)}$$

$$b = \begin{cases} 1.68\ for\ D = 0.7\ cm \\ 1.78\ for\ D = 0.3\ cm \\ 1.8\ for\ D = 0.05\ cm \end{cases} \qquad \text{(Eq. 6.6)}$$

Further studies of the role of runup in controlling the elevation of the berm by Takeda and Sunamura (1982) and based on previous results by Hunt (1959) have modified this expression to:

$$B_h = 0.125 H_b^{5/8} (gT^2)^{3/8} \qquad \text{(Eq. 6.7)}$$

The physical process behind it is the same for all the beaches and has been described clearly by Komar (1998): After the wave breaks, the water rushes forward up the beach face, carrying sand with it, losing velocity as it goes because it is opposed by gravity and friction and because of water losses through percolation. Bascom (1953) noted that, for the same reason than overtopping, the upward growth of the berm depends mainly on the largest waves, since they are the ones overtopping the crest.

Bascom pointed out the resulting paradox: even though storms tend to destroy the summer berm, they also build up a berm to a higher elevation, because it is when higher runup and wave height values are registered. This happens even when the beach face is being eroded and the extent of the berm is reduced, as it is the case the erosion profiles of Malgrat (e.g. A5-9, A6-4).

6.3 Storm induced changes in the mouth of the River Tordera

This section aims to further develop the study of the evolution of the area surrounding the River Tordera made in Chapter 1. Figure 6.17 shows again the response of the area to the storm (left) and its recovery (right). Storm the response of the area to the storm are given again

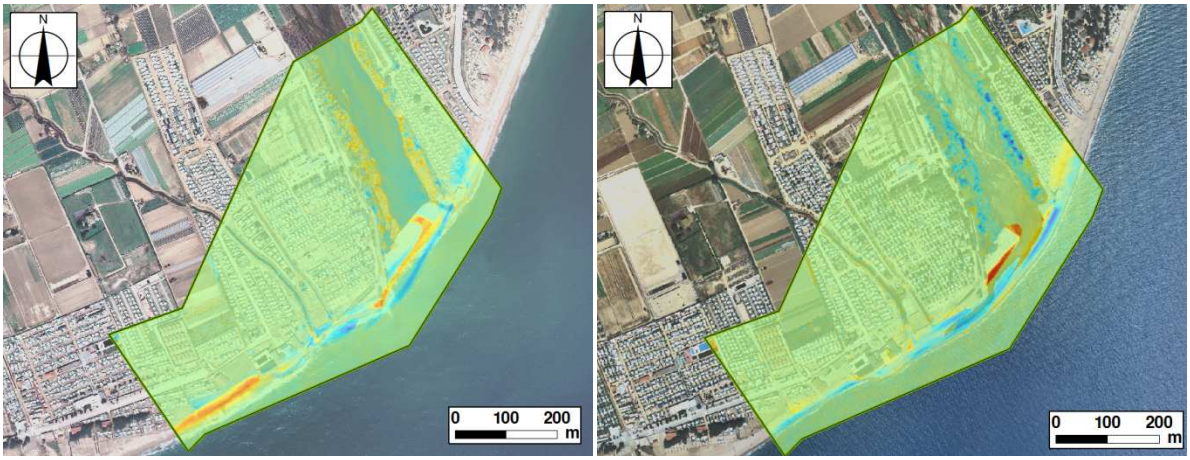

Figure 6.17. Area 4: Left: Changes produced by the storm. Right: Recovery.

The area has two special characteristics, (1) it is located in the place where the coast modifies its orientation and (2) it is affected by the dynamics of the River Tordera.

The sub-balances made for the beach response to the storm given in Chapter 1 and repeated here (see Fig. 6.18) show that the order of magnitude of the sediment lost in the bar is the same that the one of the sediment gained outside the river mouth. This could suggest that the river flow transported the sediment. However, the amount of sediment involved in the process is quite high for a small river as the Tordera.

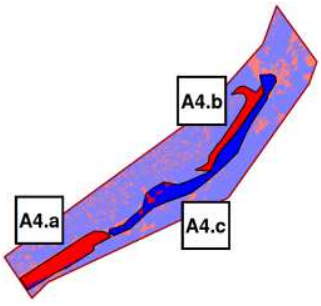

A4.a	**-7166 m³**
A4.b	**-4406 m³**
A4.c	**+6771 m³**

Figure 6.18. Area 4: Sub areas, beach response to the storm.

The Tordera has a mean water flow of 5 m^3/s, which can rise significantly during *Torderades* (see Chapter 2). The sediment transport capacity of the river has been estimated in about 25000 m^3/year (Jiménez, 2007).

The vast majority of this sediment is generally transported during extreme events, but the quantities given by the sub-balances are 20% of the year total capacity, which seems a very high value. The storm of Sant Esteve 2008 produced a rise of the water level of the river on 27th December, but the photographs taken in different locations during the event show that the water hardly overflowed the river banks. The flow associated to the river channel has been estimated to be about 25 m^3/s (Agència Catalana de l'Aigua, 2002).

In addition, it has been said in previous sections that S'Abanell suffered from longshore sediment transport, and that the flow of the material is directed towards the river mouth. The high sediment volumes involved in LST due to the artificial beach nourishment may account for the vast majority of the aggradation in front of the river mouth, prevailing over the sediment transported by the river.

However, even though if it was a secondary role, the river did have an impact on the process because the aerial photographs (see Fig. 6.19) show that the water flow was strong enough to break the sand bar. The shape of the resulting channel gives another hint to reinforce the hypothesis that the sand from S'Abanell had a great impact on the area: the channel is not directed towards the sea, it is curved towards Malgrat. This reflects that the water and sediment flow was weaker than the wave-induced processes.

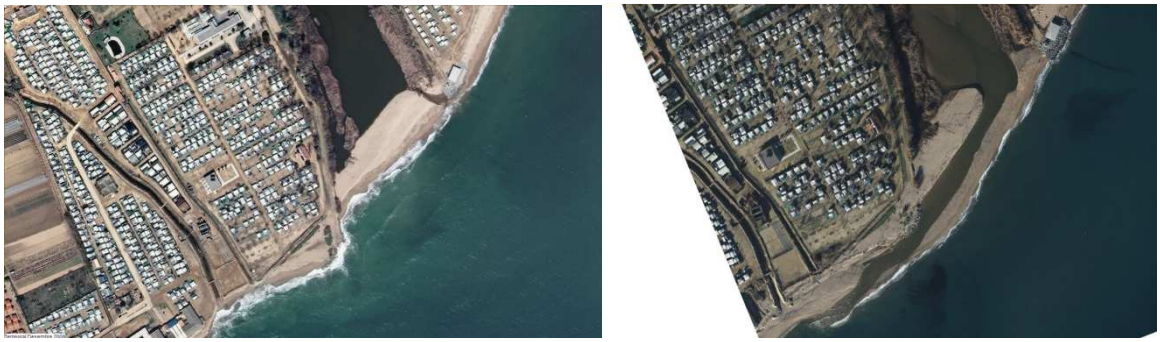

Figure 6.19. The mouth of the River Tordera before (left) and after (right) the storm of Sant Esteve 2008 (ICC).

Chapter 7

CONCLUSIONS

At present, the application of LIDAR to the study and monitoring of the Catalan coast is being developed by the Institut Cartogràfic de Catalunya. In this framework, this work has used LIDAR data to analyze the morphological changes induced by the storm of Sant Esteve 2008 on the Tordera-Blanes area.

The studied event was a type III significant storm characterised by wave heights that reached nearly 8 metres. The combination of the highly energetic waves and the reflective characteristics of the beaches of the study area resulted in extremely pronounced runup.

The analysis of the LIDAR elevation data has permitted to detect the spatial patterns of the emerged beach response to the storm and establish homogeneous areas. In addition, it has proved to be a powerful tool to easily calculate volumetric sediment balances both globally and in shore-normal profiles.

The intrinsic limitation of LIDAR topographic data is that it does not provide information about the submerged part of the beach. However, it has been possible to overcome this limitation using two modelling tools: the Convolution Method and the SBEACH numerical model. The first method has shown poor performance in the beaches of the study area, which are highly reflective and limited by an important human pressure. By contrast, it has been possible to calibrate the SBEACH model to match the measured emerged volume changes.

Furthermore, the results of the SBEACH model for the submerged part of the beach have shown that, especially in S'Abanell, the beach storm-induced changes happened primarily in the emerged part of the beach. If further research shows that this is the common behaviour for the study area, LIDAR will prove to be an even more useful tool to monitor the area, because the lack of bathymetric data would not be an important drawback.

The beach of S'Abanell was severely eroded by the event, and its behaviour matched the theoretical response of a beach to a storm closely because the waves reached it in a nearly normal angle. However, the erosion was much stronger in the northern half of the beach, which had been artificially nourished prior to the storm. In addition, the erosion rate decreased smoothly from north to south, which could be explained by the effects of longshore sediment transport boosted by the available sediment of the nourishment. In some areas the waves reaches the maritime promenade, which means that the beach could not fulfil its protective role.

The response of the beach of Malgrat to the event was deeply affected by longshore sediment transport, because the wave reached it in various oblique angles. This resulted in a heterogeneous beach response, with accretion and erosion profiles. The accretion was located in specific areas that acted as sediment barriers: changes of beach orientation and

artificial groynes. The application of two-dimensional models to this area could lead to significant mistakes, whereas LIDAR measurements described the behaviour accurately.

Overwash occurred along the entire study area, but could not be reflected by LIDAR in S'Abanell. However, data collected in Malgrat permitted to estimate it very precisely, and this is a very encouraging result because overwash modelling is generally difficult.

The storm-induced changes in the mouth of River Tordera have not been studied with as much detail as the open beaches, but it has been seen that the maritime processes were dominant over the river dynamics.

Finally, the LIDAR elevation data obtained by the ICC in summer 2009 shows that the recovery of the beach at that time was not complete. The beach of Malgrat had recovered much more than S'Abanell, a fact certainly linked to the highest anthropic pressure existing in S'Abanell.

BIBLIOGRAPHY

Agència Catalana de l'Aigua. (2002). *"Planificació de l'espai fluvial de la conca de la Tordera: estudi hidràulic"*. P210411/SRLC/ME-01. October 2002. Ed. 1 – Rev.2.

Badosa, E. et al. (2009). "Informe de Seguiment de l'Estat Socioecològic de la Conca de la Tordera". L'Observatori. Agència Catalana de l'Aigua (ACA), Institut de Ciència i Tecnologia Ambientals (ICTA) de la Universitat Autònoma de Barcelona i Ajuntament de Sant Celoni.

CIIRC. (2010). *"Estat de la zona costanera a Catalunya"*. Centre internacional d'investigació dels recursos costaners. Laboratori d'enginyeria marítima. Universitat Politècnica de Catalunya. June 2010.

Coastal Engineering Manual. (1998). *"Coastal Engineering Manual: Cross-shore sediment transport processes"*. U.S. Coastal and Hydraulics Laboratory. Amy Corps of Engineers. Part III-Chapter 2, Part V-Chapter 4 EC 1110-2-292. March 1998.

Coastal Overwash. (2004). *"Coastal Overwash. Part 1: Overview of Processes"* . Tecnical note 14 de la us army. Engineer Research and Development Center, Regional Sediment Management Demonstration Program. Technical Note-14. September 2004.

De Mas, C., Södergren, J. and Larson, M. (thesis supervisor) (2011). *"Modelling coastal erosion in Bjärred, Lomma municipality. Long-term evolution and protective measures"*. Master's thesis. Division of Water and Resources Engineering, Lund University, Sweden.

Dean, R.G.(2002). *"Beach Nourishment Theory and Practice".* Advanced Series on Ocean Engineering, Vol. 18. World Scientific.

Elko, N.A. and Wang, P. (2007). *"Immediate profile and planform evolution of a beach nourishment project with hurricane influences".* Coastal Engineering. Volume 54, Issue 1, January 2007, p. 49–66.

Ferreira, Ó., Dias, J., Gama, C. and Taborda, R. (1995). *"Quantification of beach erosion caused by storms on the Portuguese coast"*. Directions in European Coastal Management. Healy and Doody (eds). Samara Publishing Limited, Cardigan, 1995. ISBN: 1-873692-06-4.

García, C. and Sala, M. (1998). *"Aplicación de fórmulas de transporte de fondo a un río de gravas: comparación con las tasas reales de trasporte obtenidas en el río Tordera"*. Ingeniería del Agua. Vol.5 Num.1 (March 1998), p. 59-72.

Gervais, M., Balouin, Y. and Belon, R. (2012). *"Morphological response and coastal dynamics associated with major storm events along the Gulf of Lions Coastline, France"*. Geomorphology, 143-144 (2012), p. 69–80.

Heurtefeux, H. (2008). *"Lidar technology and beach survey: history, experimentation and assessment"*. Beach erosion monitoring, results from BEACHMED-e/OpTIMAL Project, 2008.

Heurtefeux, H., Lesaignoux, A. and Denamiel, C. (2008). *"Assessment, validation and further uses of Lidar survey in the Western part of the French Mediterranean Sea*. *Beach erosion monitoring*", results from BEACHMED-e/OpTIMAL Project, 2008.

Homar, A. (2010). *"Evaluation of the longshore sediment transport capacity at the catalan coast"*. Barcelona 2010. UPC.

IGC, Institut geològic de Catalunya. *"Llibre verd de l'Estat de la zona costanera a Catalunya".* (2010).

Ilich, K., Bishopp, S., Li, F. and Bicknell, C. (2009). *"Erosive capacity of storms on a typical sandy beach. Cross-Shore sediment transport modelling"*. 5th Western Australian State Coastal Conference 2009.

Jiménez, J.A., Sallenger, A.H., and Fauver, L. (2006). "*Sediment transport and barrier island changes during massive overwash events*". Coastal engineering conference. ASCE, American Society of Civil Engineers, 2006. Conf. 30; Vol. 3, p. 2870-2879. ISSN 0893-8717.

Jiménez, J.A. et al. (2007). *"Informe sobre la problemática actual de la playa de S'Abanell".* Solicitud de las Asociaciones de Campings y Hosteleria de Blanes al CSIC sobre la problemática de erosión en la playa de S'Abanell.

Komar, P.D. (1998). "Beach processes and sedimentation". College of Oceanic & Atmospheric Sciences, Oregon State University. Prentice Hall, ISBN: 0-13-754938-5.

Kriebel, D.L. and Dean, R.G. (1993). *"Convolution method for time-dependent beach-profile response"*. Journal of Waterway, Port, Coastal and Ocean Engineering. 1993.119 p. 204-226.

Laudier, N.A. and MacMahan, J. (thesis advisor) (2009). *"Wave overtopping of a barrier beach"*. Thesis. Naval Postgraduate School Monterey California. September 2009.

Maspataud, A., Ruiz, M.H. and Hequette, A. (2009). *"Spatial variability in post-storm beach recovery along a macrotidal barrel beach, southern Nord Sea"*. Journal of Coastal Research, SI 56 (Proceedings of the 10th International Coastal Symposium), p. 88-92. Lisbon, Portugal. ISSN 0749-0258.

Mendoza, E.T. and Jiménez, J.A. (2006). *"Storm-induced beach erosion potential on the Catalonian coast"*. Journal of Coastal Research, SI 48 (Proceedings of the 3rd Spanish Conference on Coastal Geomorphology), p.81-88. Las Palmas de Gran Canaria – Spain, ISSN 0749-0208.

Mendoza, E.T., Jiménez, J.A. and Mateo, J. (2011). *"A coastal storms intensity scale for the Catalan sea (NW Mediterranean)"*. Natural Hazards and Earth System Sciences, 11, p. 2453-2462, 2011.

Morton, R.A. Paine, J.G. and Gibeaut, J.C. (1994). *"Stages and durations of Post-Storm Beach Recovery, Southeastern Texas Coast, U.S.A."*. Journal of Coastal Research 10 4, p. 884-908. Fall 1994.

Morton, R.A. (2002). *"Factors controlling storm impacts on coastal barriers and beaches – A preliminary basis for near real-time forecasting"*. Journal of Coastal Research 18 3, p. 486-501. Summer 2002.

Pla de Ports de Catalunya 2007-2015: Estudi del medi costaner. Departament de Política Territorial i Obres Públiques, Generalitat de Catalunya. ISBN 978-84-393-8417-5.

Reis, M.T., Hu, K., Hedges, T.S. and Mase, H. (2008). *"A comparison of empirical, semiempirical, and numerical wave overtopping models"*. Journal of Coastal Research 24 2B, p. 250-262. March 2008.

Ruiz, A. and Kornus, W. (2003). *"Experiencias y aplicaciones del LIDAR".* Presentation of the 5th Geomatic Week of Barcelona, 2003. Institut Cartogràfic de Catalunya.

Ruiz, A., Kornus, W. and Talaya, J. (2008). *"Coastal applications of LIDAR in Catalonia"*. Institut Cartogràfic de Catalunya, Session 5.

Ruiz García, A. (2009). *"Aportación del LIDAR aerotransportado al cálculo de cambios en playas tras temporales"*. Actas de las Jornadas Técnicas "Las nuevas técnicas de información geográfica al servicio de la gestión de zonas costeras: Análisis de la evolución de playas y dunas." Revista Catalana de Geografia IV época, volum XIV, núm. 37. July 2009.

Sallenger, A. H., Stockdon, H.F., Fauver, L., Hansen, M., Thompson, D., Wright, C.W. and Lillycrop, J. (2006). *"Hurricanes 2004: An overview of their characteristics and coastal change"*. Estuaries and Coasts, Vol.29, Nº6A, p. 880-888. December 2006.

Servei Meteorològic de Catalunya. (2008). *"Butlletí climàtic mensual. Desembre de 2008"*. Departament de Medi Ambient i Habitatge, Generalitat de Catalunya. December 2008.

Shore Protection Manual. (1984). Coastal Engineering Research Centre, U.S. Amy Corps of Engineers.

Sierra, J.P. and Lo Presti, A. (1998). *"Estudio comparativo de criterios de rotura de oleaje regular"*. Ingenieria del Agua. Vol.5 Num. I (march 1998), p. 23-34.

Stockdon, H.F., Holman, R.A., Howd, P.A. and Sallenger Jr, A.H. (2006). *"Empirical parameterization of setup, swash, and runup"*. Coastal Engineering 53 (2006), p. 573-588.

Stockdon, H.F., Sallenger Jr, A.H., Holman, R.A. and Howd, P.A. (2007). *"A simple model for the spatially-variable coastal response to hurricanes"*. International Journal of Marine Geology, Geochemistry and Geophysics 238 (2007), p.1-20.

Türker, U. and Kabdas, M.S. *"The effects of sediment characteristics and wave height on shape-parameter for representing equilibrium beach profiles"*. Ocean Engineering 33 (2006), p. 281–291.

Wise, R.A., and Smith, S.J. (1996). *"SBEACH: Numerical model for simulating storm-induced beach change. Report 4: Cross-Shore Transport Under Random Waves & Model Validation with SuperTank & Field Data".* Technical Report CERC-98-9. April 1996. Headquarters, U.S. Army Corps of Engineers.

Websites:

Blanes en imatges. [December 2012].
www.blanesenimatges.wordpress.com

Coastal & Hydraulics Laboratory, US Army Corps of Engineers [December 2012].
chl.erdc.usace.army.mil

Institut Cartogràfic de Catalunya [September 2012].
www.icc.cat

La Natura a la Baixa Tordera [December 2012].
natura-ordera.blogspot.com.es

Laboratori d'Enginyeria Marítima, Universitat Politècnica de Catalunya - Vucoma project. [September 2012]
lim050.upc.es/vucoma

National Oceanic and Atmospheric Administration. [December 2012].
www.noaa.gov

Observatori del riu Tordera. [December 2012].
www.observatoritordera.cat

Puertos del Estado [September 2012].
www.puertos.com

Servei Meteorològic de Catalunya [September 2012].
www.meteo.cat

US Geological Surver [December 2012].
www.usgs.gov

XIOM, *Xarxa d'Instruments Oceanogràfics i Meteorològics* [September 2012].
www.xiom.cat